

## **Role of physical processes in determining the nature of fisheries in the eastern Arabian Sea**

**D. Shankar<sup>1,2,\*</sup>, R. Remya<sup>1,2</sup>, A.C. Anil<sup>1</sup>, V.Vijith<sup>3</sup>**

<sup>1</sup>CSIR-National Institute of Oceanography, Dona Paula, Goa 403004, India

<sup>2</sup>Academy of Scientific and Innovative Research (AcSIR), CSIR-NIO, Goa, India

<sup>3</sup>Cochin University of Science and Technology, Kochi, India

\*Corresponding author: shankar@nio.org

### **Abstract**

We use available data and model simulations to make a case for physical forcing of the spatial variation in the nature of fisheries off the west coast of India in the eastern Arabian Sea (EAS). The approach is heuristic, but builds the case on the basis of model simulations and well-established implications of specific physical processes for the marine ecosystem. We address three questions.

First, we show that it is differences in the physical forcing lead to a carnivore-dominated fishery in the northeastern Arabian Sea (NEAS) and a planktivore-dominated fishery in the southeastern Arabian Sea (SEAS). In the NEAS, the growing season for phytoplankton is longer because the upwelling during the summer monsoon (June–September) is followed by convective mixing during the winter (November–February) monsoon. Detrainment, again leading to a phytoplankton bloom, follows the convective-mixing season. The long duration of the growing season permits the existence of a longer food chain, leading to a carnivore-dominated fishery. In the NEAS, the phytoplankton also tend to be small owing to weaker upwelling during the summer monsoon and limitations imposed by silicates, turbulence, and light during the winter monsoon. In the SEAS, the stronger upwelling implies larger phytoplankton that can be directly fed on by fish like the oil sardine. The growing season in the SEAS is also limited to the summer monsoon, predisposing the ecosystem towards a shorter food chain.

Second, we show that it is the differences in physical forcing that lead to the weaker fishery in the central-eastern Arabian Sea (CEAS) compared to the SEAS. Though the growing season in both SEAS and CEAS is comparable, the upwelling is weaker in the CEAS, implying a limitation of nitrate and a dominance of small phytoplankton in contrast to the SEAS, where large phytoplankton dominate. Hence, the phytoplankton biomass is less in the CEAS compared to the SEAS and the region cannot support a fishery comparable to the SEAS.

Third, we show that it is the difference in physical forcing that leads to a sharp decline in the catch of oil sardines from the SEAS to the CEAS even as the catch of mackerel does not change much. Not only does the stronger upwelling in the SEAS compared to the CEAS imply a larger size of the phytoplankton in the former, but the phytoplankton biomass is also higher in the SEAS. The zooplankton standing stock, as estimated using the backscatter measured by the acoustic Doppler current profilers (ADCPs) deployed on moorings, is determined more by the vertical movement of the depth of the 20°C isotherm (D20)-. Hence, the standing stock of zooplankton tends to be lowest when upwelling peaks, i.e., during the summer monsoon. This is also the time when the phytoplankton biomass peaks. The phytoplankton surplus is greater in the SEAS compared to the CEAS because of the stronger upwelling, which implies higher primary productivity and a shallower D20, in the SEAS. This phytoplankton surplus can be fed on by the oil sardine, which prefers diatoms. In contrast, the higher zooplankton standing stock in the CEAS competes with the oil sardine off Karnataka and Goa, where the mackerel, which feed on zooplankton, is the dominant

fishery. The weaker upwelling implies lower primary productivity and a deeper D20 (higher zooplankton standing stock) in the CEAS.

This limitation of the mature habitat by the physical forcing and the seasonal reversal of the currents limits the spawning regimes of these fish because the carnivorous (planktivorous) fish like the Bombay Duck (oil sardine) can spawn only in those regions from where they can make it to their mature habitat in the NEAS (SEAS).

## 1. Introduction

India has a coastline ~7517 km long, of which ~5423 km is for the Indian mainland and ~2094 km for the island territories (<http://iomenvis.nic.in/index.aspx?langid=1>). The Indian exclusive economic zone (EEZ) extends over  $2 \times 10^6$  km<sup>2</sup>, of which  $\sim 0.86 \times 10^6$  km<sup>2</sup> is in the eastern Arabian Sea (EAS; off the west coast of India),  $\sim 0.56 \times 10^6$  km<sup>2</sup> is in the western Bay of Bengal (BoB; off the east coast of India), and the rest,  $\sim 0.6 \times 10^6$  km<sup>2</sup>, is around the Andaman and Nicobar Islands in the southeastern BoB (Fig. 1a). Fishing constitutes a major economic activity in the Indian EEZ, and, with a fisherfolk population over  $3.5 \times 10^6$  (CMFRI, 2007a), India is among the largest marine fishing and fish-exporting countries of the world (FAO, 2016). The fish catch estimates in India are based on landings data, which show that the average landings have increased from  $0.83 \times 10^6$  tonnes during 1961–1970 to  $2.44 \times 10^6$  tonnes during 1991–2000 and  $2.49 \times 10^6$  tonnes during 2001–2005. 67.9% of the catch in the mainland EEZ (i.e., excluding the EEZ around the Andaman and Nicobar Islands) is from the EAS, with the EEZ in the western BoB contributing 32.1% (CMFRI, 2007a).

With respect to fisheries, the west-coast EEZ has been traditionally divided into two regions with the border drawn just north of 15°N. The northwest (NW) region, with a total coastline length of ~2320 km, consists of two states, Gujarat and Maharashtra, and the southwest (SW) region, with a total coastline length of ~1021 km, consists of three states, Goa, Karnataka, and Kerala (Fig. 1b, Table 1). The NW and SW regions contribute almost equally to the west-coast catch, with the landings percentage being 50.8% (SW) and 49.2% (NW) during 2001–2005 (CMFRI, 2007a; Table 1).

Using data from CMFRI (1995), Madhupratap et al. (2001) showed that the fisheries in the NW region are dominated by carnivorous fish and that of the SW region by planktivorous fish. As we show later, this inference holds for more recent data as well, suggesting that this change in the nature of fisheries from south to north along the Indian west coast is characteristic of the Indian west-coast fisheries and is not restricted to certain years.

The fisheries, which constitute the higher trophic levels, are related to the lower trophic levels, comprising zooplankton, phytoplankton, and the microbial loop. These lower trophic levels are, in turn, related to the physical forcing, which determines the supply of nutrients to the surface mixed

layer. The physical forcing in the North Indian Ocean (NIO), including the EAS, exhibits a strong seasonality owing to the seasonally reversing monsoon winds (see, for example, Wyrski, 1971; Schott and McCreary, 2001; Shankar et al., 2002), and it drives the seasonal cycles of phytoplankton and zooplankton (Banse, 1968, 1984, 1987, 1994; Prasad, 1969; Nair, 1980; Banse and McClain, 1986; Naqvi, 1991; Banse and English, 1993; Brock et al., 1994; Goswami and Padmavati, 1995; Madhupratap et al., 1996a,b; McCreary et al., 1996; Nair et al., 1999; Wiggert et al., 2000, 2005, 2006, 2009; Naqvi et al., 2002, 2006; Dwivedi et al., 2006, 2008; Parab et al., 2006; Lévy et al., 2007; Habeebrehman et al., 2008; Koné et al., 2009; McCreary et al., 2009; Vinayachandran et al., 2009; Jyothibabu et al., 2010; Hood et al., 2017).

The physical forcing has been linked in the literature to the fisheries of the west-coast EEZ (Banse, 1959, 1968; Pillai et al., 1980; Pillai, 1983; Madhupratap et al., 1994; Longhurst and Wooster, 1990; Yohannan and Abdurahman 1998; Jayaprakash, 2002; Vivekanandan et al., 2005; Xu and Boyce, 2009; Manjusha et al., 2013; Kripa et al., 2015a) and even the Maldives Islands (Anderson et al., 2011), which lie to the west of Kerala in the Lakshadweep Sea (Fig. 1b). For example, the larger fishery of the west coast (two-thirds of the total landings) compared to the east coast has been attributed to the higher primary productivity of the former (Madhupratap et al., 2001; Vivekanandan et al., 2005), but this difference in primary productivity itself is driven by physical processes (Banse, 1984, 1994; Madhupratap et al., 1996a,b; Prasannakumar et al., 2002; Lévy et al., 2007; McCreary et al., 2009; Vinayachandran et al., 2009; Koné et al., 2009; Hood et al., 2017). All these papers connecting physical phenomena to fisheries attempt to link the variability observed in selected oceanographic variables like sea level, sea-surface temperature (SST), and dissolved oxygen to fisheries through a set of heuristic arguments, but are limited in their scope by the data and the methods used. A more comprehensive, but still heuristic, analysis of the links between the physical forcing in the NIO and satellite-derived chlorophyll-*a* was carried out by Lévy et al. (2007), who showed that the changes in the physical forcing over space and time allowed a division of the summer and winter blooms of phytoplankton into distinct regions. Several papers have linked the higher primary productivity off NW and SW India during the winter (November–February) and summer (June–September) monsoons, respectively, to the higher fish catch in these regions (Banse, 1968; Madhupratap et al., 2001; Vivekanandan et al., 2005). Thus, there is a strong historical basis for linking the physical forcing to the fisheries off the Indian west coast, but most studies have been piecemeal, restricting their focus to a few years or a small part of the EAS (Pillai et al., 1980; Pillai, 1983; Longhurst and Wooster, 1990; Yohannan and Abdurahman 1998; Jayaprakash, 2002; Vivekanandan et al., 2005; Xu and Boyce, 2009; Manjusha et al., 2013; Kripa et al., 2015a) or have

been based on model studies and restricted to the links between the physical forcing and chlorophyll-*a* (Lévy et al., 2007). A few papers extended their analysis to the entire EAS (Banse, 1968; Madhupratap et al., 1994), but our understanding of the physical forcing has evolved significantly since then (Schott and McCreary, 2001; Shankar et al., 2002).

While pointing to the change in the nature of fisheries along the Indian west coast, Madhupratap et al. (2001) concluded that their observation of a dominance of carnivores (planktivores) in the NW (SW) region was unexplained. Hence, this is the first of three questions that we address in this paper: why is the fishery in the NW (SW) region dominated by carnivores (planktivores)? In order to make the case for a physical forcing of this spatial variation in the nature of fisheries in the NW and SW regions of the Indian EEZ, we rely largely on data that are already published or are publicly available. In other words, we draw our inferences mostly from the available information. We show that differences in physical forcing lead to a longer duration of primary production in the NW region, particularly Gujarat, permitting a longer food chain and implying a carnivore-dominated fishery; the shorter duration of primary production in the SW region, particularly Kerala, implies a shorter food chain and a planktivore-dominated fishery. The second question we address concerns the lower productivity off Karnataka, Goa, and Maharashtra in comparison to Kerala, the southernmost of the three states in the SW region. We link the lower productivity north of Kerala to weaker upwelling, which limits the nutrient supply to the surface mixed layer. The third question we address is the reason for the dominance of the oil sardine off Kerala. We show that the zooplankton-phytoplankton seasonal cycles are mismatched, suggesting a huge phytoplankton surplus off Kerala; we hypothesise that this surplus phytoplankton leads to the domination of the oil sardine in this region.

The paper is organised as follows. The sources of fisheries data and climatological data of the physical and biogeochemical variables are listed in Section 2. In addition to these data, we use a physical and a coupled physical-ecosystem model; these models are also described in Section 2. The background information, based on the data sets used, is presented in Section 3; while the focus is kept on the elements essential to answering the questions posed above, we have chosen to explain the relevant physical processes in reasonable detail owing to the inter-disciplinary nature of this paper. In Section 4, we show that the available data and model results can be used to infer the links between the physical forcing and the nature of fisheries and answer the three questions posed above. Section 5 discusses the results and their implications and concludes the paper.

## **2. Data and models**

This section describes the data sets and models used in this paper.

## **2.1. Data sources**

The fishery data used in this paper are based on the fish-landing statistics compiled in reports published by the Central Marine Fisheries Research Institute (CMFRI). The phytoplankton biomass estimates are based on a weekly climatology of near-surface satellite derived chlorophyll-*a* concentration measured by SeaWiFS (Sea-Viewing Wide Field-of-View Sensor) at a spatial resolution of 9 km (Lévy et al., 2006, 2007). The photosynthetic pigment chlorophyll-*a* can be used as a proxy for phytoplankton biomass and the associated primary production due to its presence in the phytoplankton cells (Falkowski and Kiefer, 1985).

For zooplankton biomass estimates, we use as a proxy the backscatter estimated from the echo intensity measured by acoustic Doppler current profilers (ADCPs); the backscatter data used here have been reported by Aparna et al. (2018), who provided a detailed description of the method used to estimate the backscatter (following Deines, 1999) and validated its use as a proxy for zooplankton biomass. These ADCPs were deployed on three moorings on the continental slope at a water-column-depth of ~1100 m off the Indian west coast. One mooring each was deployed at 9°N (off Kerala), ~15.15°N (off Goa), and ~20°N (just south of the coast off Gujarat, but we refer to this mooring as lying off Gujarat); the mooring details are listed in Table 2. These west-coast moorings are serviced during October–November each year (Amol et al., 2014; Aparna et al., 2018). All ADCPs deployed are broadband and of make RD Instruments and the data were collected at an hourly interval with a bin size of 8 m (Amol et al., 2014; Amol, 2014). We use a climatology created by Aparna et al. (2018) using data from 153 kHz ADCPs, which were deployed at a depth of ~200 m; the water-column depth at these locations is ~1100 m. Roughly 10% of the range is lost owing to surface echoes, implying that data are not available for the top ~20 m. At least three years of data during October 2012 to November 2016 from these ADCPs are available at all three locations (Table 2).

We also use data on near-surface currents from a climatology of ship drifts (Mariano et al., 1995) and from the OSCAR (Ocean Surface Currents Analyses Real-time; Bonjean and Lagerloef, 2002) product to describe the circulation. The OSCAR currents were averaged over 2001–2015 to create the climatology. Other data sets used are the temperature and salinity climatology of Chatterjee et al. (2012), the oxygen climatology of Garcia et al. (2014), and the altimeter sea-level anomalies (SLAs) from AVISO (Archiving Validation and Interpretation of Satellite Oceanographic; AVISO, 1996); the altimeter data were averaged over 1993–2014 to create the climatology.

## **2.2. Models**

We use the results from two model simulations, one reported by Shankar et al. (2016) and the other

by Vijith et al. (2016). Model details are available in these papers and both models have been validated extensively (Kurian and Vinayachandran, 2007; Vinayachandran et al., 2007; Chatterjee et al., 2013, 2017; Mukherjee et al., 2017; Mukhopadhyay et al., 2017).

Shankar et al. (2016) used a state-of-the-art oceanic general circulation model (OGCM) called MOM (Modular Ocean Model; Griffies, 2009) to show how the physical forcing leads to a shallower mixed layer in the southern part of the northeastern Arabian Sea compared to its northern part. The specific model version used by them was MOM4p1. The model setup, physics, and forcing are given in Tables 3, 4, and 5, respectively

Vijith et al. (2016) used a coupled physical-ecosystem model based on MOM4p1; the physical set-up in Vijith et al. differs somewhat from that in Shankar et al. (2016), with the major difference being the wind forcing data set. Vijith et al. used a merged product of 3-hourly ECMWF (European Centre for Medium-range Weather Forecasting) reanalysis (ERA-INTERIM) and daily QuikSCAT (Quik scatterometer) data instead of daily OMIP (Ocean Model Inter-comparison Project; Röske 2001) data used by Shankar et al.; the model set-up, physics, and forcing details are given in Tables 3, 4, and 5, respectively. The differences in the forcing lead to minor differences in the simulated circulation. The ecosystem model used is TOPAZ (Tracers of Phytoplankton with Allometric Zooplankton; Dunne et al., 2010, 2013), and the relevant model details are given in Table 6. Vijith et al. used the model to describe the biogeochemical processes that distinguish the southern and northern parts of the northeastern Arabian Sea. Their results did not extend to the rest of the EAS. We use the same model simulation, but present results for the entire EAS in Section 4. These results — extension of the results of Shankar et al. (2016) and Vijith et al. (2016) from the northeastern Arabian Sea to the entire EAS — are the only ones that have not been published earlier: all the data and other model results used to infer the links between the physical forcing and the fisheries in the EAS are available in the literature.

### **3. The background**

This section is essentially a summary of existing knowledge, but it is necessitated by the fact that this existing knowledge forms the basis for the inferences that constitute our results. We begin with a description of the seasonal cycle of the physical forcing in the EAS (Section 3.1), restricting our attention to the aspects relevant to the fisheries questions posed earlier. Then follows a description of the seasonal cycle of phytoplankton (Section 3.2) and zooplankton (Section 3.3); a similar description of the seasonal cycle of the microbial loop or picoplankton is not possible as we still do not have enough data to document the spatio-temporal variability. We end this section with a

description of the relevant aspects of the fisheries in the EAS (Section 3.4). In order to avoid repetition, we restrict this section to this description as available in the literature: a discussion of the inter-connections between the physical forcing, the phytoplankton and zooplankton, and the fisheries is deferred to Section 4, in which we infer these links based on the evidences presented in this section.

### ***3.1. Seasonal cycle of circulation and hydrography in the EAS***

The physical processes of interest for biogeochemistry and fisheries are upwelling, entrainment, and detrainment. All three processes are potential drivers of phytoplankton blooms (McCreary et al., 2001, 2009; Lévy et al., 2007; Hood et al., 2017), triggering a cascade of ecosystem processes up the food chain or food web. We begin with a brief description of these processes and their implications for the ecosystem, followed by a description of the variability of the circulation and hydrography in the EAS.

#### ***3.1.1. Upwelling and downwelling, entrainment and detrainment***

Upwelling and entrainment inject nutrients into the surface mixed layer (ML), promoting primary production. The difference between the two processes is, however, significant not merely because they constitute different physical processes, but because they have different biogeochemical implications.

##### **3.1.1.1 Upwelling and downwelling**

When upwelling occurs, the thermocline shallows and the ML becomes thinner owing to a positive or upward vertical component of velocity that pushes up the ML base. During upwelling, this vertical velocity is upward at the base of the ML and decays to near-zero values at the surface. This decrease in vertical velocity within the ML is a measure of the much larger changes in the thermocline, as manifest in the changes in, say, the depth of the 20°C isotherm (called D20 hereafter), compared to the changes in sea level. The ocean is stratified and the resulting baroclinicity (pressure surfaces do not match the density surfaces) implies that the range of the seasonal cycle of D20, which lies within the thermocline, is of the order of a few tens of metres (or the range of the seasonal cycle of the ML depth — MLD hereafter — is of the order of several metres to tens of metres) compared to the few tens of centimetres associated with the seasonal cycle of sea level (Shankar, 1998, 2000). (It is this rough correspondence between the movement of the thermocline and the sea surface that makes satellite altimeter data useful for studying ocean circulation and climate. See, for example, Prakash et al. (2013) for a study linking the sea level to the thermocline and the oxycline in the seas around India.) As a consequence of the upward vertical velocity during upwelling, material is advected, or

transported, into the surface ML from the nutrient-rich layer below, creating conditions favourable for phytoplankton growth. When downwelling occurs, the vertical velocity is negative or downward, implying transfer of material away from the ML; hence, nutrients are not supplied to the ML during downwelling, making it unfavourable for phytoplankton growth. This process is shown schematically in Fig. 2.

Upwelling and downwelling are associated with horizontal divergence and convergence, respectively, of mass. For an eastern ocean boundary like the EAS, upwelling (downwelling) occurs along with an equatorward (poleward) alongshore boundary current, associated with which is a fall (rise) in sea level and isotherms sloping up (down) towards the coast, reflecting a shallowing (deepening) of the thermocline and therefore a decrease (an increase) in D20 (see Fig. 2). The alongshore current tends to be in quasi-geostrophic balance with the pressure field, which is related to the sea level and D20. Upwelling (downwelling) can be forced by an alongshore wind if it blows equatorward (poleward) along the eastern boundary, as happens in classical eastern-boundary-current systems like the California Current or the Canary Current (Sverdrup et al., 1942; McCreary, 1981). The alongshore wind forces an offshore (onshore) Ekman drift, leading to a fall (rise) in sea level and an upsloping (downsloping) of isotherms owing to the divergence (convergence) of mass associated with upwelling (downwelling). This relation of the alongshore wind to the alongshore current, sea level, and D20 is shown schematically in Fig. 2. In contrast, a cross-shore wind will drive an alongshore Ekman drift and cannot, therefore, force upwelling or downwelling.

Note that the definition of upwelling, as the term is used here, differs from that used in several papers dealing with biology. Here, upwelling refers to a vertical velocity that is upward; this is the same definition used in papers like that by Lévy et al. (2007). It does not necessarily imply that cold, sub-surface water *surfaces*, as is often implied in biology and fisheries papers. For example, when Madhupratap et al. (2001) state that upwelling in the EAS is restricted to the regime south of roughly 15°N, it is only the surfacing of cold waters whose extent is thus restricted, not that of the upward vertical velocity or the fall in sea level or shallowing of the thermocline, all of which, as we show in Section 3.1.2, are evident throughout the EAS.

There is one problem, however, with vertical velocity: it is several orders of magnitude smaller than the horizontal velocity and cannot be measured directly. Even in OGCMs, the vertical velocity is a diagnostic field, implying that it is estimated from computations of the horizontal velocity (Griffies, 2009). In other words, the vertical velocity, the best indicator of upwelling, must be inferred from other measurements.



### 3.1.1.2 Entrainment and detrainment

In contrast to upwelling or downwelling, entrainment is not associated with vertical velocity. Entrainment occurs when the turbulence available in the surface ML exceeds that required to maintain the near-uniform density in the ML: this excess turbulent energy is used for mixing between the water of the ML and the denser water underlying it (Turner and Kraus, 1967; Kraus and Turner, 1967; Denman, 1973; Kim, 1976; Shetye, 1986; Wiggert et al., 2005; McCreary et al., 2001, 2009). In this process, small eddies transfer properties in both directions across the base of the ML and there is no vertical advection as happens with upwelling or downwelling. Entrainment is essentially a turbulent mixing process that can be driven by the wind blowing on the ocean surface or by a destabilisation of the usually stable stratification by evaporative cooling at the surface. When entrainment is driven by changes in buoyancy, it is often referred to as convective mixing (see, for example, Banse, 1968). Since it is only the magnitude of the wind that matters for mixing, entrainment is not direction-specific: the wind may be alongshore or cross-shore, and both will drive the same level of entrainment if their magnitude is the same. This process is depicted schematically in Fig. 3. When entrainment occurs, the ML deepens and nutrients from the nutrient-rich waters below the ML can be entrained into it, again promoting phytoplankton growth. Entrainment can also inject into the ML the phytoplankton seeds lying dormant in the sub-surface chlorophyll maximum layer (SCML), which is found commonly at the base of the ML (Cullen, 2015), or from the thermocline waters below it.

While entrainment is not linked to vertical velocity and mixing due to entrainment can occur irrespective of whether upwelling or downwelling is taking place, it is evident that a shallow ML, which is promoted by upwelling, will be more conducive to mixing than a deep ML because the latter will require more turbulent energy just to maintain its depth.

Entrainment usually cools the ML because temperature decreases with increasing depth in the ocean. Stratification, however, depends on salinity in addition to temperature, implying that there are cases in which entrainment can occur without a decrease in SST. Such situations occur when a thin layer of fresher water overlies saltier water of the same temperature, as often happens in the BoB (Shetye et al., 1996; Sengupta and Ravichandran, 2001; Vinayachandran et al. 2002; Schott and McCreary, 2001; Thadathil et al., 2007) or the southeastern Arabian Sea (Shetye et al., 1991; Thadathil and Ghosh, 1992; Shenoi et al., 2004, 2005; Kurian and Vinayachandran, 2006) or farther north in the EAS (Shankar et al., 2005; Shankar et al., 2016). In this case, the isothermal layer (the layer over which temperature is almost the same as the SST) is deeper than the ML, whose depth is determined by both temperature and salinity. In such a situation, entrainment will lead to mixing between waters

of differing salinities but same temperature, precluding a change in the SST. This isothermal layer underlying the ML is called the barrier layer because it presents a barrier to the cooling of the surface (Lukas and Lindstrom, 1981; Vialard and Delecluse, 1998). Note that the temperature can even increase within the barrier layer if the resulting decrease in density is compensated by salinity increasing rapidly enough to ensure a stable stratification. Such temperature inversions within the barrier layer have been reported from the northern and western BoB (Shetye et al., 1996; Sengupta and Ravichandran, 2001; Vinayachandran et al., 2002; Thadathil et al., 2007) and the southeastern Arabian Sea (Thadathil and Ghosh, 1992; Durand et al., 2004; Shenoi et al., 2004). The barrier layer has implications for the ecosystem too: if the SCML occurs at the base of the isothermal layer instead of at the base of the ML, as can happen in the northern BoB (Amol et al., 2018b), entrainment will not lead to the nutrients or phytoplankton seeds being injected into the ML until the barrier layer is eroded.

Detrainment, which is also referred to as re-stratification, occurs when the ML shallows rapidly, as happens when the Sun warms the ocean surface after winter. As the ML shallows, the available nutrients are confined within a smaller depth range, leading to phytoplankton blooms (Sverdrup, 1953; McCreary et al., 1996, 2001, 2009; Ryabchenko et al., 1998). The existing nutrients within the ML are rapidly exhausted by the bloom because there is no supply of nutrients from below: hence, detrainment blooms are short-lived in comparison to blooms driven by upwelling or entrainment. Nevertheless, since the depth-averaged light intensity is high in the thin MLs, detrainment blooms tend to be highly productive (McCreary et al., 2001, 2009). Detrainment can also occur if the ML is stabilised by the influx of freshwater due to in situ rainfall or river runoff, as happens in the EAS (Shankar, 1998; Shankar and Shetye, 1999; Shankar et al., 2005; Shenoi et al., 2005) and the BoB (Shetye et al., 1991; Sengupta and Ravichandran, 2001; Vinayachandran et al. 2002; Schott and McCreary, 2001). Horizontal advection of low-salinity surface water is also a possible cause of detrainment (Shankar et al., 2016).

### *3.1.2. Seasonal cycle of the physical forcing in the EAS*

Since the vertical velocity cannot be measured, the variables of interest for upwelling, which is a dynamical process, are D20, sea level, and the alongshore current; for entrainment and detrainment, the variables of interest are the MLD, the wind field, the buoyancy flux in the ML, and the stratification at the base of the ML; this stratification can be estimated from vertical profiles of temperature and salinity.

### 3.1.2.1. Upwelling and downwelling

We start by presenting the variation in time at the three ADCP locations because the zooplankton biomass estimates are restricted to these locations and the temporal variation is easier to follow in these curves. We consider the ADCP moorings at 9°N, 15.15°N, and 20°N to be representative of the southeastern Arabian Sea (SEAS; off Kerala), central-eastern Arabian Sea (CEAS; off Karnataka, Goa, and Maharashtra), and northeastern Arabian Sea (NEAS; off Gujarat), respectively; note that the northernmost mooring lies just southwest off Gujarat in the southern NEAS, but we consider it representative of the NEAS. D20 begins shallowing in the SEAS after January, when it reaches its maximum depth (Fig. 4b); in the CEAS and the NEAS, the shallowing starts after March. The variation of SLA is similar (Fig. 4a), but the SLA in the NEAS shows little variation during November–March. The West India Coastal Current (WICC), which is the boundary current in the EAS (Shankar and Shetye, 1997), flows poleward during November–January at all three locations, but reverses to flow equatorward by April. The SLA decreases and D20 shallows through the summer monsoon. The minima of SLA (D20) in the SEAS, CEAS, and NEAS occur during August (September), October (October), and September (September), respectively (Fig. 4a,b). The equatorward WICC in the SEAS and NEAS (CEAS) starts weakening after July (August), and it reverses during October (November) in the SEAS and CEAS (NEAS; Fig. 4c). Therefore, upwelling may be said to occur during May–October at all three locations. During November–March, downwelling, manifest in a rise in sea level, deepening of the thermocline (D20), and a poleward WICC, occurs at all three locations.

The seasonal cycle of the WICC is linked to that of the SLA in the EAS (Shankar and Shetye, 1997, Shankar, 1998; Shetye, 1998). High SLA occurs off the west coast of India in November in conjunction with a poleward WICC (Fig. 5). These high SLAs spread westward over time (McCreary et al., 1993; Shankar and Shetye, 1997; Shankar et al., 2002; Shankar, 1998; Shetye, 1998), but the rate of westward movement depends on latitude: the high SLAs move westward faster in the SEAS than farther north along the coast. By January, an anticyclonic sea-level feature exists in the SEAS and the current flows around it with the high SLAs to its right; this sea-level high has been called the Lakshadweep High (LH; Bruce et al., 1994; Shankar and Shetye, 1997). As the high SLAs move westward, with the westward spread occurring faster south of ~13°N, the sea level tends to decrease near the coast and the near-coastal WICC reverses to flow equatorward. By May, the high SLAs are replaced by lower sea level near the coast even north of 13°N and the WICC flows equatorward throughout the EAS. The sea level continues to decrease and the low SLAs also move westward over time, again with the rate of westward movement being higher in the SEAS. During

the summer monsoon, a low-SLA counterpart of the LH forms in the SEAS, with cyclonic flow around it. This low-SLA feature, associated with which is upwelling, has been called the Lakshadweep Low (LL; Shankar and Shetye, 1997; Shankar, 1998; Shetye, 1998).

Model simulations show that the LH and LL are forced by coastal Kelvin waves (McCreary et al., 1993; Shankar and Shetye, 1997), which propagate with the coast on their right in the northern hemisphere (Gill, 1982). The LH is associated with downwelling coastal Kelvin and Rossby waves and it moves westward owing to the westward propagation of the Rossby waves that constitute it (Shankar and Shetye, 1997; Bruce et al., 1998). These Rossby waves are equatorial Rossby waves and their westward speed decreases as  $1/y^2$ , where  $y$  is the distance from the equator. Therefore, the wave propagates offshore much faster in the SEAS than farther north. For example, the Rossby wave speed at  $10^\circ\text{N}$  is  $\sim 10$  cm/s ( $\sim 8.6$  km/day), but it decreases to  $\sim 2.5$  cm/s ( $\sim 2.1$  km/day) at  $20^\circ\text{N}$ ; hence, the Rossby wave takes over a month to cross the Lakshadweep Sea (Shankar et al., 2004a), but will take over 4–5 months to propagate the same distance off Gujarat. As the wave propagates offshore, it takes with it the current and SLA signals associated with it. Therefore, the strongest current occurs along the front of the wave, which is adjacent to the west coast only in November (Fig. 5). As the SLA peak moves offshore, the sea level decreases towards the coast, leading to a reversal of the coastal current. Since this offshore movement occurs earlier in the SEAS owing to the higher Rossby wave speed there, the WICC tends to reverse earlier off Kerala than farther poleward in the EAS (Shankar and Shetye, 1997; Shankar, 1998), as had been observed earlier (Sharma, 1968; Longhurst and Wooster, 1990). During March, for instance, the WICC tends to flow equatorward off Kerala even as it continues to flow poleward farther north along the coast (Fig. 5). Hence, upwelling tends to occur earlier off Kerala than off Karnataka or Goa. Likewise, the LL is associated with upwelling coastal Kelvin and Rossby waves. Model simulations show that the forcing for the LH comes largely from the alongshore winds off the Indian east coast, implying a dominance of what has been called “remote forcing”, rather than the local winds or “local forcing” (McCreary et al., 1993; Shankar and Shetye, 1997; Shankar et al., 2002). The LL too is largely forced remotely from the east coast of India (McCreary et al., 1993; Shankar and Shetye, 1997; Shankar et al., 2002), but the local winds too make a contribution (Shankar et al., 2002; Suresh et al., 2013). It is the arrival of the downwelling coastal Kelvin wave during October that leads to a reversal in the WICC, which then flows poleward, and an increase in SLAs off the Indian west coast. An important point to note is that dynamics constrains the Kelvin wave to propagate only poleward along an eastern ocean boundary like the Indian west coast, but the direction of the alongshore current associated with it can be poleward, as happens with a downwelling Kelvin wave, or

equatorward, as happens with an upwelling Kelvin wave (McCreary, 1981; Gill, 1982).

Apart from the slower offshore movement with increasing latitude owing to the decrease in Rossby wave speed with increasing distance from the equator, Fig. 5 also suggests a difference in the offshore movement of the LL and LH in the SEAS. The low SLAs associated with the LL do not extend as far westward in the southern Arabian Sea (up to 66°E from June to September) as do the high SLAs associated with the LH (beyond 62°E from November to January). The faster offshore movement of the LH is easier to understand in the context of the one-and-half-layer reduced-gravity model (Gill, 1982; Shankar and Shetye, 1997; Shankar, 1998). The Rossby wave speed in this model, which has one active upper layer and an isostatic lower layer (see, for example, Appendix A of Shankar, 1998) is given by  $C_R = \beta g H (\rho_2 - \rho_1) / f^2 \rho$ , where  $g$  is the acceleration due to gravity,  $H$  is the thickness of the active upper layer,  $\rho_1$  and  $\rho_2$  are the densities of the upper (lighter) and lower (denser) layers, respectively,  $\rho$  is the average density of sea water,  $f$  is the Coriolis acceleration, and  $\beta$  is the rate of change of Coriolis acceleration with latitude. In the context of this model, the sea level is given by  $\eta = H(\rho_2 - \rho_1) / \rho$ . The thickness of the upper layer changes significantly between the summer monsoon, when the layer is thin owing to upwelling, and the winter monsoon, when downwelling thickens the layer. The layer thickness in the simulation of Shankar and Shetye (1997) changed from over 100 m during January to less than 40 m during July (see their Fig. 3) and this difference is evident in the slower offshore propagation of the LL. Note that the Rossby wave speed for the LH and LL is the same in a linear model and this is one of the distortions introduced by linearisation (compare Figs. 3.5 and 3.6 in Shankar, 1998).

In Fig. 5, we have shown the spatial variation as a function of time by using 12 panels; in Fig. 4, we have shown the temporal variation of the variables of interest at the three ADCP mooring locations, thereby discretising the alongshore variation and dropping the cross-shore variation. Since all the above variables are functions of time and the two horizontal coordinates, the alongshore and cross-shore distance from an origin, it is necessary to discard one dimension among time, alongshore distance from the southern tip of India (8°N), and the cross-shore distance from the coast for describing the variability in two dimensions. Following Shankar et al. (2016) and Vijith et al. (2016), we drop the cross-shore distance in Fig. 6 and present the variables as functions of time and the alongshore distance following the 1000 m isobath; though the alongshore distance is used as the coordinate, we refer to these figures as time-latitude plots to avoid confusing alongshore and cross-shore distance measures. Fig. 6 complements Fig. 5, in which time appears as a discrete variable (varying from one panel to another). So all the data in Fig. 6 are presented for the continental slope, on which the WICC is trapped (Shetye et al., 1990, 1991; Shetye and Gouveia, 1998), enabling the

use of models without bathymetry to simulate the large-scale circulation of the NIO (see , for example, McCreary et al., 1993; Shankar and Shetye, 1997; Han et al., 2001; Han and McCreary, 2001; Shankar et al., 2002). The WICC does, however, leave its imprint on the coastal sea level (Banse, 1968; Shetye and Almeida, 1985; Shankar, 1998, 2000) and recent work shows a strong relation between the slope and shelf WICC (Amol et al., 2012; Amol, 2014). Most of our discussion is therefore restricted to the continental slope, but we examine the consequences of our results for the shelf in Section 5.2. Furthermore, instead of using the calendar year as the time axis, we plot the seasonal cycle beginning with April because it is easier to follow the seasonal evolution of the physical forcing with this choice of the abscissa: it does not split the winter monsoon between the end (November–December) and beginning (January–February) of the calendar year.

Upwelling, manifest in a decrease in sea level (Fig. 6a) and a shallowing of D20 (Fig. 6b), occurs all over the EAS during the summer monsoon, but it is stronger south of 13°N (SEAS), i.e., off Kerala, compared to farther north along the Indian west coast. For example, during the summer monsoon, the SLA drops below -10 cm and D20 shallows to ~80–90 m at 10°N, but the corresponding values for SLA and D20 at 15°N (22°N) are -8 cm (-4 cm) and ~130 m (~150 m), respectively. SLA off Kerala (8–13°N) begins decreasing after peaking in January–February, but the equatorward flow strengthens only in April. The SLA in the EAS reaches its minimum in August along with D20; the equatorward WICC peaks in July (Fig. 6c). The tilt of the SLA and D20 fields (from left to right along the time axis as one moves poleward along the 1000 m isobath from 8°N to ~16°N) implies that the upwelling starts later as one moves poleward along the coast, a feature noted for the first time shortly after the International Indian Ocean Expedition (IIOE; Sharma, 1968) and explained almost three decades later (Shankar and Shetye, 1997).

In summary, therefore, upwelling occurs in the EAS during May–October, but the data suggest that it begins earlier, maybe by February or March, in the SEAS, and downwelling occurs during November–March. Note that our focus has been on vertical advection because it brings up nutrients during upwelling, but horizontal advection by the prevailing currents is also important: nutrients, phytoplankton, and zooplankton are advected by the circulation. Horizontal advection is critical for a significant part of the fish life cycle as well because the fish larvae are advected by the currents. The currents are also known to determine the direction in which fish shoals move (Laevastu and Hayes, 1981; Madhupratap et al., 1994).

#### 3.1.2.2. Entrainment and detrainmen

The surface ML, whose depth provides a measure of the entrainment mixing, is generally shallow in

the EAS: MLD is less than 30 m at the mooring locations in the SEAS and CEAS throughout the year (Fig. 4d). The MLD exhibits a seasonal cycle, being shallow during the summer monsoon in conjunction with upwelling (Fig. 4a) and low D20 (Fig. 4b) and deepening along with D20 when downwelling occurs during the winter monsoon. The MLD in the SEAS (CEAS) ranges from less than 10 m during August (September) to ~25 m (~30 m) during January (December). In the NEAS too, the MLD exhibits a seasonal cycle, with shallow (deep) MLs occurring during the summer (winter) monsoon. The range in the NEAS is much higher, however, compared to the SEAS or CEAS: the minimum, at ~10 m during October at the end of the summer-monsoon upwelling, is comparable to the minimum in the SEAS and CEAS, but the maximum, ~55 m during January, is much higher in the NEAS. Downwelling, as manifest in D20, peaks during March, but the MLD shallows after January in the NEAS. This striking difference between the NEAS and the rest of the Indian west coast is evident in the time-latitude plot, which shows that the deeper MLs are confined poleward of ~18°N during the winter monsoon (Fig. 6d). As shown by Shankar et al. (2016), the poleward advection of fresher water by the WICC inhibits ML deepening in the southern part of the NEAS; hence, the deepest MLs occur during January (February) south (north) of ~23°N. This deepening of the ML in the NEAS during the winter monsoon has been attributed to convective mixing driven by dry, cool northeasterly winds blowing from the Indian subcontinent (Banse, 1968; Shetye et al., 1992; Madhupratap et al., 1996b; Dwivedi et al., 2006, 2008; Lévy et al., 2007; Koné et al., 2009; Shankar et al., 2016), but the role of advection distinguishes the regime of highest latent heat flux in the southern NEAS from the regime of deepest MLs in the northern NEAS (Shankar et al., 2016). This deepening of the ML in the NEAS during October–February drives entrainment mixing (Banse, 1968; Madhupratap et al., 1996b; Lévy et al., 2007; Koné et al., 2009; Shankar et al., 2016).

Once the Sun crosses the equator and the northern hemisphere warms in March, the ML shallows rapidly in the NEAS (Figs. 4d,6d), leading to detrainment; in the southern NEAS, the detrainment occurs in February (Shankar et al., 2016) owing to the freshening of the surface in the southern NEAS by fresher water advected from the south by the poleward WICC (Shankar et al., 2016). The WICC reverses in April (Figs. 4c,6c), marking the upwelling phase of the seasonal cycle, and the ML continues to shallow (Figs. 4d,6d) as SLA decreases (Figs. 4a,6a) and D20 shallows (Figs. 4b,6b), but now due to upwelling, not detrainment.

### ***3.2. Seasonal cycle of phytoplankton***

Collecting phytoplankton samples to document the seasonal cycle is tough owing to the time required to process the samples, the long coastline, the strong seasonality, and variation across years

(interannual variability) and within a season (intraseasonal variability). Hence, descriptions of the seasonal cycle of phytoplankton rely almost exclusively on satellite measurements of chlorophyll-*a*. In the EAS, such descriptions have been available for over 25 years (Banse and McClain, 1986; Banse and English, 2000; Lévy et al., 2007; Aparna et al., 2018). We use the weekly SeaWiFS climatology of Lévy et al. (2006) to describe the seasonal cycle of phytoplankton.

Spatial maps of the satellite-derived chlorophyll-*a*, a proxy for phytoplankton biomass, show high chlorophyll during both summer and winter monsoon in the NEAS off Gujarat, but there is only one peak, during August, in the SEAS off Kerala and in the CEAS (Fig. 7; Banse, 1987; Lévy et al., 2007; McCreary et al., 2009; Koné et al., 2009; Resplandy et al., 2011; Shankar et al., 2016; Hood et al., 2017). To map the spatio-temporal variation, we plot the chlorophyll concentration as a function of time and distance along the 1000 m isobath. The two peaks in the NEAS and the single peak in the SEAS are evident in Fig. 8a. For comparing with the seasonal cycle of zooplankton biomass, it is useful to map the seasonal cycle of phytoplankton at the three ADCP mooring locations (Fig. 8b); the two peaks off Gujarat (20°N) and the single peak off Goa and Kerala are evident. As noted by Lévy et al. (2007), however, the peak represents but one aspect of a phytoplankton bloom: of equal interest is its duration, and one way to measure the bloom duration is to start from a minimum and follow the curve to the maximum and on to the next minimum.

Off Kerala, in the SEAS, the bloom can be said to start in May because the chlorophyll concentration in May is only slightly higher than that in April (Fig. 8b). Note that the start of the summer-monsoon phytoplankton bloom occurs earlier, during March, in Lévy et al. (2007, their Figs. 3 and 5) because they average over a much larger region covering the near-coastal SEAS, the Gulf of Mannar, and part of the east coast of Sri Lanka (Figure 3 of Lévy et al., 2007) and use the minimum to denote the start of the bloom. We ignore the mathematical minimum used by Lévy et al., choosing to treat the period of low chlorophyll concentration during December–April as marking a broad “minimum” in the seasonal cycle (Fig. 8b). At its peak in August, the concentration exceeds 1.6 mg/m<sup>3</sup>; then the concentration decreases and reaches its minimum level seen in May (April) again by November (December). Note that the ADCP mooring at 9°N is located in a patch of lower chlorophyll concentration compared to 8°N and 10°N (Fig. 8a): the peak concentration in the SEAS, at both 8°N and 10°N, exceeds 2.2 mg/m<sup>3</sup>. As may be expected from the poleward migration of upwelling along the Indian west coast (Fig. 6a,b), the bloom starts earlier, in April, in the southern SEAS (~8°N) compared to the northern SEAS (~13°N), where it starts in June, but the bloom at 8°N ends in October, a month earlier than farther north along the Kerala coast. In summary, therefore, the summer bloom off most of the Kerala coast can be considered to occur during May–November, a



duration of six months, but the bloom close to the southern tip of India at 8°N lasts a month longer.

Off Goa, in the CEAS, the bloom starts in a similar manner in May, when the concentration is slightly higher than in April, but it peaks in July, a month earlier than off Kerala (Fig. 8a,b). (As with the SEAS, the bloom onset occurs earlier, during April, in Lévy et al. (2007).) The peak concentration off Goa is 1 mg/m<sup>3</sup> and the concentration decreases thereafter, but more slowly than off Kerala (Fig. 8b). The bloom can be said to end in December, following which there is little change in the concentration till May. So the bloom off Goa, though not as strong as off Kerala (see Fig. 7b–d), also lasts six months. This mooring location off Goa can be considered representative of the central part of the Indian west coast as the chlorophyll concentration is weaker in the latitude band ~14–19°N compared to south (north) of 14°N (19°N) (Fig. 8a).

Off Gujarat, in the NEAS, it is more difficult to interpret the duration owing to the relatively sharp minimum occurring in October between the summer and winter blooms (Fig. 8a,b). The summer bloom starts in June (during May in Lévy et al., 2007) and peaks in August, with the peak concentration exceeding 1 mg/m<sup>3</sup> (Fig. 8b). The concentration decreases after August, hitting a minimum in October, but the concentration in October is still higher than the minimum concentrations achieved during May–June. The winter bloom starts in October and peaks in February; the sharp minimum in October implies that Lévy et al. (2007) pick the same starting point for the winter bloom. The peak concentration in winter is a little higher than during the summer bloom at 20°N, but the summer bloom peak is stronger than the winter bloom peak north of ~24°N in the northern NEAS (Fig. 8a). Following the peak in February, the chlorophyll concentration decreases and the bloom disappears by April. So the summer bloom lasts four months (June–September) and the winter bloom six months (October–March), but the winter bloom succeeds the summer bloom off Gujarat even in the southern NEAS, implying a combined duration of almost 10 months (June–March).

### ***3.3. Seasonal cycle of zooplankton***

Zooplankton analysis is even more time-consuming and satellites cannot sense zooplankton. Hence, a reasonable description of the seasonal cycle of zooplankton biomass, with a sampling interval that can be considered adequate, is possible only through a proxy, the backscatter measured by ADCPs deployed on moorings. Only one study of the seasonal cycle of zooplankton is available to date in our region of interest (Aparna et al., 2018) and we use the ADCP backscatter data to describe the seasonal cycle of zooplankton standing stock.

Contrary to the canonical assumption that the zooplankton seasonal cycle will follow that of

phytoplankton (Subramanyan, 1959; Heinrich, 1962), the backscatter, a proxy for zooplankton biomass, is almost invariant in time in the upper ocean, whose depth is identified roughly by D20 (Fig. 8c–e). Aparna et al. (2018) showed that the degree of variance of backscatter was low both above and below D20 and reached its maximum around this depth, implying that the backscatter above and below D20 was almost invariant in time. The bottom of this layer of near-invariant backscatter, denoted roughly by D20 in Figs. 8c–e, does, however, undergo a seasonal cycle associated with the upwelling and downwelling off the Indian west coast (Figs. 4a–d, 8c–e). Aparna et al. noted that the reason D20 matches the depth of this invariant-backscatter layer is the existence of the oxygen-minimum zone (OMZ) below this layer. Tracking a specific oxygen level, 0.6 ml/l (1.2 ml/l) off Gujarat and Goa (Kerala), shows that the oxygen variation in the vertical follows D20 (Fig. 8c–e): upwelling (downwelling) pushes up (down) the top of the OMZ, and the zooplankton are confined to the oxygenated near-surface waters (Aparna et al., 2018). The variation of the depth of this near-invariant-backscatter layer shows no relation to the MLD (Fig. 8c–e; Aparna et al., 2018). The vertical gradient of the backscatter is much higher around D20 than around the MLD.

In other words, in any depth bin (of, say, a few metres) above D20, the backscatter is near-invariant over time (Fig. 8c–e), and the column integrated backscatter or zooplankton standing stock does not respond to the seasonal changes in the phytoplankton biomass (Aparna et al., 2018). The lack of response of zooplankton standing stock to a decrease in phytoplankton biomass can be explained by invoking the microbial loop (Madhupratap et al., 1992, 1994, 1996b; Smith and Madhupratap, 2005), but this alternate pathway does not explain the lack of response in the zooplankton standing stock to an increase in phytoplankton biomass (Aparna et al., 2018).

Aparna et al. (2018) showed that the column-integrated backscatter or zooplankton standing stock will be minimum (maximum) when the thickness of this layer above D20 is minimum (maximum). The lowest (highest) zooplankton standing stock is therefore seen in September–October (February–March; Fig. 8b), when upwelling (downwelling) peaks in the EAS (Fig. 4b). Thus, the zooplankton standing stock is lowest when the phytoplankton biomass peaks (Fig. 8b). The depth of this layer of near-invariant backscatter is comparable off Goa and Kerala (Figs. 4b, 8d,e), but the weaker upwelling during the summer monsoon (Fig. 4a,b) and the convective mixing during the winter monsoon (Fig. 4d) lead to a deeper thermocline, as denoted by D20, in the NEAS (Figs. 4d, 8c), and the zooplankton standing stock is therefore higher in the NEAS compared to the rest of the EAS (Fig. 8b).

Aparna et al. offered three possible explanations for this lack of correlation between the phytoplankton and zooplankton cycles. One possible reason is the loophole theory, according to

which phytoplankton species grow exclusively to form dense blooms when physico-chemical perturbations open a “loophole” in the microbial loop. A possible predator-prey mismatch can occur as a consequence, providing a mechanism to such potential blooming species to escape the pressure of grazing by predators (Irigoiien et al., 2005; D’Costa et al., 2008), which are microzooplankton in this case. A second possible reason is that the size or type of the phytoplankton species that bloom can have a cascading effect on food-web dynamics. In this case, while food is not a limiting factor, the type of food available is, and the diversity of zooplankton species and their specific food preferences imply again a potential predator-prey mismatch. A third possible reason is that the zooplankton standing stock is at the upper limit of what can be sustained by the environment. In other words, the space available for this trophic level is filled to the maximum and therefore the zooplankton standing stock cannot increase in response to an increase in phytoplankton biomass. Since the species of zooplankton change seasonally in the EAS (Madhupratap et al., 1996a; Raghukumar and Anil, 2003; Smith and Madhupratap, 2005), this explanation implies that this seasonal change in species does not change the space required by them: hence, the species must have a similar morphology over the year in a given part of the EAS.

### ***3.4. Fisheries in the EAS***

The fish landings data show a difference in the nature of fisheries between the NW and SW regions. One way to estimate the difference in fisheries between these regions is to compute the mean trophic level based on the landings. Using data for 1953–2002, Vivekanandan et al. (2005) estimated a mean trophic level of 3.32 for the NW region, with a range from 3.27 during 1953–1962 to 3.38 during 1983–1992 and 1993–2002. The mean trophic level for the SW region was 3.14, with a range from 2.94 during 1963–1972 to 3.28 during 1993–2002. The mean trophic level was stabler in the NW region, which had a lower coefficient of variation (2.8%) than the SW region (5.4%). Use of mean trophic level to discern the nature of fisheries is, however, problematic because the mean hides a lot of variability around it. The fish caught also change with mechanisation, change in gear, and fishing effort, apart from regional taste preferences, and a general preference in the fishing community for higher-level predators owing to their higher market price, making it difficult to infer a significant difference between the mean trophic levels across decades and regions.

Yet, this difference in fisheries is evident if one examines the top groups fished in the two regions (Madhupratap et al., 2001; Raghukumar and Anil, 2003). The data for 1985–1993 (CMFRI, 1995; Madhupratap et al., 2001) show that carnivorous fish like Bombay Duck, ribbon fish, croakers, catfish, elasmobranchs, and pomfrets dominate the fishery of the NW region (see also Table 2 of Vivekanandan et al., 2005); some groups, like Bombay Duck, are exclusive to this region and are not

found in the south (Pazhayamadom et al., 2015). On the other hand, planktivorous fish like oil sardines, perches, carangids, and mackerels dominate the fishery of the SW region; the oil sardine is almost exclusive to the SW region and is hardly found in the north (see also Table 2 of Vivekanandan et al., 2005). This difference is also seen in the data for 2001–2005 (CMFRI, 2007a; Table 7), implying that the inference drawn by Madhupratap et al. (2001) is still valid (Pazhayamadom et al., 2015). This regional distinction in the composition of fisheries leads to the first of three questions we seek to answer: “Why do carnivorous (planktivorous) fish dominate the fisheries in the NW (SW) region?”

The annual landings data for the states comprising the SW region show that the total catch is lower, when adjusted for the coastline length, off Karnataka and Goa compared to Kerala, the three states that comprise the SW region. For the period 1986–2005, the catch off Kerala (Karnataka and Goa) is 550950 (255680) tonnes (Table 1) for a coastline length of 590 km (431 km). Normalising the Kerala data to the shorter coastline of Karnataka and Goa implies that the catch off Kerala is 402470 tonnes, ~1.5 times that off Karnataka and Goa. The average landings off Maharashtra for 1986–2005 is 350640 tonnes for a coastline length of 720 km (Table 1). When normalised for the coastline length of Kerala, the catch off Maharashtra is 287330 tonnes, just over half that off Kerala. Thus, the catch in the CEAS, comprising Karnataka, Goa, and Maharashtra, is 606320 tonnes during 1986–2005 (Table 1), but the catch is just 310798 tonnes, again just over half of that off Kerala, when normalised to the coastline length of Kerala. The higher catch off Kerala leads to the second of our three questions: “Why is the fish catch lower in the CEAS compared to the SEAS?” It is tempting to attribute the higher catch off Kerala to the greater effort there (5504 mechanised craft, 14151 motorised craft, and 9522 non-motorised craft with a fisherfolk population of 602234; CMFRI, 2007e) compared to Karnataka (4373 mechanised craft, 3705 motorised craft, and 7577 non-motorised craft with a fisherfolk population of 170914; CMFRI, 2007d), but we argue that the higher investment in fisheries in Kerala, and therefore the greater effort there, may be attributed to the higher potential for fisheries off Kerala. For example, Gujarat, where too the catch is high, shows a greater investment in fisheries (13047 mechanised craft, 7376 motorised craft, and 3729 non-motorised craft with a fisherfolk population of 323215; CMFRI, 2007c) than even Kerala (CMFRI, 2007e). Therefore, the investment in fisheries, or the effort, is as likely to mirror the fishery potential as the catch is to mirror the effort, and the above normalisation of the landings with respect to the coastline is a useful measure of the fishery potential of the respective states.

The statewise landings data (Table 8) also show that Karnataka (CMFRI, 2007d) and Goa (CMFRI, 2007b) constitute a transition regime between Gujarat (CMFRI, 2007c) and Maharashtra (CMFRI,

2007f), where carnivorous fish like Bombay Duck dominate, and Kerala, where planktivorous fish like the oil sardine dominate (CMFRI, 2007e). The total landings of oil sardines during 1986–2005 (2001–2005) decrease from 120310 (216940) tonnes off Kerala (CMFRI, 2007e) to just 26400 (44960) tonnes off Karnataka (CMFRI, 2007d) and 13540 (31600) tonnes off Goa (CMFRI, 2007b; Table 8). In contrast, the mackerel landings decrease much less from Kerala to Karnataka, with the corresponding landings being 57670 (36750) tonnes off Kerala during 1986–2005 (2001–2005; CMFRI, 2007e) and 31390 (18320) tonnes off Karnataka (CMFRI, 2007d); off Goa, the mackerel catch was 16390 (6920) tonnes during 1986–2005 (2001–2005; CMFRI, 2007b). This distinction between Kerala and Karnataka leads to the third question: “Why does the oil sardine dominate the fisheries off Kerala?”

As one may expect in this region, the landings show significant seasonal variation. In general, the landings are lowest during the inter-monsoon season during March–May (between the winter and summer monsoons). Unfortunately, the data tend to be tabulated in terms of quarters, leading to the low catch being listed for April–June (Table 4 of Madhupratap et al., 2001). The catch in the SW region, particularly the SEAS, increases during the summer monsoon, but this is also the spawning season and a fishing ban of two months (June–July) is imposed by the states along the west coast (Madhupratap et al., 2001), making it difficult to interpret the landings data for the season. In the NW region, particularly the NEAS, the catch is highest during the winter monsoon, with the data showing a peak during the October–December quarter and a weakening during January–March (Table 4 of Madhupratap et al., 2001).

#### **4. The physical forcing and fisheries in the EAS**

##### ***4.1. Why do carnivorous (planktivorous) fish dominate the fisheries in the NW (SW) region?***

Though it has been traditional to think of India's west-coast fisheries as consisting of two regions, SW and NW, leading to Madhupratap et al. (2001) pointing to the difference in the nature of fisheries between them, statewide landings data (see Table 8 for landings data for selected fish groups) show that this difference between the SW and NW regions is more striking when we compare the SEAS (off the Kerala coast), which shows a dominance of planktivorous fish like oil sardines (CMFRI, 2007e), and the NEAS (off the Gujarat coast), which shows a dominance of carnivorous fish like Bombay Duck (CMFRI, 2007c). Hence, we recognise the lack of homogeneity within the NW and SW regions and rephrase our first question as follows: “Why do carnivorous fish dominate in the NEAS and planktivorous fish in the SEAS?”

We hypothesise that this difference in the nature of the fisheries between the SEAS and the NEAS is

caused by differences in the length of the growing season for phytoplankton and the size of phytoplankton, both of which are due to differences in the physical forcing.

#### *4.1.1. Difference in the length of the growing season*

The first reason we attribute for the difference in fisheries between the SEAS and the NEAS is the different lengths of the growing season for phytoplankton. In the SEAS, the growing season for phytoplankton is limited to May–October (Figs. 7 and 8a,b), or roughly half the year, and is due to upwelling; downwelling occurs in the SEAS during November–April (Figs. 4,5). This period of downwelling, which is not conducive for phytoplankton growth, is also marked by lower surface salinity (Fig. 9), which is due to the inflow of fresher waters from the BoB during December–February (Shetye et al., 1991; Shenoi et al., 1999; Rao and Sivakumar, 1999; Han et al., 2001; Jensen, 2001; Kurian and Vinayachandran, 2006, 2007; Durand et al., 2007). This inflow of fresher water at the surface leads to the formation of a barrier layer in the SEAS (Thadathil and Ghosh, 1992; Durand et al., 2004; Shankar et al., 2004a; Shenoi et al., 2004; Kurian and Vinayachandran, 2006, 2007), which inhibits mixing between the low-nutrient surface waters and the nutrient-rich waters below the barrier layer. Hence, the downwelling season in the SEAS is not conducive for phytoplankton growth.

In the NEAS, in contrast, the growing season is much longer. Upwelling occurs during May–October (Figs. 4,5) and is followed by convective mixing during November–January (Figs. 4d, 10), which covers three of the six months during which downwelling occurs in the EAS (Figs. 4,5). Detrainment occurs in the southern NEAS during February owing to the poleward advection of fresher surface water by the WICC (Shankar et al., 2016), enabling phytoplankton production (Figs. 7f, 8a,b) even as the increase in stratification weakens convective mixing (Fig. 10; Shankar et al., 2016). In the northern NEAS, convective mixing and the deep MLs extend into February (Figs. 4d, 10) because the mixing deepens the ML before the arrival of the fresher waters from the south (Shankar et al., 2016). Detrainment, a consequence of heating at the surface, follows in March in the northern NEAS (Fig. 4d; Shankar et al., 2016), extending the growing season in the northern NEAS by a month compared to the southern NEAS (Fig. 8a). Hence, the growing season for phytoplankton extends over roughly nine months (June–February) in the southern NEAS and ten months (June–March) in the northern NEAS (Fig. 8a).

It is known that a longer growing season for phytoplankton favours a longer food chain because more time is available for grazing across the trophic levels comprising this chain (Wyatt, 1980; Parsons et al., 1984). While we cannot quantify that a six-month growing season is (much) shorter

than a 9-10-month growing season, a six-month growing season, as seen in the SEAS and CEAS, leaves a comparable gap to be filled by the non-growing season in which the picoplankton or microbial loop will take over from diatoms. If the growing season extends to 9-10 months, the gap is less and it is likely to be easier for the ecosystem to tide over this shorter period of weaker (primary) production, when too the picoplankton and microbial loop will tend to dominate. Furthermore, the distinction drawn by Wyatt (1980) between the discontinuous (primary) production in the temperate regions and the continuous production in the tropics is based on the seasonal change in light and temperature (and therefore mixing depth), which is much stronger for the temperate and polar seas than for the tropics. Wyatt's (1980) hypothesis was that an absence of a lag would lead to an unsustainable grazing pressure during the initial period of the spring bloom, leading to the conclusion that a time lag between phytoplankton and zooplankton production is therefore a necessary feature of a discontinuous (primary) production system. Note, however, that Wyatt's (1980) assumption of continuous (primary) production in the tropical ecosystem is only partially correct. Absence of temperature and light limitation (save when the light intensity is so high that it inhibits phytoplankton growth, a possibility before the onset of the summer monsoon) in the EAS does not imply a continuous, year-long growing season. As is evident from Figs. 7 and 8a, there are seasonal changes in the phytoplankton biomass even in the NEAS, which supports a growing season that extends over much of the year and therefore is a closer approximation to Wyatt's model for a tropical ecosystem than the rest of the EAS. The limitation of upwelling to the summer monsoon places a similar, but longer, restriction on the growing season in the SEAS and CEAS. In other words, even in the EAS, we have a discontinuous production system, with production during the "off" season likely to be limited to picoplankton, which were just being discovered (Sieburth et al., 1978; Waterbury et al., 1979) when Wyatt (1980) wrote his paper.

Therefore, we infer that the longer duration of favourable physical forcing in the NEAS permits the existence of a longer food chain, implying the existence of higher trophic levels in the fisheries. Hence, carnivorous fisheries dominate in the NEAS. In the SEAS, the shorter growing season implies the dominance of a lower trophic level and favours planktivorous fisheries.

#### *4.1.2. Difference in the size of the phytoplankton*

The second reason for the difference in the nature of fisheries between the SEAS and the NEAS is that the forcing leads to a smaller size of phytoplankton in the NEAS. Smaller phytoplankton tend to lead to a longer food chain because the zooplankton have to feed on them before they are grazed by the fish (Wyatt, 1980; Parsons et al., 1984).

Stronger upwelling implies a greater supply of nutrients to the ML, permitting the growth of larger phytoplankton like diatoms (Wyatt, 1980; Parsons et al., 1984). During the summer monsoon, upwelling, as indicated in the shallowing of D20 or the decrease in sea level, is stronger in the SEAS. The range of SLA (D20) at the ADCP mooring location off Kerala (9°N) is 22 cm (60 m); the corresponding values for the mooring location off Gujarat (20°N) is 9 cm (50 m) (Fig. 4a,b). Simulations with MOM support this observation of stronger upwelling in the SEAS (Fig. 11) and the cumulation of the vertical velocity (estimated at 30 m depth) over time during July–September leads to a displacement of over 60 m off Kerala; off Gujarat, the displacement during this period is ~30 m (Fig. 12). These results are in accordance with the cumulation of the vertical velocity estimated by Lévy et al. (2007) during the summer bloom. In their study, the cumulation of vertical velocity led to a displacement of over 150 m off Kerala; off Gujarat, the displacement during the summer bloom period was ~50 m (see Fig. 4c of Lévy et al., 2007). Stronger upwelling implies greater supply of nutrients to the surface ML and the TOPAZ simulations show a higher concentration of nitrate (Fig. 13), phosphate (Fig. 14), and silicate (Fig. 15) during the summer monsoon in the SEAS compared to the NEAS. The higher nitrate concentration in the SEAS compared to the CEAS and NEAS is in agreement with observed nitrate distribution (Habeebrehman et al., 2008) and the observed distribution of nitrite at the secondary maximum (Naqvi, 1991). The existence of the OMZ over most of the EAS, with the SEAS lying outside this regime (Naqvi, 1991; Naqvi et al., 2006), implies an oxygen deficiency that shifts the primary respiratory pathway: heterotrophic bacteria use nitrate instead of oxygen to decompose organic matter, and it is nitrite, an intermediary species, that accumulates in the water column, producing the secondary nitrite maximum (SenGupta et al., 1976; Codispoti and Christensen, 1985). The silicate supply to the SEAS is also greater owing to inflow of water from the BoB during the winter monsoon; a signature of this inflow is seen in December and February (Fig. 15e,f). The higher silicate concentration spreads westward in the SEAS along with the currents associated with the westward propagating Rossby wave (Young and Kindle, 1994).

The TOPAZ simulations show that the higher nutrient supply in the SEAS not only implies higher concentration of chlorophyll there compared to the NEAS (Fig. 16), but also that this difference is due to the large phytoplankton (Fig. 17) rather than small phytoplankton (Fig. 18). These differences in nutrient and chlorophyll concentration are also evident in the time-latitude plot along the 1000 m isobath (Fig. 19). For example, at 11°N (22°N), the chlorophyll maximum due to small phytoplankton is 0.83 (0.54)  $\mu\text{g-m/kg}$  and that due to large phytoplankton is 1.05 (0.2)  $\mu\text{g-m/kg}$ . In the simulations of Koné et al. (2009; see their Plate 4), the primary production during the summer monsoon in both SEAS and NEAS was silicate-limited. Vijith et al. (2016) did not include silicate



limitation for large phytoplankton group, but an experiment with an imposed limitation of silicate showed no significant difference from the simulation without silicate limitation. In TOPAZ, large phytoplankton dominate when the nutrients are surplus and light is also sufficient (Dunne et al., 2010, 2013), conditions that are fulfilled in the SEAS when upwelling occurs. Thus, the lower chlorophyll concentration due to large phytoplankton in the NEAS during the summer monsoon is due to the weaker upwelling there compared to the SEAS.

During the winter monsoon — when downwelling replaces upwelling —, the TOPAZ simulations show a dominance of small phytoplankton in the NEAS (Figs. 17–19; Vijith et al., 2016). In TOPAZ, the Liebig limitation term, which is the minimum of the individual limitation terms for nitrate, phosphate, and iron (Dunne et al., 2010), is lowest for nitrate and the N/P ratio is lower than 16 over most of the NEAS during December–February; hence, the primary production in the NEAS is nitrate-limited in this simulation because the term for nitrate limitation is smaller than that for phosphate limitation (see Fig. 9 of Vijith et al., 2016). Silicate limitation is not considered in this simulation, but Koné et al. (2009) suggest that the primary production in the NEAS is silicate-limited. Observations are scarce, but available data also suggest that silicate limitation is important in the NEAS (Naqvi et al., 2002; Balachandran et al., 2008). Silicate limitation will impact diatom growth, again leading to a dominance of small phytoplankton.

The Liebig term is well-mixed within the ML, implying that the vertical structure of growth rate depends on the availability of light. Therefore, the growth rate decreases vertically downward depending on the penetration of light (Vijith et al., 2016). This dependence on light is also seen in recent data from the NEAS, which show that the mixing process brings into the ML phytoplankton seeds from below, but some of these phytoplankton are more accustomed to the low-light conditions in the deeper waters; hence, the growth of phytoplankton can be limited even in the presence of entrainment mixing owing to the acclimitisation of different species of phytoplankton (Roy and Anil, 2015).

The deep MLs seen in the NEAS during the winter monsoon are due to thermal buoyancy (Shankar et al., 2016), and it is in this region and during this season that one encounters the strongest turbulent mixing in the surface ML (Fig. 10d,e). Turbulence is conducive to phytoplankton growth as it implies a higher supply of nutrients due to entrainment (Wyatt, 1980; Parsons et al., 1984; McCreary et al., 2009). Studies show, however, that turbulence can also limit the growth of phytoplankton (Estrada and Bertalet, 1998; Barton et al., 2014; Garrison et al., 2014). The relationship between turbulence and phytoplankton is therefore complex.

Therefore, the phytoplankton size tends to be small in the NEAS irrespective of the season and the specific nature of the physical forcing. While support for this hypothesis is found readily in models, it is more difficult to substantiate it in observations. The problem with the observations is their bias towards the larger phytoplankton owing to the limitation of measurement techniques in the years preceding the discovery of picoplankton (Sieburth et al., 1978; Waterbury et al., 1979) and their observations in the AS in general (Liu et al., 1998; Campbell et al., 1998) and the EAS in particular (Jochem, 1995; Ramaiah et al., 1996). Data that can provide a measure of the phytoplankton biomass with reference to size are scarce because measurements of picoplankton cell abundance in the EAS are restricted to the post-2010 period (Mitbavkar and Anil, 2011); an earlier paper by Roy et al. (2006) reported the picoplankton pigment concentration, but not abundance, from the SEAS. Recent pigment data from the NEAS suggest, nevertheless, that the concentration of the pigment zeaxanthin, which is associated with picoplankton, is much higher in the NEAS than the concentration of the pigment fucoxanthin, which is associated with diatoms; correspondingly, the proportion of picoplankton and nanoplankton is much higher than that of microplankton (Roy et al., 2015). The data of Roy et al. (2015) were limited to November 2014, but their finding of a dominance of smaller phytoplankton is borne out by later data from the NEAS (Bemal, 2017). Unfortunately, similar and simultaneous data are not yet available for the rest of the EAS, making it difficult to corroborate the model simulations with observations, but the limited pigment and cell abundance data available do suggest a larger phytoplankton size in the SEAS compared to the NEAS (Bemal, 2017).

We note that the model simulation is not as good in the NEAS as one would like it to be. The summer-monsoon chlorophyll peak in the NEAS is restricted in the model to the shelf (see Fig. 18); it is only south of roughly  $18^{\circ}\text{N}$  that the higher chlorophyll concentration of the shelf spills over onto the slope. The reason for this discrepancy is not clear, but a possible explanation lies in the horizontal resolution of the model. Advection, both horizontal and vertical, are expected to strengthen as the resolution increases and we expect this model, whose horizontal resolution is  $0.25^{\circ}$ , to simulate a weaker vertical advection, which will imply a lower flux of nutrients into the ML and therefore weaker phytoplankton growth.

Suppose, however, that the model upwelling were stronger than it is in this case. A likely result is that more nutrients will be pumped into the ML, leading to a higher concentration of chlorophyll in the NEAS. The upwelling in this region will, nevertheless, still be much weaker than in the SEAS. Hence, a higher model resolution, if it leads to stronger upwelling, will imply an increase in the small phytoplankton in the NEAS: it is difficult to see the size increasing to imply higher diatom growth in

this region. Therefore, even though the model is unable to simulate the observed summer bloom in the NEAS accurately enough, resolving this problem is unlikely to change the size discrepancy between the SEAS and the NEAS.

Thus, though the data are limited and the models have their limitations, the available evidence suggests a larger phytoplankton size in the SEAS compared to the NEAS. Hence, while it is possible to sustain fisheries that can feed on diatoms (planktivorous fisheries) in the SEAS, the dominance of smaller phytoplankton predisposes the NEAS towards a longer food chain and does not favour fish like the oil sardine that can feed directly on diatoms (Raja, 1969; Rykaczewski and Checkley, 2008; van der Lingen et al., 2009; Remya et al., 2013; Checkley et al., 2017). This absence of fish that tend to be herbivorous implies a greater role for mesozooplankton, whose biomass is also greater in the NEAS owing to the deeper D20 (Fig. 8b,c). A striking aspect of the groups fished in the NEAS is the absence of the oil sardine, which dominates the fisheries of the SEAS (Table 7; Madhupratap et al., 2001). We attribute this absence of the oil sardine and similar groups that prefer diatoms or larger phytoplankton to the lower biomass of large phytoplankton in the NEAS.

#### ***4.2. Why is the fish catch lower in the CEAS compared to the SEAS?***

The observed summer-monsoon phytoplankton bloom in the EAS weakens poleward of 16°N and the high chlorophyll concentration tends to be restricted to the inner shelf poleward of ~13.5°N (Fig. 7). Along the 1000 m isobath, the observed climatological chlorophyll concentration decreases poleward of ~13.5°N and it increases again only poleward of 20°N (Fig. 8a). In the TOPAZ simulation, however, while the chlorophyll concentration decreases poleward of ~13.5°N in the EAS, it remains roughly constant poleward of this latitude (Fig. 16). Apart from the difference in the magnitude of the concentration, which is lower in the model, the main difference between the observations and model chlorophyll is seen largely in the regime of the inner shelf in the CEAS, where the observations tend to show a bloom in the Gulf of Khambhat (Cambay) and the shallow shelf adjoining it (Fig. 7), but this high chlorophyll concentration is not simulated by the model (Fig. 16).

Notwithstanding these differences, the model is able to simulate the decrease in the chlorophyll concentration from the SEAS to the CEAS. The weaker upwelling in the CEAS implies a lower concentration of nitrate (Koné et al., 2009). As a consequence, the chlorophyll due to large phytoplankton shows a sharper decrease from the SEAS to the CEAS compared to the chlorophyll due to small phytoplankton (Figs. 17–19) in spite of silicate not being a limiting factor (Koné et al., 2009).

The bias towards a smaller size of the phytoplankton in the CEAS predisposes the ecosystem towards a longer food chain, but the growing season in the CEAS is similar to that in the SEAS. The similar duration of the growing season is due to the duration of upwelling being similar, roughly six months, and the convective mixing that follows the upwelling in the NEAS being restricted poleward of  $\sim 18^{\circ}\text{N}$  (Figs. 6, 11, 12). Hence, the fisheries are weaker in the CEAS compared to the SEAS, and this lower potential stock off Karnataka and Goa (CMFRI, 2007b,d,e) compared to Kerala (CMFRI, 2007e) is reflected in the landings data.

#### **4.3. Why does the oil sardine dominate the fisheries off Kerala?**

As discussed above, the growing season in the SEAS is shorter than in the NEAS and a shorter food chain is therefore favoured in this region, implying a potential dominance of planktivorous fish. The growing season in the CEAS is comparable to that in the SEAS, but the dominant fishery changes from the oil sardine in the SEAS to mackerel in the CEAS. The landings for oil sardine show a sharp drop from Kerala to Karnataka and Goa; the oil sardine is almost absent farther north in the EAS (CMFRI, 2007b–f). The landings for mackerel do not, however, show a similar change from Kerala to Karnataka. We argue here that this change in the fisheries and the lower stock of the oil sardine poleward of the SEAS can be attributed to the physical forcing.

The summer-monsoon peak in phytoplankton biomass at the mooring location off Kerala is almost twice that at the mooring location off Goa; the SeaWiFS data show that the high chlorophyll concentration is largely restricted south of  $\sim 13.5^{\circ}\text{N}$ , which is just north of the state border between Kerala and Karnataka (Fig. 1), and the minimum during July–August occurs around  $17^{\circ}\text{N}$  (Figs. 7,8a), which is just north of Goa (Fig. 1). The intensity of upwelling, whether inferred from SLA (Figs. 6a,11a) or D20 (Figs. 6b,11b), shows that the strong upwelling is restricted to the same latitude regime. The higher primary production, as seen in the satellite data, off Kerala in comparison to Karnataka may therefore be reasonably attributed to the stronger upwelling in the SEAS. This restriction of the strong-upwelling regime to the coast of Kerala is linked to the dynamics of the Lakshadweep Low: the poleward decrease in the speed of the westward propagating Rossby wave limits this cyclonic sea-level feature associated with upwelling to the SEAS (Shankar and Shetye, 1997), with a sharp change taking place around  $13.5^{\circ}\text{N}$  (Fig. 5; Shankar, 1998). The simulation with TOPAZ shows that not only is the chlorophyll concentration higher in the SEAS than in the CEAS (Figs. 17,19c), but that large phytoplankton dominate in the SEAS (Figs. 17,19d). Therefore, not only is the phytoplankton biomass higher off Kerala, but this part of the EAS also shows a dominance of larger phytoplankton.

The data also show that D20 is deeper in the CEAS owing to the weaker upwelling (Fig. 6). The near-invariance of ADCP backscatter above D20 in the EAS (Fig. 8c–e) therefore implies a larger zooplankton standing stock in the CEAS compared to the SEAS during January–September; it is only during October–December, when D20 is deeper in the SEAS than in the CEAS that the zooplankton standing stock in the SEAS exceeds that in the CEAS (Fig. 8b). That the zooplankton standing stock is low during the summer monsoon, when the phytoplankton biomass, based on satellite measurements of chlorophyll-*a*, peaks in the EAS, implies that the phytoplankton are unlikely to be grazed entirely by the zooplankton during this period. A bigger discrepancy in the phytoplankton and zooplankton biomass occurs in the SEAS because the chlorophyll concentration in the SEAS is almost twice that in the CEAS (Fig. 8b). The excess phytoplankton biomass is therefore available for grazing by the fish that can feed directly on the phytoplankton, and it is in the SEAS that this direct grazing of phytoplankton by fish is facilitated because the large phytoplankton, i.e., diatoms, are more abundant there than in the CEAS (Figs. 17,19d).

The oil sardine feeds on both larger phytoplankton (diatoms) and zooplankton, but shows a preference for the diatoms (Raja, 1969; Rykaczewski and Checkley, 2008; van der Lingen et al., 2009; Remya et al., 2013; Checkley et al., 2017). Though data are patchy, studies suggest that the oil sardine shows a marked preference for diatoms off Kerala (Venkatraman, 1960) and up to Mangalore (Dhulkhed, 1962), which is located just north of the Kerala-Karnataka border. In Karwar, just south of Goa, on the other hand, phytoplankton and zooplankton in the food of the oil sardine were found to be distributed in a 2:3 ratio, suggesting a dominance of feeding on zooplankton (Noble, 1962, 1964). Such regional distinctions in the food preference of the oil sardine had been noted earlier too in the EAS, leading the authors to suggest the existence of more than one “race” of oil sardines in the region (Devanesan, 1943; Devanesan and Chidambaram, 1943). The mackerel also feeds on both diatoms and zooplankton off Karwar (Noble, 1962, 1964), but is believed to prefer zooplankton (Raja, 1969).

While these data on food preferences are patchy and show seasonal variation (Remya et al., 2013) in addition to variation in space, they are in line with the expectation from the spatial variations in the physical forcing. The key difference between the SEAS and CEAS therefore lies in the weaker upwelling in the CEAS, which implies lower biomass and smaller size of phytoplankton, and, by implying a deeper D20, also leads to the higher standing stock of zooplankton in the CEAS. Hence, not only is the preference of oil sardine for diatoms in the SEAS (Remya et al., 2013) more likely to be met in this region, the competition for them from zooplankton is also lower in this region, permitting them to grow more abundantly in the SEAS and dominate the fisheries of the region.

Farther north, in the CEAS, not only is the diatom biomass lower, but the zooplankton also provide stiffer competition for fish at the lower trophic levels like the oil sardine. Hence, though the oil sardine changes its diet in the CEAS to feed on the more abundant zooplankton there, it gives way in this region to the mackerel, which prefers zooplankton. Therefore, the landings of oil sardine decline sharply from Kerala to Karnataka and Goa, but not the landings of mackerel.

## **5. Discussion**

The arguments in the preceding section are heuristic, but we do not think it is possible at least at this stage to model the interactions from the physical forcing to the fisheries in the EAS. In this section, we discuss a few implications of the results and the shortcomings of both data and models before concluding with a summary of the results.

### ***5.1. Natural and political boundaries, oceanography and fisheries***

Fisheries data are based on fish landings at fishing jetties. The data used in this paper are statewide summaries (CMFRI, 2007b–f). A major problem with data tabulated on the basis of political boundaries is that the natural boundaries do not respect them.

One example lies in the SEAS, which is largely limited to Kerala, but does spill over to the southern part of the Karnataka coast. The boundary of the SEAS is determined by the meridional extent of the Lakshadweep High and Low (Shankar and Shetye, 1997; Shankar, 1998), which constitute the physical forcing for the region. Based on these features, which are evident in both, the physical forcing (Figs. 5,6) and the biological response as seen in chlorophyll-*a* data (Figs. 7,8a), the northern limit of the SEAS is roughly around 13.5°N and therefore includes Mangalore, the major city in southwestern Karnataka (Fig. 1b). Therefore, one expects fishing to be more productive off southern Karnataka than off northern Karnataka.

Likewise, the NEAS spills over beyond the Gujarat coast to ~19°N because the convective mixing extends to the coast of Maharashtra (Figs. 1b,10). Therefore, the Maharashtra coast, which is part of the CEAS, may be divided into two parts. It is only the northern part of the Maharashtra coast, north of ~19°N (roughly the latitude of Mumbai), that comes under the influence of winter convective mixing, which extends the growing season beyond the summer-monsoon upwelling regime and makes a longer food chain viable. That's why the Bombay Duck, a carnivorous fish, is also caught off Maharashtra in addition to Gujarat and indeed derives its name from Bombay, the earlier name of Mumbai. The Bombay Duck, however, has not been reported south of 15°N (Pazhayamadom et al., 2015), which is taken as the rough boundary between the NW and SW regions. The landings data are summarised statewide, making it difficult to ascertain if there is a north-south difference along

the 720-km-long coastline of this state, but the physical forcing and the fisheries suggest the existence of such a difference. An added complication around Mumbai is the wide shelf (Fig. 1b), which may limit the fishing by the Maharashtra boats to the inner shelf.

It is possible to break the statewise summaries into a distribution along the coast by analysing the landings data for individual jetties. Doing so will not, however, solve the problem because the fishing vessels are not restricted to fishing in the vicinity of the jetties at which they are registered. It is not possible, therefore, to establish from the fish landings data where the fish were caught: all that can be done is to determine where they were brought onshore.

Hence, if one wishes to make progress in linking the physical forcing and the fisheries, which is important for predicting the potential impact of changes in the regional climate, it is essential to determine where the fish are caught rather than relying on landings data alone.

## ***5.2. Extension to the continental shelf***

Most of the fishery studies are from the continental shelf, but the dynamics or the physical forcing is best documented and understood for the continental slope. Nevertheless, as is evident from both observational studies — whether one considers tide gauges (Banse, 1968; Shetye and Almeida, 1985; Shankar, 1998, 2000; Shankar, 1998, 2000; Aparna et al., 2012), which are located at the coast, or hydrography (Shetye et al., 1990, 1991) or surface-current data from current-meter moorings (Shetye et al., 2008) or ADCP moorings (Amol, et al., 2018a) or HF (high-frequency) radars (Mukhopadhyay et al., 2017) — and modelling studies (Amol et al., 2012; Amol, 2014), the WICC, which is the boundary current in the EAS, leaves its imprint on the shelf, including the inner shelf (Shetye et al., 2008; Amol et al., 2018a); a similar relation of the boundary current to the near-coastal current is seen in the western BoB as well (Mukhopadhyay et al., 2017). This relation of the boundary current to the near-coastal current implies that the above discussion of the seasonal cycle in the context of the outer shelf and slope is valid, with some differences, for the inner shelf as well (see Figs. 5 and 7 for the observed circulation and chlorophyll-*a*, respectively, and Figs. 13–18 for the model-simulated nutrients and chlorophyll-*a*). The presence of bottom topography modifies the coastal Kelvin waves associated with the boundary current on the continental slope to coastally trapped waves (CTWs) or continental shelf waves (Wang and Mooers, 1976; Huthnance, 1978; Brink, 1982a,b; Brink and Chapman, 1987). As with Kelvin waves, these shelf waves or CTWs propagate with the coast on their right in the northern hemisphere, i.e., from south to north along the Indian west coast. Analysis of these CTWs shows an unambiguous link between the WICC on the slope and shelf (Amol et al., 2012; Amol, 2014; Amol, et al., 2018a).

In spite of the significant connection between the slope and shelf circulations, one does expect a few differences between them. First, the sub-surface, nutrient-rich water is likely to upwell to the surface in the SEAS and southern part of the CEAS (Ramasastry and Mryland, 1959; Banse, 1968; Shetye et al., 1990), leading to higher primary production; such strong upwelling will also, however, push up the low-oxygen waters, which will be mixed by the strong summer-monsoon winds with the oxygenated waters of the surface ML. Second, the shelf topography and the existence of the bottom will limit the extent of convective mixing during winter in the NEAS; implications for the nutrient chemistry are unclear, but it is possible that silicate limitation in the NEAS (Naqvi et al., 2002; Balachandran et al., 2008) is more prevalent in the inner shelf. Thus, light limitation, as suggested by Roy and Anil (2015), is more likely to prevail over silicate limitation on the slope, but we need more extensive studies that sample across the shelf-slope boundary to test this idea. Our understanding of shelf dynamics also needs to improve considerably to permit a more detailed analysis of the shelf ecosystem.

### ***5.3. Implications of localisation of mature habitat for the life cycle***

The physical forcing shows seasonal variation owing to the monsoonal climate of this region. The WICC reverses seasonally, flowing equatorward (poleward) during the summer (winter) monsoon, and it is linked to seasonal upwelling (downwelling) (Figs. 5,6). The implication of this seasonal cycle of the forcing is evident in the seasonal cycle of phytoplankton in the EAS (Figs. 7,8a).

Phytoplankton blooms have a life span of a few days, implying a direct response to the changes in the forcing. Fish, in contrast, have a much longer life cycle that can extend beyond a year. Therefore, the spatial variation in the extent of the habitat of the mature adult has implications for the entire life cycle. As we have seen, some carnivorous fish like Bombay Duck or largely planktivorous fish like the oil sardine are geographically limited by the physical forcing, with no reports of the former south of 15°N (Pazhayamadam et al., 2015), and the latter restricted largely south of ~16°N. The life cycle of the fish, from spawning to maturity, has to obey the cyclicity of the seasons and the limitations of geography. Since the geographical extent of the mature habitat is limited, the spawning areas are likely to be the regions from where the fish can make it to their eventual habitat in the mature stage. In other words, the physical forcing not only limits the Bombay Duck (oil sardine) to the NEAS (SEAS) during the mature stage, the seasonal reversal of the WICC implies that these species are likely to spawn in the regions from where they are best placed to make it to their mature habitat. Thus, the seasonal reversal of the WICC must place limits on the possible spawning grounds. While migration is common for sardines elsewhere too in the world oceans (see, for example, Watanabe et al., 1995; Checkley et al., 2009a,b; Demer et al., 2012; van der Lingen et



al., 2010), the boundary currents in these basins are unidirectional and do not reverse seasonally like the WICC. The EAS ecosystem is therefore more complex and the seasonality demands that observations be made at a higher frequency to map the changes in the lower and higher trophic levels.

#### **5.4. *Interannual variability***

This distinction between the seasonality of the physical forcing and the lower trophic levels and the multi-year life cycle of the fish makes it difficult to interpret interannual variability in fish catch. Careful analysis is required to link the interannual variability of the forcing to the interannual variability in the fisheries. It is evident that substantial interannual variability in the physical forcing due to, say, basin-scale climate modes like El Nino or the Indian Ocean Dipole (Saji et al., 1999; Webster et al., 1999; Aparna et al., 2012; Parvathi et al., 2017) must be reflected in the marine ecosystem (see, for example, Jayaram et al., 2013; Shalin and Sanilkumar, 2014), but it is easier to link interannual variability of the physical forcing to that of the lower trophic levels than to extrapolate from the physical forcing or, say, chlorophyll-*a* to fisheries, as has been attempted by some authors (Longhurst and Wooster, 1990; Manjusha et al., 2013; Kripa et al., 2015a). It is also important to recognise the limitations of a correlation analysis because a significant correlation does not necessarily imply a cause-and-effect relationship (Mann, 1993; Madhupratap et al., 1994; Nuzzo, 2014).

#### **5.5. *Climate change and anthropogenic impacts***

In this paper, we have dealt with the spatial variability in the nature of fisheries in the EAS using fish-landings data over the last few decades. While we have assumed the spatial variability to be roughly static — ignoring predator-prey interactions and competition among species (see, for example, Winkelmann et al., 2014) —, and therefore discussed it in the context of the climatological seasonal cycle, the fisheries data do suggest that changes are taking place over time. For example, less than 1% of the oil sardine catch in the Indian EEZ occurred off the Maharashtra coast during 1961-1986, the percentage seems to have increased during 1987–2006, suggesting a poleward shift in the northern limit of the habitat of the mature oil sardine (Kripa et al., 2015b). The tendency has been to link such shifts to climate change, but it is recognised that it is difficult to make a categorical statement owing to the simultaneous changes in the nature of fishing gear and increase in mechanisation and fishing effort (Madhupratap et al., 2001; Kripa et al., 2015b). Therefore, the impact of climate change for fisheries is not easy to decipher, and we believe that it is critical to understand first the reason for the nature of the distribution of fisheries in order to be able to predict

sensibly the implications of climate change for the fisheries in the EAS.

Separating the natural changes in climate from the changes caused due to anthropogenic effects is, likewise, a difficult task. For example, while some studies have tended to blame fertiliser concentration in river discharge for increasing hypoxia in the CEAS (Naqvi et al., 2000), the evidence for such a trend is lacking and modelling studies suggest that the physical forcing controls the interannual variability of hypoxia and anoxia in the region (Parvathi et al., 2017). Likewise, there have been reports linking the sewage discharged off Mumbai and Karachi to the occurrence of *Noctiluca scintillans* blooms in the NEAS (do Rosário Gomes et al., 2014), but there are no reports corroborating such an increase between either city and the southern NEAS, where these blooms have been noted (Sarma et al., 2018).

One possible anthropogenic effect, however, is due to the construction of dams on the major rivers draining into the EAS. In the NEAS, the large rivers like the Indus (Milliman et al., 1984) and the Narmada have seen significant dam construction and therefore a reduction in the discharge and the silicate supply to the EAS. Data show that the construction of dams has reduced the discharge of the Indus from a potential 90 km<sup>3</sup> per year to just 5 km<sup>3</sup> per year; the suspended sediment load has reduced from a potential 250 million tonnes to just 10 million tonnes (Milliman and Farnsworth, 2011). Likewise, the discharge of the Narmada has reduced from a potential 38 km<sup>3</sup> per year to 23 km<sup>3</sup> per year and the suspended sediment load from a potential 70 million tonnes to 15 million tonnes (Milliman and Farnsworth, 2011); since the data for the Narmada are prior to the construction of the Sardar Sarovar dam, the discharge is expected to decrease significantly. The implied reduction in the silicate supply can have consequences for the ecosystem if it is indeed silicate-limited, as suggested by some observational (Naqvi et al., 2002; Balachandran et al., 2008) and modelling (Koné et al., 2009) studies. Indeed, in the simulation of Koné et al. (2009; see their Plate 4), the EAS, except for the central part of the CEAS in the neighbourhood of Goa, is silicate-limited. We do not have a good data set on river discharge into the EAS as most of the rivers are ungauged, making it necessary to build a modelling framework to simulate the discharge (Shankar et al., 2004b; Suprit and Shankar, 2008; Suprit, 2010; Suprit et al., 2012), which is a pre-requisite for estimating the silicate flux from land into the EAS.

Nevertheless, in spite of the significant barriers to estimating the impact of climate change on the fisheries in the Indian EEZ, it is evident that the economic implications demand such predictions. Therefore, while linking climate change to changes in fisheries is tricky and will require a significant shift in the way biological oceanographers and fishery scientists approach their subjects, it is imperative to break these disciplinary barriers to make progress. Capturing the linkages and

processes that determine the flow of matter and energy through this food web all the way to the high-trophic-level carnivorous fish demands a trans-disciplinary programme so that these processes can be implemented in models.

### ***5.6. Limitations of models***

What is presented above is a set of arguments that link the physical forcing through a set of plausible connections to the differences observed in the nature of the fisheries in the EAS. Among the “data sets” used in this paper are the results of simulations with a physical and an ecosystem model. A discussion of the limitations of the specific models used in this paper was presented towards the end of Section 4.1.2, but there are more generic limitations as well. At this stage, we do not think it is possible to model these differences in the fisheries because the ecosystem models that simulate biogeochemistry of the marine environment (for example, TOPAZ: Dunne et al., 2010, 2013; BIOFENNEL: Fennel et al., 2006, 2008; PISCES: Aumont and Bopp, 2006) do not account for the trophic levels higher than the zooplankton. In these models, grazing on phytoplankton is assumed to be due to zooplankton, but the ADCP backscatter data, which suggest that the zooplankton standing stock on the continental slope of the EAS is at its lowest when the phytoplankton biomass peaks in the SEAS and CEAS, imply the existence of alternate pathways for consumption of the phytoplankton that bloom during the summer monsoon. The existence of fish like the oil sardine, which shows a marked preference for diatoms or large phytoplankton at least in the SEAS, suggests that some of these alternate pathways do operate in nature. Therefore, for models of the marine ecosystem to reproduce sensibly the observations, they will have to factor in these pathways. Hence, while the arguments made in this paper are heuristic, in that we argue possibilities based on pieces of evidence and provide tentative linkages between the pieces of this jigsaw puzzle, it does not seem possible to model the processes at least at this stage. Yet, what — whether zooplankton or low-trophic-level fish like the oil sardine — feeds on the phytoplankton that bloom is an important question because the answer has both ecological and economic implications.

It is also likely that deterministic models like TOPAZ and its equivalents will have problems simulating the response to an increase in phytoplankton. While it may be possible to factor in the lack of response of zooplankton, as seen in the ADCP backscatter data, it will be challenging to allow for grazing by herbivorous or planktivorous fish. A key difference between zooplankton and fish is that the former are ubiquitous and have a short life span, permitting the assumption of a purely local response to a phytoplankton bloom. Fish, in contrast, have a longer life cycle and are not as ubiquitous: the fish will have to find the phytoplankton before they can graze on them. This non-localisation of grazing by fish introduces an indeterminate time lag that may prove difficult, at the

least, to parameterise in models.

Another complication arises from the existence of mixotrophs, which combine phototrophy and heterotrophy and are found to be abundant in oligotrophic systems (Bird and Kalff, 1987; Arenovski et al., 1995; Zubkov and Tarran, 2008; Hartmann et al., 2012). This dual nature complicates the model-building exercise by adding an additional layer of complexity in the ecosystem web, but we note that models are now beginning to include mixotrophs (see, for example, Ghyoot et al., 2017).

The marine ecosystem in the tropics is complex because of the higher biodiversity compared to the temperate or polar seas; this higher diversity is seen at all trophic levels (Raghukumar and Anil, 2003). Experimental and theoretical studies show that high diversity makes the community more stable and leads to an increase in productivity (Tilman, 1999; Raghukumar and Anil, 2003).

### ***5.7. Limitations of the ADCP backscatter data***

Though practically all the data used in this paper, save the few model simulations, are available in the literature, the ADCP backscatter data used as a proxy for zooplankton (Aparna et al., 2018) are almost contemporaneous. Since the answer to the of the third question depends on the zooplankton-phytoplankton mismatch inferred from the backscatter data, a brief discussion of the limitations of these data is presented here.

The ADCP data provide a temporal resolution or duration of sampling that cannot be matched by other available instruments or methods for studying zooplankton. Therefore, the ADCP backscatter, though a vital tool for linking physical processes to the marine ecosystem, has some limitations. First, the data can be used only to infer the biomass and provide no information on the zooplankton species distribution, which changes in seasonally in the EAS (Madhupratap et al., 1996a; Raghukumar and Anil, 2003; Smith and Madhupratap, 2005). This seasonal change in species can have implications for ecosystem dynamics, but these aspects of the ecosystem cannot be analysed with the backscatter data, which must, therefore, be complemented with carefully planned zooplankton observations. Second, the backscatter data are not available in the top 15–20 m and therefore the ADCPs do not provide data within the shallow ML over a part of the year (Fig. 8c–e). Aparna et al., (2018) overcame this limitation by extrapolating the backscatter from the topmost ADCP bin to the surface. How the zooplankton biomass varies within the top 15–20 m and across the base of the ML needs to be quantified using net hauls in this limited depth range to justify this extrapolation. Such an exercise has to be carried out at all mooring locations in all seasons to verify that the degree of variance of backscatter is indeed low above D20, permitting the inference of near-invariance drawn by Aparna et al. Third, the backscatter is but a proxy for zooplankton biomass. To

convert the backscatter to biomass demands a sustained campaign to calibrate the ADCP backscatter with direct measurement of zooplankton biomass using multiple plankton nets. The calibration reported by Aparna et al. (2018) was restricted to sampling over a few days, but a sustained calibration campaign is critical if the promise and potential of the backscatter data for ecosystem studies is to be realised.

The other issue that comes up is the role of oxygen: Aparna et al. (2018) argue that it is the depletion of oxygen within the OMZ that restricts the depth of the near-invariant, high-backscatter layer above D20. Yet, these ADCP data show the diel cycle of vertical migration characteristic of zooplankton, suggesting a contradiction because the migration occurs from this high-backscatter layer into the oxygen-depleted OMZ waters below. Note, however, that the higher mesozooplankton biomass above the OMZ is evident even in the zooplankton data reported in the literature (Padmavati et al., 1998; Madhuratap et al., 2001; Raghukumar and Anil, 2003). The data also show that certain species characterise the oxygen-poor waters (Raghukumar and Anil, 2003). Calanoid copepods, for example, may be divided into four categories: (1) those that live above 200 m, (2) those that are predominantly surface-living, with their biomass tailing off in deeper waters, (3) those that live in the oxygen-poor waters below 300 m, and (4) those that are distributed throughout the water column. So there are zooplankton that inhabit only the oxygen-rich surface waters and zooplankton that prefer the oxygen-deficient OMZ. In other words, not all zooplankton are known to migrate vertically. Data from other regions also show that the same zooplankton do not migrate up and down daily: doing so would require a prohibitive amount of energy and the downward (upward) migration likely occurs only when the migrating species are satiated (hungry and sense availability of food) (Thorisson, 2006). Hence, the argument made by Aparna et al. (2018) and in this paper is that the existence of diel vertical migration in the EAS backscatter data does not imply that the decline in oxygen in the OMZ cannot be invoked to explain the decrease in zooplankton biomass below D20.

### ***5.8. Summary of results***

The spatial changes in the fisheries of the EAS are dictated by the physical forcing. The strong seasonality of the forcing leads to a strong seasonality of the biological response. The fish, like the lower trophic levels, have to respond to the seasonal changes in the forcing. The growing season in the NEAS, where convective mixing follows upwelling, is over nine months, permitting the existence of a longer food chain and therefore the existence of carnivorous fish like the Bombay Duck. The dominance of smaller phytoplankton in the NEAS also lengthens the food chain because the small phytoplankton cannot be fed on directly by lower-trophic-level fish like the oil sardine, which is therefore not found in this region. In the SEAS, the growing season is restricted to the

summer monsoon, when upwelling occurs, and a few months of significant primary production thereafter, predisposing the region to a shorter food chain and the dominance of planktivorous fish like the oil sardine and mackerel. The growing season in the CEAS is comparable to that in the SEAS, but the upwelling is weaker in the CEAS, implying a restriction of phytoplankton size and a smaller fishery owing to the lower primary production. In the SEAS, the phytoplankton biomass is much higher than in the CEAS, but the standing stock of zooplankton is lower owing to the stronger upwelling, which implies a shallower D20 (depth of the 20°C isotherm). The excess phytoplankton in the SEAS is therefore available for grazing by the oil sardine, which preferentially feeds on diatoms, leading to a much larger catch of this fish off Kerala compared to Karnataka or Goa. In contrast, the catch of mackerel, which feeds on zooplankton, does not change as much from Kerala to Karnataka. The spatial variation during the summer and winter monsoons is depicted schematically in Fig. 20; in Fig. 21, we show a schematic diagram depicting the temporal variation of the physical forcing and the phytoplankton and zooplankton biomass and their relation to the nature of fisheries in the NEAS, CEAS, and SEAS. Note that seasonality is not shown for the fisheries in the temporal schematic (Fig. 21). This neglect does not imply a lack of seasonal variation in the fisheries in the EAS, but merely reflects the discussion in this paper, in which the seasonal changes in the physical forcing are related to the annual fish catch.

This paper has used a set of heuristic arguments based on known connections between the physical forcing, the lower trophic levels, and fisheries to show that the change in the nature of the fisheries from south to north along the Indian west coast is determined by the physical forcing. It provides ideas that need to be tested with better data sets and experiments that can help improve models. Understanding the spatial variability of the fisheries in the region and their temporal variation over the year is a necessary pre-requisite, however, for a reliable prediction of the effect of a changing climate on the Indian fisheries.

### **Acknowledgements**

The work reported in this paper was carried out under OCEAN FINDER, a project funded by the Council of Scientific and Industrial Research (CSIR), India, and TRIMFish. The physical model was run on the high-performance-computing (HPC) systems at CSIR-CMMACS and CSIR-NIO; the support provided by Ashalata Marandi at CSIR-CMMACS and the staff handling these HPC systems is gratefully acknowledged. The physical ecosystem model (based on TOPAZ) simulation was carried out in SahasraT (CrayXC40) located at the Supercomputer Education and Research Centre (SERC), Indian Institute of Science, Bengaluru. The analysis was carried out using Ferret, a software from PMEL (NOAA), USA and the figures have been made using Ferret and GMT (Generic

Mapping Tools). Inkscape, a vector graphics software, was used to create the schematic diagrams. We acknowledge Dr. S.G. Aparna, Mr. Suchandan Bemal, and Dr. P. Amol for helpful discussions, Prof. P.N. Vinayachandran and Ms. V. Thushara for help with TOPAZ, Mr. Charls Antony, Mr. Anil Kumar, and Mr. Vineet Jain for helping with the figures, and Mr. P. Vipin for helping digitise state boundaries. Critical comments from two anonymous reviewers helped improve the manuscript. R. Remya acknowledges CSIR and INCOIS, India for financial support. This is CSIR-NIO contribution 9195.

## References

Adcroft A. and Campin J.M., Rescaled height coordinates for accurate representation of free-surface flows in ocean circulation models, *Ocean Model*, 2004, 7:269–284.

Amol, P., 2014. *Intraseasonal variability of currents along west coast of India*. Ph.D. thesis. Goa University, Goa, India.

Amol, P., Shankar, D., Aparna, S. G., Shenoi, S.S.C., Fernando, V., Shetye, S., Mukherjee, A., Agarvadekar, Y., Khalap, S.T., Satelkar, N.P., 2012. Observational evidence from direct current measurements for propagation of remotely forced waves on the shelf off the west coast of India. *Journal of Geophysical Research*, **117**, C05017, doi:10.1029/2011JC007606.

Amol, P., Shankar, D., Fernando, V., Mukherjee, A., Aparna, S.G., Fernandes, R., Michael, G., Khalap, S., Satelkar, N.P., Agarvadekar, Y., Gaonkar, M. G., Tari, A.P., Kankonkar, A., Vernekar, S.P., 2014. Observed intraseasonal and seasonal variability of the West India Coastal Current on the continental slope. *Journal of Earth System Science*, **123**, 1045–1074.

Amol, P., Vijith, V., Fernandes, V., Pednekar, P. and Singh, J. Impact of local and remote winds on the shelf circulation off the central west coast of India, *Ocean Dynamics*, 68 (12), 2018a, 1607-1623.

Amol, P., Vinayachandran, P. N., Shankar, D., Thushara, V., Vijith, V., Chatterjee, A. and Kankonkar, A., Effect of freshwater advection and winds on the vertical structure of chlorophyll in the northern Bay of Bengal, Manuscript submitted to *Deep Sea Research II*, 2018b.

Anderson, R.C., Adam, M.S., Goes, J.I., 2011. From monsoons to mantas: seasonal distribution of *Manta alfredi* in the Maldives. *Fisheries Oceanography*, **20**, 104–113, doi:10.1111/j.1365-2419.2011.00571.x.

Antonov, J. I., D. Seidov, T. P. Boyer, R. A. Locarnini, A. V. Mishonov, H. E. Garcia, O. K. Baranova, M. M. Zweng, and D. R. Johnson, World Ocean Atlas 2009, Vol. 2, Salinity, NOAA Atlas NESDIS 69, 2010 edited by S. Levitus, p. 184, U.S. Gov. Print. Off., Washington, D. C.

Aparna, S.G., McCreary, J.P., Shankar, D., Vinayachandran, P.N., 2012. Signatures of Indian Ocean Dipole and El Niño–Southern oscillation events in sea level variations in the Bay of Bengal. *Journal of Geophysical Research*, **117**, C10012, doi:10.1029/2012JC008055.

Aparna, S.G., Desai, D.V., Shankar, D., A.C., Anil, 2018. Seasonal cycle of zooplankton standing stock inferred from ADCP backscatter measurements in the eastern Arabian Sea, manuscript

submitted to *Progress in Oceanography*, 2018.

Arenovski, A.L., Lim, E.L., Caron, D.A., 1995. Mixotrophic nanoplankton in oligotrophic surface waters of the Sargasso Sea may employ phagotrophy to obtain major nutrients. *Journal of Plankton Research*, **17**, 801–820, doi:10.1093/plankt/17.4.801.

Aumont, O., and L., Bopp, 2006. Globalizing results from ocean in situ iron fertilization studies. *Global Biogeochemical Cycles*, **20**, GB2017, doi:10.1029/2005GB002591.

AVISO, 1996. *AVISO user handbook: Merged TOPEX/Poseidon products. Tech. rep.*, CNES, Toulouse, France.

Balachandran, K.K., Laluraj, C.M., Jyothibabu, R., Madhu, N.V., Muraleedharan, K.R., Vijay, J.G., Maheswaran, P.A., Ashraff, T.T.M., Nair, K.K.C, Achuthankutty, C.T., 2008. Hydrography and biogeochemistry of the north western Bay of Bengal and the north eastern Arabian Sea during winter monsoon. *Journal of Marine Systems*, **73**, 76–86.

Banse, K., 1959. On upwelling and bottom trawling off the southwest coast of India. *Journal of Marine Biological Association of India*, **1**, 33–49.

Banse, K., 1968. Hydrography of the Arabian Sea shelf of India and Pakistan and effects on demersal fishes. *Deep-Sea Research*, **15**, 45–79, doi:10.1016/0011-7471(68)90028-4.

Banse, K., 1984. Overview of the hydrography and associated biological phenomena in the Arabian Sea, off Pakistan. *Marine geology and oceanography of Arabian Sea and coastal Pakistan*, edited by J. D. Haq and B. U. Milliman, 271–303, Van Nostrand Reinhold, N. Y.

Banse, K., 1987. Seasonality of phytoplankton chlorophyll in the central and northern Arabian Sea. *Deep-Sea Research Part A*, **34**, 713–723, doi:10.1016/0198-0149(87)90032-X.

Banse, K., 1994. Overview of research efforts and results in the Arabian Sea, 1960–1990. *Biogeochemistry of the Arabian Sea. Proceedings of the Indian Academy of Sciences*, Lotus Printers, New Delhi, India, 7–25.

Banse, K., English, D.C., 1993. Revision of satellite-based phytoplankton pigment data from the Arabian Sea during the northeast monsoon. *Journal of Marine Research*, **2**, 83–103.

Banse, K., English, D.C., 2000. Geographical differences in seasonality of CZCS-derived phytoplankton pigment in the Arabian Sea for 1978–1986. *Deep-Sea Research Part II: Topical Studies in Oceanography*, **47**, 1623–1677, doi:10.1016/S0967-0645(99)00157-5.

Banse, K., McClain, C.R., 1986. Winter blooms of phytoplankton in the Arabian Sea as observed by the Coastal Zone Color Scanner. *Marine Ecology Progress Series*, **34**, 201–211.

Barton, A.D., Ward, B.A., Williams, R.G., Follows, M.J., 2014. The impact of fine-scale turbulence on phytoplankton community structure. *Limnology and Oceanography: Fluids and Environments*, **4**, 34–49, DOI:10.1215/21573689-2651533.

Bemal, S., Diversity and trophodynamics of Synechococcus in the Eastern Arabian Sea. Ph.D. Thesis, 2017, Academy of Scientific and Innovative Research, Ghaziabad, India.

Bird, D.F., Kalff, J., 1987. Algal phagotrophy: regulating factors and importance relative to



- photosynthesis in Dinobryon (Chrysophyceae). *Limnology and Oceanography*, **32**, 277–284.
- Bonjean, F., Lagerloef, G.S.E., 2002. Diagnostic model and analysis of the surface currents in the tropical Pacific Ocean. *Journal of Physical Oceanography*, **32**, 2938–2954, doi:10.1175/1520-0485(2002)032 <2938:DMAATOT>2.0.CO;2.
- Brink, K.H., 1982a. The effect of bottom friction on low-frequency coastal trapped waves. *Journal of Physical Oceanography*, **12**, 127–133.
- Brink, K.H., 1982b. A comparison of long coastal trapped wave theory with observations off Peru. *Journal of Physical Oceanography*, **12**, 897–913.
- Brink, K.H., Chapman, D.C., 1987. *Programs for computing properties of coastal-trapped waves and wind-driven motions over the continental shelf and slope*. Technical report, Second ed., Woods Hole Oceanographic Institution, Woods Hole, Massachusetts.
- Brock, J., Sathyendranath, S., Platt, T., 1994. A model study of seasonal mixed-layer primary production in the Arabian Sea. *Proc. Indian Acad. Sci. (Earth Planet. Sci.)*, **103**, 163–176.
- Bruce, J.G., Johnson, K.V., and Kindle, J.C., 1994. Evidence for eddy formation in the eastern Arabian Sea during the northeast monsoon. *Journal of Geophysical Research: Oceans*, **99**, 7651–7664.
- Bruce, J.G., Kindle, J.C., Kantha, L.H., Kerling, J.L., Bailey, J.F., 1998. Recent observations and modeling in the Arabian Sea Laccadive High region. *Journal of Geophysical Research*, **103**, 7593–7600.
- Campbell, L., Landry, M.R., Constantinou, J., Nolla, H.A., Brown, S.L., Liu, H., Caron, D.A., 1998. Response of microbial community structure to environmental forcing in the Arabian Sea. *Deep-Sea Research Part II: Topical Studies in Oceanography*, **45**, 2301–2325.
- Chatterjee, A., Shankar, D., Shenoi, S.S.C., Reddy, G.V., Michael, G.S., Ravichandran, M., Gopalkrishna, V.V., Rao, E.P.R., Bhaskar, T.V.S.U., Sanjeevan, V.N., 2012. A new atlas of temperature and salinity for the North Indian Ocean. *Journal of Earth System Science*, **121**, 559–593, doi:10.1007/s12040-012-0191-9.
- Chatterjee, A., Shankar, D., McCreary, J.P., Vinayachandran, P.N., 2013. Yanai waves in the western equatorial Indian Ocean. *Journal of Geophysical Research*, **118**, 1556–1570, doi:10.1002/jgrc.20121.
- Chatterjee, A., Shankar, D., McCreary, J.P., Vinayachandran, P.N., Mukherjee, A., 2017. Dynamics of Andaman Sea circulation and its role in connecting the equatorial Indian Ocean to the Bay of Bengal. *Journal of Geophysical Research*, **122**, 3200–3218, doi:10.1002/2016JC012300.
- Checkley, Jr, D.M., Alheit, J., Oozeki, Y., Roy, C., 2009a. *Climate change and small pelagic fish*. Cambridge University Press, Cambridge, U.K.
- Checkley Jr, D.M., Ayon, P., Baumgartner, T.R., Bernal, M., Coetzee, J.C., Emmett, R., Guevara-Carrasco, R., Hutching, L., Ibaibarriaga, L., Nakata, H., Oozeki, Y., Planque, B., Schweigert, J., Stratoudakis, Y., van der Lingen, C.D., 2009b. Habitats. In: D. Checkley, J. Alheit, Y. Oozeki, & C. Roy (Eds.), *Climate Change and Small Pelagic Fish*, Cambridge University Press, Cambridge, U.K., 12–44, doi:10.1017/CBO9780511596681.005.

- Checkley Jr, D.M., Asch, R.G., Rykaczewski, R.R., 2017. Climate, anchovy, and sardine. *Annual Review of Marine Science*, **9**, 469–493, doi:10.1146/annurev-marine-122414-033819.
- CMFRI, F., 1995. Marine fish landings in India during 1985–93. *Marine Fisheries Information Service, Technical and Extension Series*, **136**, 1–28.
- CMFRI, 2007a. *Marine fisheries profile India*, <http://www.cmfri.org.in/data-publications-/5/2007>.
- CMFRI, 2007b. *Marine fisheries profile Goa*, <http://www.cmfri.org.in/data-publications-/5/2007>.
- CMFRI, 2007c. *Marine fisheries profile Gujarat*, <http://www.cmfri.org.in/data-publications-/5/2007>.
- CMFRI, 2007d. *Marine fisheries profile Karnataka*, <http://www.cmfri.org.in/data-publications-/5/2007>.
- CMFRI, 2007e. *Marine fisheries profile Kerala*, <http://www.cmfri.org.in/data-publications-/5/2007>.
- CMFRI, 2007f. *Marine fisheries profile Maharashtra*, <http://www.cmfri.org.in/data-publications-/5/2007>.
- Codispoti, L.A., and Christensen, J.P., 1985. Nitrification, denitrification and nitrous oxide cycling in the eastern tropical South Pacific Ocean. *Marine Chemistry*, **16**, 277–300, doi:10.1016/0304-4203(85)90051-9.
- Cullen, J.J., 2015. Subsurface chlorophyll maximum layers: enduring enigma or mystery solved? *Annual Review of Marine Science*, **7**, 207–239, doi:10.1146/annurev-marine-010213-135111.
- D'Costa, P.M., Anil, A.C., Patil, J.S., Hegde, S., D'Silva, M.S., Chourasia, M., 2008. Dinoflagellates in a mesotrophic, tropical environment influenced by monsoon. *Estuarine, Coastal and Shelf Science*, **77**, 77–90.
- Deines, K.L., 1999. Backscatter estimation using broadband acoustic Doppler current profilers. *Proceedings of the IEEE sixth working conference on current measurement, San Diego, CA*, 249–253, doi: 10.1109/CCM.1999.755249.
- Demer, D.A., Zwolinski, J.P., Byers, K.A., Cutter, G.R., Renfree, J.S., Sessions, T.S., Macewicz, B.J., 2012. Prediction and confirmation of seasonal migration of Pacific sardine (*Sardinops sagax*) in the California Current Ecosystem. *Fishery Bulletin*, **110**, 52–70.
- Denman, K.L., Miyake, M., 1973. Upper layer modification at Ocean Station Papa: Observations and simulation. *Journal of Physical Oceanography*, **3**, 185–196.
- Devanesan, D.W., 1943. A brief investigation into the causes of the fluctuation of the annual fishery of the oil sardine of Malabar, *Sardinella longiceps* Cuv. & Val., determination of its age and an account of the discovery of its eggs and spawning grounds. *Madras Fish. Bull*, **28**, 1–38.
- Devanesan, D.W., Chidambaram, K., 1943. On the alleged existence of races in the population of the oil sardine, *Sardinella longiceps* in the Arabian Sea. *Proc. 30<sup>th</sup> Indian Sci. Congr., Calcutta*, Abstract.
- Dhulkhed, M. H., 1962. Observations on the food and feeding habits of the Indian oil sardine, *Sardinella longiceps* Val. *Indian Journal of Fisheries*, **9A(1)**, 37–47.

- Dunne, J.P., Gnanadesikan, A., Sarmiento, J.L., Slater, R.D., 2010. Technical description of the prototype version (v0) of tracers of phytoplankton with allometric zooplankton (TOPAZ) ocean biogeochemical model as used in the Princeton IFMIP model. *Biogeosciences*, **7**, 3593–3624.
- Dunne, J.P., John, J.G., Shevliakova, E., Stouffer, R.J., Krasting, J.P., Malyshev, S.L., Milly, P.C., Sentman, L.T., Adcroft, A.J., Cooke, W., Dunne, K.A., Griffies, S.M., Hallberg, R.W., Harrison, M.J., Levy, H., Wittenberg, A.T., Phillips, P.J., and Zadeh, N., 2013. GFDL's ESM2 global coupled climate–carbon earth system models. Part II: carbon system formulation and baseline simulation characteristics. *Journal of Climate*, **26**, 2247–2267, doi:10.1175/JCLI-D-12-00150.1.
- Durand, F., Shetye, S.R., Vialard, J., Shankar, D., Shenoi, S.S.C., Éthé, C., Madec, G., 2004. Impact of temperature inversions on SST evolution in the South-Eastern Arabian Sea during the pre-summer monsoon season. *Geophysical Research Letters*, **31**, L01305, doi:10.1029/2003GL018906.
- Durand, F., Shankar, D., de Boyer Montégut, C., Shenoi, S.S.C., Blanke, B., Madec, G., 2007. Modeling the barrier-layer formation in the southeastern Arabian Sea. *Journal of Climate*, **20**, 2109–2120, doi:10.1175/JCLI4112.1.
- Dwivedi, R.M., Raman, M., Parab, S., Matondkar, S.G.P., Nayak, S., 2006. Influence of northeasterly trade winds on intensity of winter bloom in the Northern Arabian Sea. *Current Science*, **90**, 1397–1406.
- Dwivedi, R.M., Raman, M., Babu, K.N., Singh, S.K., Vyas, N.K., Matondkar, S.G.P., 2008. Formation of algal bloom in the northern Arabian Sea deep waters during January–March: a study using pooled in situ and satellite data. *International Journal of Remote Sensing*, **29**, 4537–4551.
- Estrada, M., and Berdalet, E., 1998. *Effects of turbulence on phytoplankton*. In: Physiological ecology of harmful algal blooms (Eds. DM Anderson, AD Cembella, and GM Hallegraeff), NATO ASI Series Volume G41, 601–608, Springer-Verlag, Berlin Heidelberg.
- Falkowski, P., and Kiefer, D.A., 1985. Chlorophyll a fluorescence in phytoplankton: relationship to photosynthesis and biomass. *Journal of Plankton Research*, **7(5)**, 715–731, doi:10.1093/plankt/7.5.715.
- FAO, 2016, *The State of World Fisheries and Aquaculture 2016*. Contributing to food security and nutrition for all, Food and Agriculture Organization, Rome, 200 pp.
- Fennel, K., Wilkin, J., Levin, J., Moisan, J., O'Reilly, J., Haidvogel, D., 2006. Nitrogen cycling in the Middle Atlantic Bight: Results from a three-dimensional model and implications for the North Atlantic nitrogen budget. *Global Biogeochemical Cycles*, **20**, GB3007, doi:10.1029/2005GB002456.
- Fennel, K., Wilkin, J., Previdi, M., Najjar, R., 2008. Denitrification effects on air-sea CO<sub>2</sub> flux in the coastal ocean: Simulations for the northwest North Atlantic. *Geophysical Research Letters*, **35**, L24608. *Journal of Experimental Marine Biology and Ecology*
- Garcia, H. E., Locarnini, R. A., Boyer, T. P., Antonov, J. I., Zweng, M. M., Baranova, O. K., and Johnson, D. R., World Ocean Atlas 2009, Vol. 4, Nutrients (Phosphate, Nitrate, Silicate), NOAA Atlas NESDIS 71, 2010, edited by S. Levitus, p. 398, U.S. Gov. Print. Off., Washington, D. C.
- Garcia, H. E., Locarnini, R. A., Boyer, T. P., Antonov, J. I., Baranova, O. K., Zweng, M. M., Reagen,

- J. R., and Johnson, D. R., World Ocean Atlas 2013, Vol. 4, Dissolved Inorganic Nutrients (Phosphate, Nitrate, Silicate), NOAA Atlas NESDIS 76, 2014, edited by A. Mishonov, 25 pp., U.S. Gov. Print. Off., Washington, D. C.
- Garrison, H.S., and Tang, K.W., 2014. Effects of episodic turbulence on diatom mortality and physiology, with a protocol for the use of Evans Blue stain for live–dead determinations. *Hydrobiologia*, **738**, 155-170, doi:10.1007/s10750-014-1927-0.
- Ghyoot, C., Lancelot, C., Flynn, K.J., Mitra, A., Gypens, N., 2017. Introducing mixotrophy into a biogeochemical model describing an eutrophied coastal ecosystem: The Southern North Sea. *Progress in Oceanography*, **157**, 1–11, doi:10.1016/j.pocean.2017.08.002
- Gill, A., 1982. *Atmosphere-Ocean Dynamics*. Academic Press, New York, 662
- Griffies, S. M., 2009. *Elements of MOM4p1*. GFDL Ocean Group Tech. Rep. 6, NOAA Geophysical Fluid Dynamics Laboratory, Princeton, N. J., 444 pp.
- Griffies S.M. and Hallberg R.W., Biharmonic friction with a Smagorinsky viscosity for use in large-scale eddy-permitting ocean models. *Mon. Weather Rev.*, 2000, 128:2935–2946.
- do Rosário Gomes, H., Goes, J.I., Matondkar, S.G.P., Buskey, E.J., Basu, S., Parab, S., Thoppil, P., 2014. Massive outbreaks of *Noctiluca scintillans* blooms in the Arabian Sea due to spread of hypoxia. *Nature Communications*, **5**, 4862, doi:10.1038/ncomms5862.
- Goswami, S.C., and Padmavati, G., 1996. Zooplankton production, composition and diversity in the coastal waters of Goa, *Indian Journal of Marine Sciences*, **25**, 91–97.
- Habeebrehman, H., Prabhakaran, M.P., Jacob, J.P., Sabu, P., Jayalakshmi, K.J., Achuthankutty, C.T., Revichandran, C., 2008. Variability in biological responses influenced by upwelling events in the Eastern Arabian Sea. *Journal of Marine Systems*, **74**, 545–560, doi:10.1016/j.jmarsys.2008.04.002.
- Han, W., and McCreary, J.P., 2001. Modeling salinity distributions in the Indian Ocean. *Journal of Geophysical Research*, **106**, 859–877.
- Han, W., McCreary, J.P., Kohler, K.E., 2001. Influence of precipitation minus evaporation and Bay of Bengal rivers on dynamics, thermodynamics, and mixed layer physics in the upper Indian Ocean. *Journal of Geophysical Research*, **106**, 6895–6916.
- Hartmann, M., Grob, C., Tarran, G.A., Martin, A.P., Burkill, P.H., Scanlan, D.J., Zubkov, M.V., 2012, Mixotrophic basis of Atlantic oligotrophic ecosystems. *Proceedings of the National Academy of Sciences*, **109**, 5756–5760.
- Heinrich, A.K., 1962. The life histories of plankton animals and seasonal cycles of plankton communities in the oceans. *ICES Journal of Marine Science*, **27**, 15–24, doi:10.1093/icesjms/27.1.15.
- Hood, R.R., Beckley, L.E., Wiggert, J.D., 2017. Biogeochemical and ecological impacts of boundary currents in the Indian Ocean. *Progress in Oceanography*, **156**, 290-325.
- Huthnance, J.M., 1978. On coastal trapped waves: Analysis and numerical calculation by inverse iteration. *Journal of Physical Oceanography*, **8**, 74–92.

- Irigoien, X., Flynn, K.J., Harris, R.P., 2005. Phytoplankton blooms: a 'loophole' in microzooplankton grazing impact? *Journal of Plankton Research*, **27**, 313–321.
- Jackett D.R., McDougall T.J., Feistel R., Wright D.G. and Griffies S.M., Algorithms for density, potential temperature, conservative temperature, and freezing temperature of seawater, *J Atmos Ocean Technol.*, 2006, 23:1709–1728.
- Jayaprakash, A.A., 2002. Long term trends in rainfall, sea level and solar periodicity: A case study for forecast of Malabar sole and Oil sardine fishery. *Journal of the Marine Biological Association of India*, **44**, 163–175.
- Jayaram, C., Kochuparambil, A.J., Balchand, A.N., 2013. Interannual variability of chlorophyll-a concentration along the southwest coast of India. *International Journal of Remote Sensing*, **34**, 3820–3831, doi: 10.1080/01431161.2012.762482.
- Jensen, T.G., 2001. Arabian Sea and Bay of Bengal exchange of salt and tracers in an ocean model. *Geophysical Research Letters*, **28**, 3967–3970.
- Jochem, F.J., 1995. Phototrophic picoplankton community structure in three different pelagic regimes in the Arabian Sea. *Marine Ecology Progress Series*, **117**, 307–314.
- Jyothibabu, R., Madhu, N.V., Habeebrehman, H., Jayalakshmy, K.V., Nair, K.K.C., Achuthankutty, C.T., 2010. Re-evaluation of 'paradox of mesozooplankton' in the eastern Arabian Sea based on ship and satellite observations. *Journal of Marine Systems*, **81**, 235–251.
- Kim, J.-W., 1976. A generalized bulk model of the oceanic mixed layer. *Journal of Physical Oceanography*, **6**, 686–695.
- Koné, V., Aumont, O., Lévy, M., Resplandy, L., 2009. Physical and biogeochemical controls of the phytoplankton seasonal cycle in the Indian Ocean: A modeling study. *Indian Ocean Biogeochemical Processes and Ecological Variability* (eds J. D. Wiggert, R. R. Hood, S.Wajih. A. Naqvi, K. H. Brink and S. L. Smith), American Geophysical Union, Washington, D. C.. doi:10.1029/2008GM000700.
- Kraus, E.B., Turner, J.S., 1967. A one-dimensional model of the seasonal thermocline II. The general theory and its consequences. *Tellus*, **19**, 98–106.
- Kripa, V., Prema, D., Jeyabaskaran, R., Khambadkar, L.R., Nandakumar, A., Anilkumar, P.S., Ambrose, T.V., Bose, J., Nair, P.G., Pillai, V.N., 2015a. Inter-annual variations of selected oceanographic parameters and its relation to fishery of small pelagics off Kochi, southwest coast of India. *Journal of the Marine Biological Association of India*, **57**, 52–57, doi: 10.6024/jmbai.2015.57.2.1861–08.
- Kripa, V., Vivekanandan, E., Zacharia, P.U., Gopalakrishnan, A., 2015b. *Climate change influences on India's marine fisheries*, Third International Symposium on the Effects of Climate Change on the World's Oceans, Santos, Brazil.
- Kurian, J., and Vinayachandran, P.N., 2006. Formation mechanisms of temperature inversions in the southeastern Arabian Sea. *Geophysical Research Letters*, **33**, doi:10.1029/2006GL027280.
- Kurian, J., and Vinayachandran, P.N., 2007. Mechanisms of formation of the Arabian Sea mini warm

pool in a high-resolution Ocean General Circulation Model. *Journal of Geophysical Research*, **112**, doi:10.1029/2006JC003631.

Laevastu, T., and Hayes, M.L., 1981. *Fisheries oceanography and ecology*, Fishing News Books: Farnham, U.K.

Large W. G., McWilliams J. C., Doney S. C., Oceanic vertical mixing: a review and a model with a nonlocal boundary layer parameterization. *Rev. Geophys.*, 1994, 32:363–403.

Lévy, M., André, J.-M., Shankar, D., Durand, F., Shenoi, S.S.C., 2006. A quantitative method for describing the seasonal cycles of surface chlorophyll in the Indian Ocean. In: Frouin, R. J., Agarwal, V. K., Kawamura, H., Nayak, S., Pan, D. (Eds.), *Remote Sensing of the Marine Environment*, Vol. 6406 (p. 640611), International Society for Optics and Photonics.

Lévy, M., Shankar, D., André, J.-M., Shenoi, S.S.C., Durand, F., de Boyer Montégut, C.D., 2007. Basin-wide seasonal evolution of the Indian Ocean's phytoplankton blooms. *Journal of Geophysical Research*, **112**, doi:10.1029/2007JC004090, C12014.

Liu, H., Campbell, L., Landry, M.R., Nolla, H.A., Brown, S.L., Constantinou, J., 1998. *Prochlorococcus* and *Synechococcus* growth rates and contributions to production in the Arabian Sea during the 1995 Southwest and Northeast Monsoons. *Deep-Sea Research Part II: Topical Studies in Oceanography*, **45**, 2327–2352.

Locarnini, R. A., Mishonov, A. V., Antonov, J. I., Boyer, T. P., Garcia, H. E., Baranova, O. K., Zweng, M. M. and D. R. Johnson, World Ocean Atlas 2009, Vol. 1, Temperature, NOAA Atlas NESDIS 68, 2010, edited by S. Levitus, p. 184, U.S. Gov. Print. Off., Washington, D. C.

Longhurst, A.R., and Wooster, W.S., 1990. Abundance of oil sardine (*Sardinella longiceps*) and upwelling on the southwest coast of India. *Canadian Journal of Fisheries and Aquatic Sciences*, **47**, 2407–2419.

Lukas, R.B., Lindstrom, E.J., 1991. The mixed layer of the western equatorial Pacific Ocean. *Journal of Geophysical Research*, **96**, 3343–3357.

Madhupratap, M., Haridas, P., Ramaiah, N. and Kutty, C.T.A., Zooplankton of the south west coast of India. Abundance, composition, temporal and spatial variability in 1987. In : oceanography of the Indian Ocean, (ed) B.N. Desai, 1992, Oxford & IBH, 99-112.

Madhupratap, M., Shetye, S.R., Nair, K.N.V., Nair, S.R.S., 1994. Oil sardine and Indian mackerel: their fishery, problems and coastal oceanography. *Current Science*, **66**, 340-348.

Madhupratap, M., Gopalakrishnan, T.C., Haridas, P., Nair, K.K.C., Aravindakshan, P.N., Padmavati, G., Paul, S., 1996a. Lack of seasonal and geographic variation in mesozooplankton biomass in the Arabian Sea and its structure in the mixed layer. *Current Science*, **71**, 863–868.

Madhupratap, M., Prasannakumar, S., Bhattathiri, P.M.A., Dileep Kumar, M., Raghukumar, S., Nair, K.K.C., Ramaiah, N., 1996b. Mechanism of the biological response to winter cooling in the northeastern Arabian Sea. *Nature*, **384**, 549–552.

Madhupratap, M., Nair, K.N.V., Gopalakrishnan, T.C., Haridas, P., Nair, K.K.C., Venugopal, P., Gauns, M., 2001. Arabian Sea oceanography and fisheries of the west coast of India. *Current Science*, **81**, 355–361.

- Manjusha, U.J., Jayasankar, J., Remya, R., Ambrose, T.V., Vivekanandan, E., 2013. Influence of coastal upwelling on the fishery of small pelagics off Kerala, south-west coast of India. *Indian Journal of Fisheries*, **60**, 37–42.
- Mann, K.H., 1993. Physical oceanography, food chains, and fish stocks: a review. *ICES Journal of Marine Science*, **50**, 105–119, <https://doi.org/10.1006/jmsc.1993.1013>.
- Mariano, A.J., Ryan, E.H., Perkins, B.D., Smithers, S., 1995. *The Mariano Global Surface Velocity Analysis 1.0*. Tech. Rep. USCG Report CG-D-34-95, USCG.
- McCreary, J.P., 1981. A linear stratified ocean model of the coastal undercurrent. *Philosophical Transactions of the Royal Society of London A: Mathematical, Physical and Engineering Sciences*, **302**, 385–413.
- McCreary, J.P., Kundu, P.K., Molinari, R.L., 1993. A numerical investigation of dynamics, thermodynamics and mixed-layer processes in the Indian Ocean. *Progress in Oceanography*, **31**, 181–244.
- McCreary, J.P., Kohler, K.E., Hood, R.R., Olson, D.B., 1996. A four-component ecosystem model of biological activity in the Arabian Sea. *Progress in Oceanography*, **37**, 193–240.
- McCreary, J.P., Kohler, K.E., Hood, R.R., Smith, S., Kindle, J., Fischer, A.S., Weller, R.A., 2001. Influences of diurnal and intraseasonal forcing on mixed-layer and biological variability in the central Arabian Sea. *Journal of Geophysical Research*, **106**, 7139–7155.
- McCreary, J.P., Murtugudde, R., Vialard, J., Vinayachandran, P.N., Wiggert, J.D., Hood, R.R., Shankar, D., Shetye, S.R., 2009. Biophysical processes in the Indian Ocean. *Indian Ocean Biogeochemical Processes and Ecological Variability* (eds. J.D. Wiggert, R.R. Hood, S.W.A. Naqvi, K.H. Brink and S.L. Smith), American Geophysical Union, Washington, D. C., 9–32, doi:10.1029/2008GM000768.
- Milliman, J.D., Quraishee, G.S., Beg, M.A.A., 1984. Sediment discharge from the Indus River to the Ocean: Past, present and future, In: *Marine Geology and Oceanography of Arabian Sea and Coastal Pakistan*, edited by B. U. Haq and J. D. Milliman, pp. 65–70, Van Nostrand Reinhold, New York.
- Milliman, J.D., Farnsworth, K.L., 2013. *River discharge to the coastal ocean: a global synthesis*: Cambridge University Press, Cambridge, U.K.
- Mitbavkar, S., and Anil, A.C., 2011. Tiniest primary producers in the marine environment: an appraisal from the context of waters around India. *Current Science*, **100**, 986–988.
- Morel, A., and Antoine, D., Heating rate within the upper ocean in relation to its biooptical state, *J. Phys. Oceanogr.*, 24(7), 1994, 1652-1665.
- Mukherjee, A., Shankar, D., Chatterjee, A., Vinayachandran, P.N., 2017. Numerical simulation of the observed near-surface East India Coastal Current on the continental slope. *Climate Dynamics*, 1–32, doi:10.1007/s00382-017-3856-x.
- Mukhopadhyay, S., Shankar, D., Aparna, S.G., Mukherjee, A., 2017. Observations of the sub-inertial, near-surface East India Coastal Current. *Continental Shelf Research*, **148**, 159–177.
- Nair, K.K.C, Madhupratap, M., Gopalakrishnan, T.C., Haridas, P., Gauns, M., 1999. The Arabian

- Sea: Physical environment, zooplankton and myctophid abundance, *Indian Journal of Marine Sciences*, **28**, 138–145.
- Nair, V.R., 1980. Zooplankton biomass along the west coast of India and its effect on the fishery. *Journal of the Indian Fisheries Association*, **10**, 11–15.
- Naqvi, S.W.A., 1991. Geographical extent of denitrification in the Arabian Sea in relation to some physical processes. *Oceanologica Acta*, **14**, 281–290.
- Naqvi, S.W.A., Jayakumar, D.A., Narvekar, P.V., Naik, H., Sarma, V.V.S.S., D'souza, W., Joseph, S., George, M.D., 2000. Increased marine production of N<sub>2</sub>O due to intensifying anoxia on the Indian continental shelf. *Nature*, **408**, 346–349.
- Naqvi, S.W.A., Sarma, V.V.S.S., Jayakumar, D.A., 2002. Carbon cycling in the northern Arabian Sea during the northeast monsoon: Significance of salps. *Marine Ecology Progress Series*, **226**, 35–44.
- Naqvi, S.W.A., Narvekar, P.V., Desa, E., 2006. Coastal biogeochemical processes in the North Indian Ocean (14, S-W). In: *The Sea* (eds. Robinson A.R., Brink K.H.), **14**, Chapter 19, 723–781, Wiley, Hoboken.
- Noble, A., 1962. Food and feeding habits of the Indian mackerel, *Rastrelliger kanagurta* (Cuvier) at Karwar. *Indian Journal of Fisheries*, **9**, 701–713.
- Noble, A., 1964. Food and feeding habits of the Indian oil sardine *Sardinella longiceps Valenciennes* at Karwar. *Indian Journal of Fisheries*, **12**, 77–87.
- Nuzzo, R., 2014. Scientific method: Statistical errors, *Nature*, **506(7487)**, 150–152, doi: 10.1038/506150a.
- Padmavati, Haridas, P., Nair, K. K. C., Gopalakrishnan, T. C., Shiney, P., Madhupratap, M., 1998. Vertical distribution of mesozooplankton in the central and eastern Arabian Sea during the winter monsoons. *Journal of Plankton Research*, **20**, 343–354.
- Papa F., Durand F., Rossow W. ., Rahman A. and Bala S., Satellite altimeter-derived monthly discharge of the Ganga–Brahmaputra river and its seasonal to interannual variations from 1993 to 2008. *J. Geophys. Res.*, 2010, 115:C12013.
- Parab, S.G., Matondkar, S.G.P., Gomes, H.d.R., Goes, J.J., 2006. Monsoon driven changes in phytoplankton populations in the eastern Arabian Sea as revealed by microscopy and HPLC pigment analysis. *Continental Shelf Research*, **26**, 2538–2558.
- Parsons, T.R., Takahashi, M., Hargrave, B., 2013. 1984. *Biological oceanographic processes*, 3<sup>rd</sup> ed., Pergamon Press, U.K.
- Parvathi, V., Suresh, I.M., Lengaigne, M., Ethé, C., Vialard, J., Levy, M., Neetu, S., Aumont, O., Resplandy, L., Naik, H., Naqvi, S.W.A., 2017. Positive Indian Ocean Dipole events prevent anoxia off the west coast of India, *Biogeosciences*, **14**, 1541–1559.
- Pazhayamadom, D. G., Chakraborty, S. K., Jaiswar, A. K., Sudheesan, D., Sajina, A. M., Jahageerdar, S., Stock structure analysis of 'Bombay duck' (*Harpadon nehereus* Hamilton, 1822) along the Indian coast using truss network morphometrics, *Journal of Applied Ichthyology*, 2015, 31, 37–44.



Pillai, V. N., Vijayarajan, K and Nandakumar, A., Oceanographic investigations, 1980, Report of the UNDP/FAO Pelagic Fishery Project, Phase-II. FIRS/IND/75/038,FAO, Rome.

Pillai, V. N., Physical characteristics of the coastal waters off the south west coast of India with an attempt to study the possible relationship with sardine, mackerel and anchovy fisheries, 1983, PhD Thesis, Cochin University of Science and Technology.

Prakash, S., Prakash, P., Ravichandran, M., 2013. Can oxycline depth be estimated using sea level anomaly (SLA) in the northern Indian Ocean? *Remote Sensing Letters*, **4**, 1097–1106, doi: 10.1080/2150704X.2013.842284.

Prasad, R.R., 1969. Zooplankton biomass in the Arabian Sea and the Bay of Bengal with a discussion on the fisheries of the region. *Proceedings of the National Institute of Sciences of India*, **35B**, 399–437.

Prasannakumar, S., Muraleedharan, P.M., Prasad, T.G., Gauns, M., Ramaiah, N., De Souza, S.N., Sardesai, S., Madhupratap, M., 2002. Why is the Bay of Bengal less productive during summer monsoon compared to the Arabian Sea? *Geophysical Research Letters*, **29**, doi: 10.1029/2002GL016013.

Raghukumar, S., and Anil, A.C., 2003. Marine biodiversity and ecosystem functioning: A perspective. *Current Science*, **84**, 884–892.

Raja, A.B.T., 1969. Indian Oil sardine. *Bulletin of the Central Marine Fisheries Research Institute*, **16**, 1–128.

Ramaiah, N., Raghukumar, S., Gauns, M., 1996. Bacterial abundance and production in the central and eastern Arabian Sea. *Current Science*, **71**, 878–882.

Ramasastri, A., Myrland, P., 1959. Distribution of temperature, salinity and density in the Arabian Sea along the South Malabar Coast (South India) during the post-monsoon season. *Indian Journal of Fisheries*, **6**, 223–255.

Rao, R.R., Sivakumar, R., 1999. On the possible mechanisms of the evolution of a mini-warm pool during the pre-summer monsoon season and the genesis of onset vortex in the South-Eastern Arabian Sea. *Quarterly Journal of the Royal Meteorological Society*, **125**, 787–809, doi:10.1002/qj.49712555503.

Remya, R., Vivekanandan, E., Manjusha, U., Nair, P.G., 2013. Seasonal variations in the diet of the Indian oilsardine, *Sardinella longiceps Valenciennes* off Cochin, Kerala. *Indian Journal of Fisheries*, **60**, 55–59.

Resplandy, L., Lévy, M., Madec, G., Pous, S., Aumont, O., Dileep Kumar, M., 2011. Contribution of mesoscale processes to nutrient budgets in the Arabian Sea. *Journal of Geophysical Research*, **116**, C11007, doi:10.1029/2011JC007006.

Roske, F., 2001. *An atlas of surface fluxes based on the ECMWF re-analysis: A climatological dataset to force global ocean general circulation models*. Technical report 323, Max-Planck Institut für Meteorologie, Hamburg, Germany.

Roy, R., Pratihary, A., Mangesh, G., Naqvi, S.W.A., 2006. Spatial variation of phytoplankton pigments along the southwest coast of India. *Estuarine, Coastal and Shelf Science*, **69**, 189–195,

doi:10.1016/j.ecss.2006.04.006.

Roy, R., and Anil, A.C., 2015. Complex interplay of physical forcing and *Prochlorococcus* population in ocean. *Progress in Oceanography*, **137**, 250–260, doi:10.1016/j.pocean.2015.06.010.

Roy, R., Chitari, R., Kulkarni, V., Krishna, M.S., Sarma, V.V.V.S., Anil, A.C., 2015. CHEMTAX-derived phytoplankton community structure associated with temperature fronts in the northeastern Arabian Sea. *Journal of Marine Systems*, **144**, 81–91, doi:10.1016/j.jmarsys.2014.11.009.

Ryabchenko, V.A, Gorchakov, V.A., Fasham, M.J.R., 1998. Seasonal dynamics and biological productivity in the Arabian Sea Euphotic Zone as simulated by a three-dimensional ecosystem model. *Global Biogeochemical Cycles*, **12**, 501–530, doi:10.1029/98GB01183.

Rykaczewski, R.R., and Checkley, Jr, D.M., 2008 Influence of ocean winds on the pelagic ecosystem in upwelling regions, *Proceedings of the National Academy of Sciences*, **105**, 1965–1970.

Saji, N.H., Goswami, B.N., Vinayachandran, P.N., Yamagata, T., 1999. A dipole mode in the tropical Indian Ocean. *Nature*, **401**, 360–363.

Sarma, V. V. S. S., Patil, J. S., Shankar, D. and Anil, A. C., Shallow convective mixing promotes massive *Noctiluca scintillans* bloom in the northeastern Arabian Sea, Manuscript accepted in *Marine Pollution Bulletin*, 2018, <https://doi.org/10.1016/j.marpolbul.2018.11.054>

Schott, F.A., McCreary, J.P., 2001. The monsoon circulation of the Indian Ocean. *Progress in Oceanography*, **51**, 1–123.

SenGupta, R.S., Rajagopal, M.D., Qasim, S.Z., 1976. Relationship between dissolved oxygen and nutrients in the north-western Indian Ocean. *Indian Journal of Marine Sciences*, **5**, 201–211.

Sengupta, D., and Ravichandran, M., 2001. Oscillations of Bay of Bengal sea surface temperature during the 1998 summer monsoon. *Geophysical Research Letters*, **28**, 2033–2036.

Shalin, S., Sanilkumar, K.V., 2014. Variability of chlorophyll-a off the southwest coast of India. *International Journal of Remote Sensing*, **35**, 5420–5433, doi: 10.1080/01431161.2014.926411.

Shankar, D., Shetye, S.R., 1997. On the dynamics of the Lakshadweep high and low in the southeastern Arabian Sea. *Journal of Geophysical Research*, **102**, 12551–12562.

Shankar, D., Shetye, S.R., 1999. Are interdecadal sea level changes along the Indian coast influenced by variability of monsoon rainfall? *Journal of Geophysical Research*, **104**, 26031–26042.

Shankar, D., 1998. *Low-frequency variability of sea level along the coast of India*. Ph.D thesis, Goa University, Goa, India.

Shankar, D., 2000. Seasonal cycle of sea level and currents along the coast of India. *Current Science*, **78**, 279–288.

Shankar, D., Vinayachandran, P.N., Unnikrishnan, A.S., 2002. The monsoon currents in the north Indian Ocean. *Progress in Oceanography*, **52**, 63–120.

Shankar, D., Gopalakrishna, V.V., Shenoi, S.S.C., Durand, F., Shetye, S.R., Rajan, C.K., Johnson, Z., Araligidad, N., Michael, G.S., 2004a. Observational evidence for westward propagation of

temperature inversions in the southeastern Arabian Sea. *Geophysical Research Letters*, **31**, L08305. doi:10.1029/2004GL019652.

Shankar, D., Kotamraju, V., Shetye, S.R., 2004b. A quantitative framework for estimating water resources in India. *Current Science*, **86**, 543–552.

Shankar, D., Shenoi, S.S.C., Nayak, R.K., Vinayachandran, P.N., Nampoothiri, G.S., Almeida, A.M., Michael, G.S., Ramesh Kumar, M.R., Sundar, D., Sreejith, O.P., 2005. Hydrography of the eastern Arabian Sea during summer monsoon 2002. *Journal of Earth System Science*, **114**, 459–474.

Shankar, D., Remya, R., Vinayachandran, P.N., Chatterjee, A., Behera, A., 2016. Inhibition of mixed-layer deepening during winter in the northeastern Arabian Sea by the West India Coastal Current. *Climate Dynamics*, **47**, 1049–1072.

Sharma, G.S., 1968. Seasonal variation of some hydrographic properties of the shelf waters off the west coast of India. *Bull. Nat. Inst. Sci. India*, **38**, 263–276.

Shenoi, S.S.C, Shankar, D., Shetye, S.R., 1999. On the sea surface temperature high in the Lakshadweep Sea before the onset of the southwest monsoon. *Journal of Geophysical Research: Oceans*, **104**, 15703–15712.

Shenoi, S.S.C, Shankar, D., Shetye, S.R., 2004. Remote forcing annihilates barrier layer in southeastern Arabian Sea. *Geophysical Research Letters*, **31**, L05307, doi:10.1029/2003GL019270.

Shenoi, S.S.C., Shankar, D., Michael, G., Kurian, J., Varma, K., RameshKumar, M.R., Almeida, A., Unnikrishnan, A.S., Fernandes, W., Barreto, N., Gnanaseelan, C., Mathew, R., Praju, K. V., Mahale, V., 2005. Hydrography and water masses in the southeastern Arabian Sea during March–June 2003. *Journal of Earth System Science*, **114**, 475–491.

Shetye, S.R., 1986. A model study of the seasonal cycle of the Arabian Sea surface temperature. *Journal of Marine Research*, **44**, 521–542.

Shetye, S.R., Gouveia, A.D., Shenoi, S.S.C., Sundar, D., Michael, G.S., Almeida, A.M., Santanam, K., 1990. Hydrography and circulation off the west coast of India during the southwest monsoon 1987. *Journal of Marine Research*, **48**, 359–378, doi:10.1357/002224090784988809.

Shetye, S.R., Gouveia, A.D., Shenoi, S.S.C., Michael, G.S., Sundar, D., Almeida, A.M., Santanam, K., 1991. The coastal current off western India during the northeast monsoon. *Deep-Sea Research Part A. Oceanographic Research Papers*, **38**, 1517–1529, doi:10.1016/0198-0149(91)90087-V.

Shetye, S.R., and Almeida, A. M., 1985. *An examination of the factors that influence the monthly-mean sea level along the coast of India*. In: IOC/Unesco workshop on regional co-operation in marine science in the central Indian ocean and adjacent seas and gulfs, Colombo, Sri Lanka, IOC workshop reports, **37**, 87–104.

Shetye, S. R., Gouveia, A. D. and Shenoi, S. S. C., Does winter cooling lead to the subsurface salinity minimum off Saurashtra, India, In: Desai BN (ed) *Oceanography of the Indian Ocean*, 1992, Oxford and India Book House, Calcutta, pp 617–625.

Shetye, S.R., Gouveia, A.D., Shankar, D., Shenoi, S.S.C., Vinayachandran, P.N., Sundar, D., Michael, G.S., Nampoothiri, G., 1996. Hydrography and circulation in the western Bay of Bengal during the northeast monsoon. *Journal of Geophysical Research*, **101**, 14011–14025.

- Shetye, S.R., 1998. West India coastal current and Lakshadweep high/low. *Sadhana*, **23**, 637–651.
- Shetye, S. R., and Gouveia, A. D., 1998. Coastal circulation in the north Indian Ocean, Coastal segment (14, S-W). In: *The Sea* (eds Robinson A.R, Brink K.H), **11**, chapter 18, Wiley, Hoboken, 523–556.
- Shetye, S.R., Suresh, I., Shankar, D., Sundar, D., Jayakumar, S., Mehra, P., Prabhudesai, R.G., Pednekar, P.S., 2008. Observational evidence for remote forcing of the West India Coastal Current. *Journal of Geophysical Research*, **113**, C11001, doi:10.1029/2008JC004874.
- Sieburth, J.M.N., Smetacek, V., Lenz, J., 1978. Pelagic ecosystem structure : heterotrophic compartments of the plankton and their relationship to plankton size fractions. *Limnology and Oceanography*, **23**, 1256–1263.
- Sindhu, B., Suresh, I., Unnikrishnan, A.S., Bhatkar, N.V., Neetu, S., Michael, G.S., 2007. Improved bathymetric datasets for the shallow water regions in the Indian Ocean. *Journal of Earth System Science*, **116**, 261–274.
- Smith, S.L., and Madhupratap, M., 2005. Mesozooplankton of the Arabian Sea: patterns influenced by seasons, upwelling, and oxygen concentrations. *Progress in Oceanography*, **65**, 214–239.
- Stacey, M. W., Pond, S. and Nowak, Z. P., A numerical model of the circulation in Knight Inlet, British Columbia, Canada. *J. Phys. Oceanogr.*, 1995, 25:1037–1062.
- Sweeney, C., Gnanadesikan, A., Griffies, S. M., Harrison, M. J., Rosati, A. J. and Samuels, B. L., Impacts of shortwave penetration depth on large-scale ocean circulation and heat transport, *J. Phys. Oceanogr.*, 2005, 35:1103–1119.
- Subrahmanyam, R., 1959. Studies on the phytoplankton on the west coast of India Part I. Quantitative and qualitative fluctuation of the total phytoplankton crop, the zooplankton crop and their interrelationship, with remarks on the magnitude of the standing crop and production of matter and their relationship to fish landings, *Proceedings of the Indian Academy of Sciences*, **L3**, Sec. B.
- Suprit, K., 2010. *Hydrological modelling of the west coast of India*. Ph.D. Thesis, Goa University, Goa, India.
- Suprit, K., Shankar, D., 2008. Resolving orographic rainfall on the Indian west coast. *International Journal of Climatology*, **28**, 643–657.
- Suprit, K., Shankar, D., Venugopal, V., Bhatkar, N.V., 2012. Simulating the daily discharge of the Mandovi River, west coast of India. *Hydrological Sciences Journal*, **57**, 686–704.
- Suresh, I., Vialard, J., Lengaigne, M., Han, W., McCreary, J.P., Durand, F., Muraleedharan, P.M., 2013. Origins of wind-driven intraseasonal sea level variations in the North Indian Ocean coastal waveguide. *Geophysical Research Letters*, **40**, 5740–5744, doi:10.1002/2013GL058312.
- Sverdrup, H.U., 1953. On conditions for the vernal blooming of phytoplankton, *ICES Journal of Marine Science*, **18**, 287–295, DOI:10.1093/icesjms/18.3.287.
- Sverdrup, H.U., Johnson, M.W., Fleming, R.H., 1942. *The Oceans: Their physics, chemistry, and general biology*: Prentice-Hall New York, <http://ark.cdlib.org/ark:/13030/kt167nb66r/>.

- Thadathil, P., and Gosh, A.K., 1992. Surface layer temperature inversion in the Arabian Sea during winter. *Journal of Oceanography*, **48**, 293–304.
- Thadathil, P., Muraleedharan, P.M., Rao, R.R., Somayajulu, Y.K., Reddy, G.V., Revichandran, C., 2007. Observed seasonal variability of barrier layer in the Bay of Bengal. *Journal of Geophysical Research: Oceans*, **112**, C02009, doi:10.1029/2006JC003651.
- Thorisson, K., 2006. How are the vertical migrations of copepods controlled? *Journal of Experimental Marine Biology and Ecology*, **329**, 86-100, doi:10.1016/j.jembe.2005.08.011.
- Tilman, D., 1999. The ecological consequences of changes in biodiversity: a search for general principles. *Ecology*, **80**, 1455–1474.
- Turner, J.S., and Kraus, E.B., 1967. A one-dimensional model of the seasonal thermocline I. A laboratory experiment and its interpretation. *Tellus*, **19**, 88–97.
- van der Lingen, C.D., Bertrand, A., Bode, A., Brodeur, R., Cubillos, L.A., Espinoza, P., Friedland, K., Garrido, S., Irigoien, X., Miller, T., C., Möllmann, R., Rodríguez-Sánchez, H., Tanaka and A., Temming, 2009. *Trophic dynamics*, In: *Climate change and small pelagic fish* (D.M. Checkley, J. Alheit, Y. Oozeki, and C. Roy, eds.), Cambridge Univ. Press, Cambridge, U.K, 112-157.
- van der Lingen, C.D., Coetzee, J.C., Hutchings, L., 2010. Overview of the KwaZulu-Natal sardine run. *African Journal of Marine Science*, **32**, 271–277.
- Venkataraman, G., 1960. Studies on the food and feeding relationships of the inshore fishes off Calicut on the Malabar coast. *Indian Journal of Fisheries*, **7(2)**, 275–306.
- Vialard, J., Delecluse, P., 1998. An OGCM study for the TOGA decade. Part I: Role of salinity in the physics of the western Pacific fresh pool. *Journal of Physical Oceanography*, **28**, 1071–1088.
- Vijith, V., Vinayachandran, P.N., Thushara, V., Amol, P., Shankar, D., Anil, A.C., 2016. Consequences of inhibition of mixed-layer deepening by the West India Coastal Current for winter phytoplankton bloom in the northeastern Arabian Sea. *Journal of Geophysical Research*, **121**, 6583–6603, doi:10.1002/2016JC012004.
- Vinayachandran, P.N., Murty, V.S.N., Ramesh Babu, V., 2002. Observations of barrier layer formation in the Bay of Bengal during summer monsoon. *Journal of Geophysical Research*, **107**, 8018, doi:10.1029/2001JC000831.
- Vinayachandran, P.N., Kurian, J., Neema, C.P., 2007. Indian Ocean response to anomalous conditions during 2006. *Geophysical Research Letters*, **34**, doi:10.1029/2007GL030194.
- Vinayachandran, P.N., Francis, P., Rao, S.A., 2009. Indian Ocean dipole: processes and impacts. *Current trends in science: Platinum Jubilee Special, Indian Academy of Sciences Bangalore*, 569–589.
- Vivekanandan, E., Srinath, M., Kuriakose, S., 2005. Fishing the marine food web along the Indian coast. *Fisheries Research*, **72**, 241–252.
- Vörösmarty, C., Fekete, B. and Tucker, B., River discharge database, version 1.0 (rivdis vl. 0), technical report, 1996, UNESCO, Paris.

- Wang, D.-P., Mooers, C.N., 1976. Coastal-trapped waves in a continuously stratified ocean. *Journal of Physical Oceanography*, **6**, 853–863.
- Watanabe, Y., Zenitani, H., Kimura, R., 1995. Population decline of the Japanese sardine *Sardinops melanostictus* owing to recruitment failure. *Canadian Journal of Fisheries and Aquatic Science*, **52**, 1609–1616.
- Waterbury, J.B., Watson, S.W., Guillard, R.R.L., Brand, L.E., 1979. Widespread occurrence of a unicellular, marine, planktonic cyanobacterium, *Nature*, **277**, 293–294.
- Webster, P.J., Moore, A.M., Loschnigg, J.P., Leben, R.R., 1999. Coupled ocean–atmosphere dynamics in the Indian Ocean during 1997–98. *Nature*, **401**, 356–360.
- Wiggert, J.D., Jones, B.H., Dickey, T.D., Brink, K.H., Weller, R.A., Marra, J., Codispoti, L.A., 2000. The Northeast Monsoon's impact on mixing, phytoplankton biomass and nutrient cycling in the Arabian Sea. *Deep-Sea Research Part II: Topical Studies in Oceanography*, **47**, 1353–1385.
- Wiggert, J.D., Hood, R.R., Banse, K., Kindle, J.C., 2005. Monsoon-driven biogeochemical processes in the Arabian Sea. *Progress in Oceanography*, **65**, 176–213.
- Wiggert, J.D., Murtugudde, R.G., Christian, J.R., 2006. Annual ecosystem variability in the tropical Indian Ocean: Results of a coupled bio-physical ocean general circulation model. *Deep-Sea Research Part II: Topical Studies in Oceanography*, **53**, 644–676.
- Wiggert, J.D., Vialard, J., Behrenfeld, M.J., 2009. Basin-wide modification of dynamical and biogeochemical processes by the positive phase of the Indian Ocean Dipole during the SeaWiFS era. *Indian Ocean Biogeochemical Processes and Ecological Variability*, **185**, 385–407, doi:10.1029/2008GM000776.
- Winkelmann, K., Genner, M.J., Takahashi, T., Rüber, L., 2014. Competition-driven speciation in cichlid fish, *Nature Communications*, **5**, 3412, doi:10.1038/ncomms4412,
- Wyatt, T., 1980. The growth season in the sea. *Journal of Plankton Research*, **2**, 81–96, doi:10.1093/plankt/2.1.81.
- Wyrtki, K., 1971. *Oceanographic atlas of the International Indian Ocean Expedition*. National Science Foundation, Washington DC.
- Xu, C., and Boyce, M.S., 2009. Oil sardine (*Sardinella longiceps*) off the Malabar Coast: density dependence and environmental effects. *Fisheries Oceanography*, **18**, 359–370, doi:10.1111/j.1365-2419.2009.00518.x.
- Yohannan, T.M., and Abdurahiman, U.C., 1998. Environmental influence on the behaviour of Indian mackerel and their availability to fishing gear along the Malabar coast. *Indian Journal of Fisheries*, **45**, 239–247.
- Young, D.K., Kindle, J.C., 1994. Physical processes affecting availability of dissolved silicate for diatom production in the Arabian Sea, *Journal of Geophysical Research*, **99**, 22619–22632.
- Zubkov, M.V., and Tarran, G.A., 2008. High bacterivory by the smallest phytoplankton in the North Atlantic Ocean. *Nature*, **455**, 224–226.

## Tables

**Table 1 :** Coastline length and fish catch of the west-coast states of India. The coastline lengths are based on the ENVIS website (<http://iomenvis.nic.in/index.aspx?langid=1>), fish catch is based on landings data given in CMFRI (2007b-f) for two periods 2001–2005 and average landings is the average for the period 1986–2005.

West-coast states of India	Coastline length (km)	Fish landings (thousands of tonnes)										Average landings
		1961–1965	1966–1970	1971–1975	1976–1980	1981–1985	1986–1990	1991–1995	1996–2000	2001–2005	1986–2005	
Gujarat	1600	92.96	82.77	123.81	191.53	239.07	273.10	467.31	631.85	442.07	453.58	
Maharashtra	720	126.27	150.53	220.72	273.48	287.60	324.74	337.03	362.04	378.75	350.64	
Goa	131	—	20.85	26.91	27.34	38.72	79.52	77.41	55.20	72.71	71.21	
Karnataka	300	55.02	79.07	90.33	117.40	133.09	210.31	153.29	173.91	200.38	184.47	
Kerala	590	264.30	348.77	406.07	331.90	340.99	493.06	559.86	574.88	576.00	550.95	

**Table 2.** Details of ADCP moorings. All the ADCPs are of frequency 153 kHz and make RD Instruments; the water-column depth at which they were deployed was ~1100 m. The ADCP in the CEAS has a data gap during 17 February to 19 October 2014.

Mooring location (Position)	Deployment date	Recovery date	Water depth (m)	Details of ADCPs on the mooring line	
				Frequency (kHz)	Depth (m)
NEAS (69.20°E, 20.00°N)	05 Oct 2012	19 Nov 2013	1134	153	167
	16 Nov 2013	02 Nov 2014	1155	153	182
	02 Nov 2014	02 Jan 2016	1122	153	171
	02 Jan 2016	09 Nov 2016	1140	153	193
CEAS (72.70°E, 15.15°N)	09 Oct 2012	08 Nov 2013	952	153	160
	11 Nov 2013	19 Oct 2014	960	153	158
	20 Oct 2014	06 Jan 2016	979	153	189
	06 Jan 2016	12 Nov 2016	976	153	178
SEAS (75.40°E, 9.05°N)	12 Oct 2012	22 Nov 2013	1105	153	171
	22 Nov 2013	24 Oct 2014	1102	153	152
	24 Oct 2014	09 Jan 2016	1164	153	202
	09 Jan 2016	15 Nov 2016	1122	153	167

**Table 3.** Set-up used for the MOM4p1 configurations in Shankar et al (2016) and Vijith et al (2016).

	<b>Shankar et al. (2016)</b>	<b>Vijith et al. (2016)</b>
Domain	Indian Ocean (30°E–120°E, 30°S–30°N)	As in Shankar et al.
Horizontal Resolution	0.25° x 0.25°	As in Shankar et al.
Vertical levels	40 levels – 25 levels in top 200 m and 5 m resolution in top 60 m.	As in Shankar et al.
Minimum depth of the ocean	15 m	As in Shankar et al.
Spin-up period	Run for 15 years and the final year's output is used.	The physical model was run for 10 years and the coupled-physical-ecosystem model was subsequently run for another 10 years. The final year's output is used.



**Table 4.** Model physics, including coordinate systems and parameterisations, used for MOM4p1 in Shankar et al. (2016) and Vijith et al. (2016).

	<b>Shankar et al. (2016)</b>		<b>Vijith et al. (2016)</b>	
<b>Physics</b>	<b>Remarks</b>	<b>References or sources</b>	<b>Remarks</b>	<b>References or sources</b>
Coordinate system	Generalised orthogonal coordinates horizontally and quasi-horizontal, rescaled height coordinate vertically	Stacey et al. (1995) Adcroft and Campin (2004)	As in Shankar et al.	As in Shankar et al.
Bottom topography	Modified ETOPO2 bathymetry	Sindhu et al. (2007)	ETOPO2	
Initial temperature and salinity fields (also used for relaxation at open boundaries)	Adds data from the Indian EEZ (Exclusive Economic Zone) to the World Ocean Atlas of Locarnini et al. (2010) and Antonov et al. (2010)	Chatterjee et al. (2012)	World Ocean Atlas 2009 for temperature, salinity, NO <sub>3</sub> , PO <sub>4</sub> , SiO <sub>4</sub> . All other variables used in TOPAZ is taken from MOM-TOPAZ test case available at <a href="ftp://ftp.gfdl.noaa.gov/perm/MOM4/mom4p1_publicrel/exp">ftp://ftp.gfdl.noaa.gov/perm/MOM4/mom4p1_publicrel/exp</a>	Locarnini et al. (2010), Antonov et al. (2010), and Garcia et al. (2010)
Tracer advection	Multi-dimensional, piecewise parabolic method (MDPPM)	<a href="http://mitgcm.org/">http://mitgcm.org/</a>	As in Shankar et al.	As in Shankar et al.
Equation of state	Nonlinear formulation	Jackett et al. (2006)	As in Shankar et al.	As in Shankar et al.
Vertical mixing	K-profile parameterisation, with a pre-specified vertical-diffusivity profile (Bryan and Lewis 1979) and a critical bulk Richardson number of 0.3 (local mixing due to double diffusion not included to avoid enhanced mixing)	Large et al. (1994)	As in Shankar et al.	As in Shankar et al.

	within the stratified water column)			
Horizontal friction	Combination of biharmonic and Laplacian mixing, with Smagorinsky mixing coefficients of 0.01 (velocity scale 0.04 m/s) and 0.1 (velocity scale 0.005 m/s), respectively	Griffies and Hallberg (2000)	As in Shankar et al.	As in Shankar et al.
Penetrative shortwave heating	In upper 100 m, calculated using a Chl-a based scheme	Morel and Antoine (1994)	As in Shankar et al.	As in Shankar et al.

**Table 5.** List of data sets used to force the MOM4p1 model in Shankar et al (2016) and Vijith et al (2016).

	Shankar et al. (2016)			Vijith et al. (2016)		
Fields (Units)	Data source	Frequency	References	Data source	Frequency	References
Wind stress (N/m <sup>2</sup> )	OMIP	Daily	Röske (2001)	ERA-INTERIM (high frequency; <36 hours)	3-hourly	<a href="http://www.ecmwf.int/en/research/climate-reanalysis/era-interim">http://www.ecmwf.int/en/research/climate-reanalysis/era-interim</a>
				QuikSCAT (low frequency; >36 hours)	Daily	<a href="http://www.ifremer.fr/cersat/en/data/data.html">http://www.ifremer.fr/cersat/en/data/data.html</a>
Wind speed (m/s)	OMIP	Daily	Röske (2001)	ERA-INTERIM (high frequency; <36 hours)	3-hourly	<a href="http://www.ecmwf.int/en/research/climate-reanalysis/era-interim">http://www.ecmwf.int/en/research/climate-reanalysis/era-interim</a>
				QuikSCAT (low frequency; >36 hours)	Daily	<a href="http://www.ifremer.fr/cersat/en/data/data.html">http://www.ifremer.fr/cersat/en/data/data.html</a>
Downward shortwave radiation (W/m <sup>2</sup> )	OMIP	Daily	Röske (2001)	ERA-INTERIM	3-hourly	<a href="http://www.ecmwf.int/en/research/climate-reanalysis/era-interim">http://www.ecmwf.int/en/research/climate-reanalysis/era-interim</a>
Downward longwave radiation (W/m <sup>2</sup> )	OMIP	Daily	Röske (2001)	ERA-INTERIM	3 hourly	<a href="http://www.ecmwf.int/en/research/climate-reanalysis/era-interim">http://www.ecmwf.int/en/research/climate-reanalysis/era-interim</a>
Air temperature (K)	OMIP	Daily	Röske (2001)	ERA-INTERIM	3-hourly	<a href="http://www.ecmwf.int/en/research/climate-reanalysis/era-interim">http://www.ecmwf.int/en/research/climate-reanalysis/era-interim</a>

<b>Specific humidity (kg/kg)</b>	OMIP	Daily	Röske (2001)	ERA-INTERIM	3-hourly	<a href="http://www.ecmwf.int/en/research/climate-reanalysis/era-interim">http://www.ecmwf.int/en/research/climate-reanalysis/era-interim</a>
<b>Precipitation (m/s)</b>	CMAP	Daily	Xie and Arkin (1997)	TRMM	Daily	<a href="http://daac.gsfc.nasa.gov/precipitation">http://daac.gsfc.nasa.gov/precipitation</a>
<b>River runoff (m/s)</b>	SAGE (UNESCO)	Monthly	Vörösmarty et al. (1996) Papa et al. (2010)	Vörösmarty et al. (1996)	Monthly	<a href="http://www.sage.wisc.edu/riverdata/">http://www.sage.wisc.edu/riverdata/</a>
<b>Chlorophyll (mg/m<sup>3</sup>)</b>	SeaWiFS	Monthly	Sweeney et al. (2005)	As Shankar et al.	As Shankar et al.	As Shankar et al.

**Table 6.** Details of the biogeochemical model TOPAZ in Vijith et al (2016).

<b>Parameter</b>	<b>Value</b>
Half-saturation coefficient for NH <sub>4</sub> and PO <sub>4</sub> uptake by large phytoplankton	$6 \times 10^{-7}$ mol kg <sup>-1</sup>
Half-saturation coefficient for NO <sub>3</sub> uptake by large phytoplankton	$6 \times 10^{-6}$ mol kg <sup>-1</sup>
Half-saturation coefficient for SiO <sub>4</sub> uptake by large phytoplankton	$1 \times 10^{-6}$ mol kg <sup>-1</sup>
Half-saturation coefficient for NH <sub>4</sub> and PO <sub>4</sub> uptake by small phytoplankton	$2 \times 10^{-7}$ mol kg <sup>-1</sup>
Half-saturation coefficient for NO <sub>3</sub> uptake by small phytoplankton	$2 \times 10^{-6}$ mol kg <sup>-1</sup>
Half-saturation coefficient for PO <sub>4</sub> uptake by diazotrophs	$6 \times 10^{-7}$ mol kg <sup>-1</sup>
Half saturation coefficient for Fe uptake by diazotrophs	$3 \times 10^{-9}$ mol kg <sup>-1</sup>
Maximum Chl:C for small phytoplankton	0.04 g Chl g C <sup>-1</sup>
Maximum Chl:C for large phytoplankton	0.06 g Chl g C <sup>-1</sup>
Maximum Chl:C for diazotrophs	0.04 g Chl g C <sup>-1</sup>
Maximum carbon assimilation rate for large and small phytoplankton	$1.5 \times 10^{-5}$ s <sup>-1</sup>
Maximum carbon assimilation rate for diazotrophs	$6 \times 10^{-6}$ s <sup>-1</sup>
Phytoplankton grazing rate constant	0.19 day <sup>-1</sup>
Depth of remineralization	187 m

**Table 7:** List of prominent groups based on landings along the west coast of India. The landings in column 3 are in thousands of tonnes and the number in parentheses represents the percentage of the total landings for the group along the Indian coast; these data are for 2001–2005. The percentage for the NW (north of 15°N) and SW (south of 15°N) regions during 2001–2005 and 1985–1993. The 2001–2005 data are from CMFRI (2007) and the 1985–1993 data are based on Table 1 of Madhupratap et al (2001); the original data for this period are from CMFRI (1995). The order, from top to bottom, is on the basis of landing. The groups identified with a \$ (#) sign are planktivorous (carnivorous).

Major group	Major species	Landings on west coast during 2001–2005 (Percentage of total landings along Indian coast)	Percentage in NW region during 2001–2005 / 1985–1993	Percentage in SW region during 2001–2005 / 1985–1993
Oil sardine \$	<i>Sardinella longiceps</i>	299 (86.3%)	1.8 / ~0	98.2 / ~100
Perches \$	<i>Nemipterus japonicus</i> , <i>N. Mesoprion</i> , <i>Epinephelus diacanthus</i>	142.9 (76.8%)	42.8 / 28.4	57.2 / 71.6
Penaeid prawns\$	<i>Parapenaeopsis stylifera</i> , <i>Metapenaeus dobsoni</i> , <i>M. monoceros</i> , <i>M. Affinis</i> , <i>Solenocera crassicornis</i> , <i>S. Choprai</i> , <i>S. Indica</i> , <i>S. Hextii</i> , <i>Fenneropenaeus indicus</i>	138 (73.5%)	60.4 / —	39.6 / —
Ribbonfishes #	<i>Trichiurus lepturus</i> , <i>Lepturacanthus savala</i> , <i>Eupleurogrammus intermedius</i> , <i>E. muticus</i>	123.6 (80.6%)	74.8 / 75.1	25.2 / 24.9
Cephalopods #	<i>Loligo duvauceli</i> , <i>Sepia aculeata</i> , <i>S. pharaonis</i>	90.3 (84.8%)	54.1 / 51.7	45.9 / 48.3
Carangids \$	<i>Megalaspis Cordyla</i> , <i>Caranx ignobilis</i> , <i>C. Malabaricus</i> , <i>Decapterus russelli</i> , <i>D. Dayi</i> , <i>D. Macrosoma</i> , <i>Selar crumenophthalmus</i>	85.9 (66.6%)	29.3 / 15.6	70.7 / 84.4
Bombay Duck #	<i>Harpadon nehereus</i> , <i>H. squamosis</i>	79.7 (69.7%)	100 / ~100	0 / ~0
Croakers #	<i>Otolithoides biauritus</i> , <i>Protonibea diacanthus</i> , <i>Johnius carutta</i> , <i>Otolithes argenteus</i> , <i>O. ruber</i>	79.7 (66.2%)	86.3 / 81.1	13.7 / 18.9
Mackerel \$	<i>Rastrelliger kanagurta</i> , <i>R. faughni</i>	74.3 (65.4%)	84.4 / 84.8	15.6 / 15.2
Tunas#	<i>Euthynnus affinis</i> , <i>Auxis thazard</i> , <i>A. Rochei</i> , <i>Katsuwonus pelamis</i> , <i>Thunnus tonggol</i> , <i>T. albacares</i>	31.7 (77.3%)	27.8 / 23.3	72.2 / 76.7
Catfishes #	<i>Tachysurus Thalassinus</i> , <i>T. Tenuispinis</i> , <i>T. jella</i>	31.3 (60.8%)	97.2 / 71.2	2.8 / 28.8

Seerfishes#	<i>Scomberomorus commerson, S. Guttatus, S. Lineolatus, Acanthocybium solandri</i>	28.7 (62.3%)	56.2 / 58.2	43.8 / 41.8
Elasmobranchs #	<i>Sharks (Scoliodon laticaudus, Rhizoprionodon acutus, Carcharhinus sorrah), Rays (Dasyatis bleekeri, D. Kuhlii, Patinachus sephen), Skates (Rhynchobatus djiddensis, Rhinobatos granulatus)</i>	28.5 (51.5%)	77.7 / 78.5	22.3 / 21.5
Pomfrets #	<i>Pampus argenteus, Parastromateus niger, P. chinensis</i>	18.8 (46.7%)	83.7 / 83.4	16.3 / 16.6

**Table 8** : Total landings for a subset of the groups listed in Table 7, but for the states constituting the NW (Gujarat and Maharashtra) and SW (Goa, Karnataka, and Kerala) regions. The data are shown for 1986-2005 and 2001-2005. Note that not all groups are present in the EEZ off all the states. The data sources are as follows: Gujarat (CMFRI, 2007c), Maharashtra (CMFRI, 2007f), Goa (CMFRI, 2007b), Karnataka (CMFRI, 2007d), and Kerala (CMFRI, 2007e).

Major fish group	Northwest coast (NW)		Southwest coast (SW)		
	Gujarat	Maharashtra	Goa	Karnataka	Kerala
	1986–2005 (2001–2005)	1986–2005 (2001–2005)	1986–2005 (2001–2005)	1986–2005 (2001–2005)	1986–2005 (2001–2005)
Bombay Duck	65.28 (54.55)	24.75 (25.60)	—	—	—
Croakers	61.69 (40.81)	25.88 (28.05)	—	3.69 (3.28)	—
Ribbon fishes	42.69 (52.23)	30.75 (39.95)	1.6 (2.11)	6.29 (9.77)	13.89 (19.15)
Elasmobranchs	17.31 (12.30)	—	—	—	—
Catfishes	16.13(19.32)	—	—	—	—
Panaeid Prawns	27.28 (24.74)	50.16 (58.65)	2.77 (2.25)	—	49.16 (38.61)
Tunas	—	—	0.99 (1.66)	—	16.78 (19.05)
Carangids	—	12.49 (13.76)	7.6 (5.61)	18.01 (13.50)	55.96 (41.65)
Mackerel	—	18.72 (9.83)	16.39 (6.92)	31.39 (18.32)	57.67 (36.75)
Oil Sardine	—	—	13.54 (31.61)	26.40 (44.96)	120.31 (216.94)



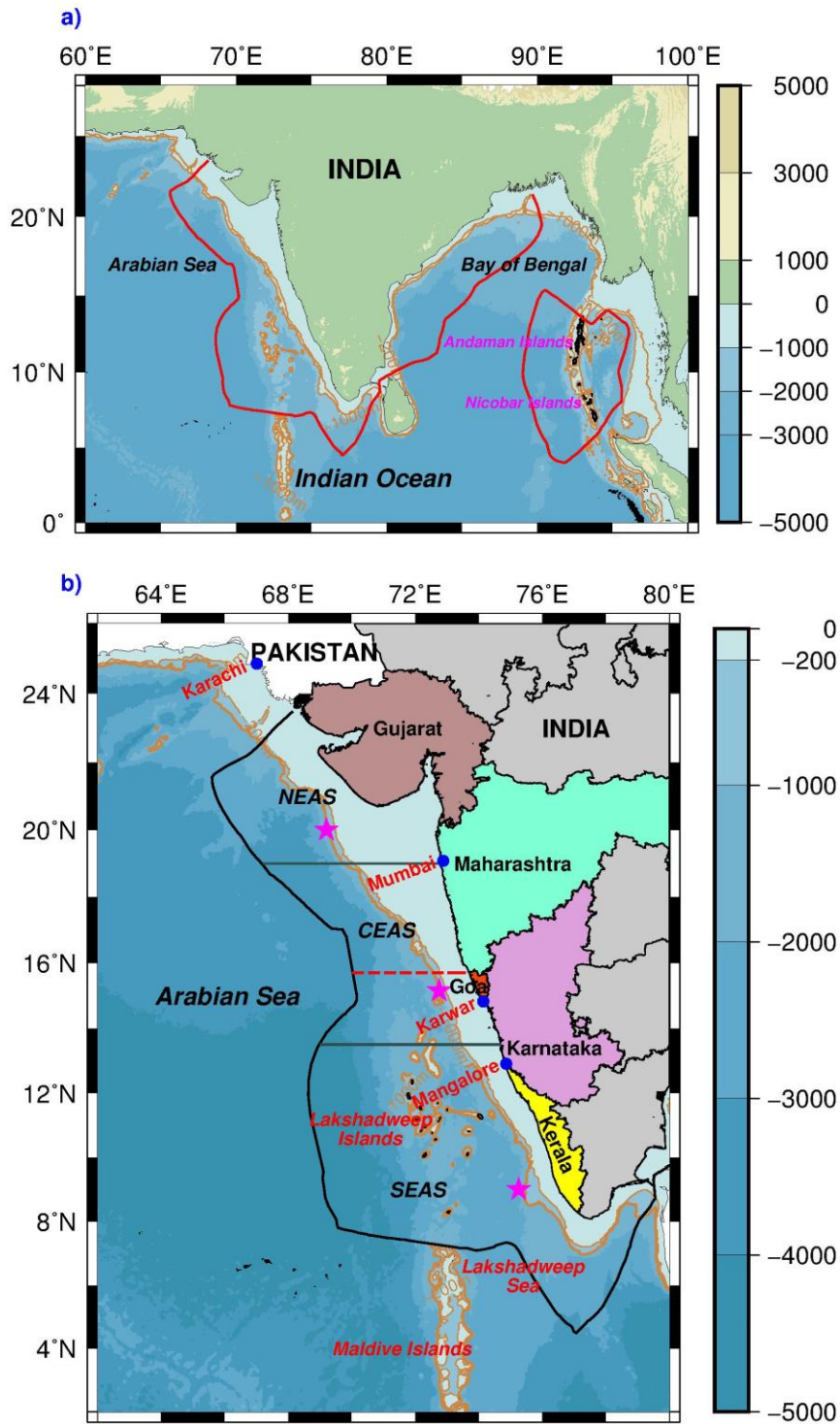


**Fig. 1:** Map showing the region of interest. (a) The Indian Ocean, with the Indian EEZ marked by a solid red curve. The colour fill shows the ocean topography in metres (Sindhu et al, 2007) and the brown curve marks the 1000 m isobath. (b) The Indian west-coast region or the eastern Arabian Sea (EAS), with the state boundaries marked. Gujarat and Maharashtra constitute the northwest (NW) region and Goa, Karnataka, and Kerala the southwest (SW) region, with a dividing line, which occurs at the northern boundary of Goa (just south of 16°N), shown by the dashed red line. The rough division between the NEAS, CEAS, and SEAS is shown by the solid black lines. Note the broad shelf off Maharashtra, particularly off Mumbai. The magenta stars show the ADCP mooring locations.

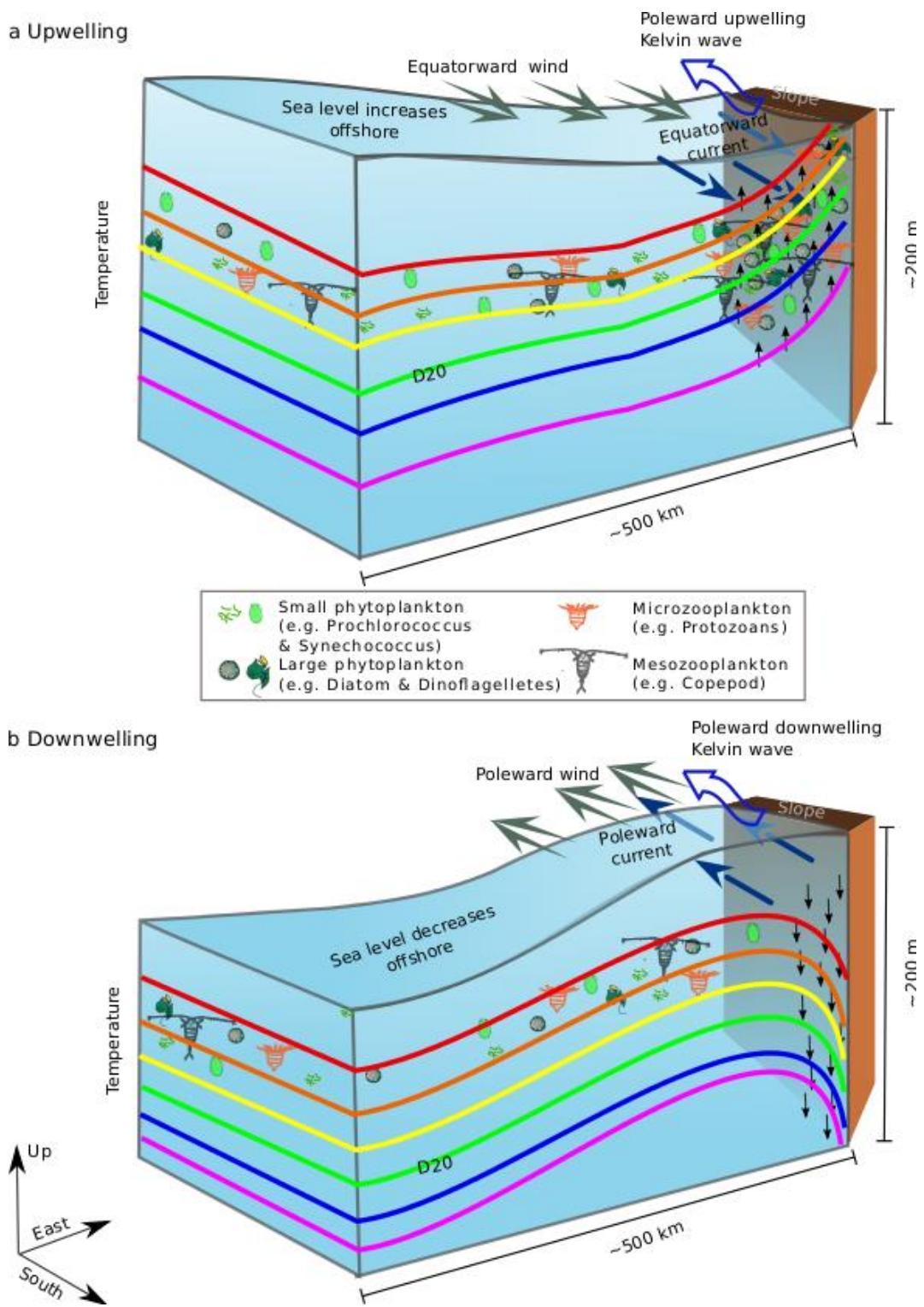


**Fig. 2.** Schematic depicting (a) upwelling and (b) downwelling at an eastern boundary; the coast is depicted by the brown wall on the right. The curves of different colours are isotherms of different temperatures. Upwelling leads to vertical transport of nutrient rich sub-surface water towards the surface and away from the surface during downwelling. Hence, these curves can also be considered as contours of nutrients. Upwelling (downwelling) is favourable (unfavourable) for plankton growth as indicated with scatter of different types of phytoplankton and zooplankton. Though the schematic suggests a direct forcing of upwelling and downwelling (vertical velocity is indicated by the vertical black arrows) by alongshore winds (big, grey arrows), these processes can be remotely forced via coastal Kelvin waves too (curved, blue arrows). Note that the Kelvin wave propagates poleward along the eastern boundary (coast on its right in the northern hemisphere) irrespective of the direction of the alongshore wind and current. The direction of coastal current is shown using solid blue arrows.

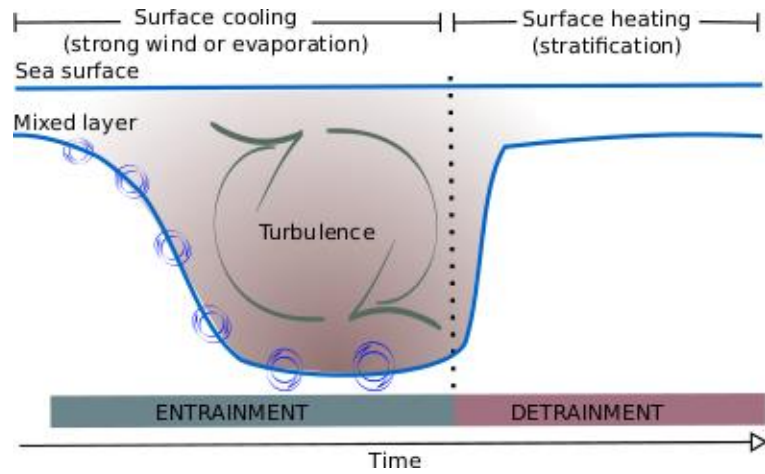


**Fig. 3.** Schematic diagram depicting entrainment and detrainment. The blue whorls represent the small eddies that are responsible for mixing. Note that detrainment is a sudden process compared to entrainment.

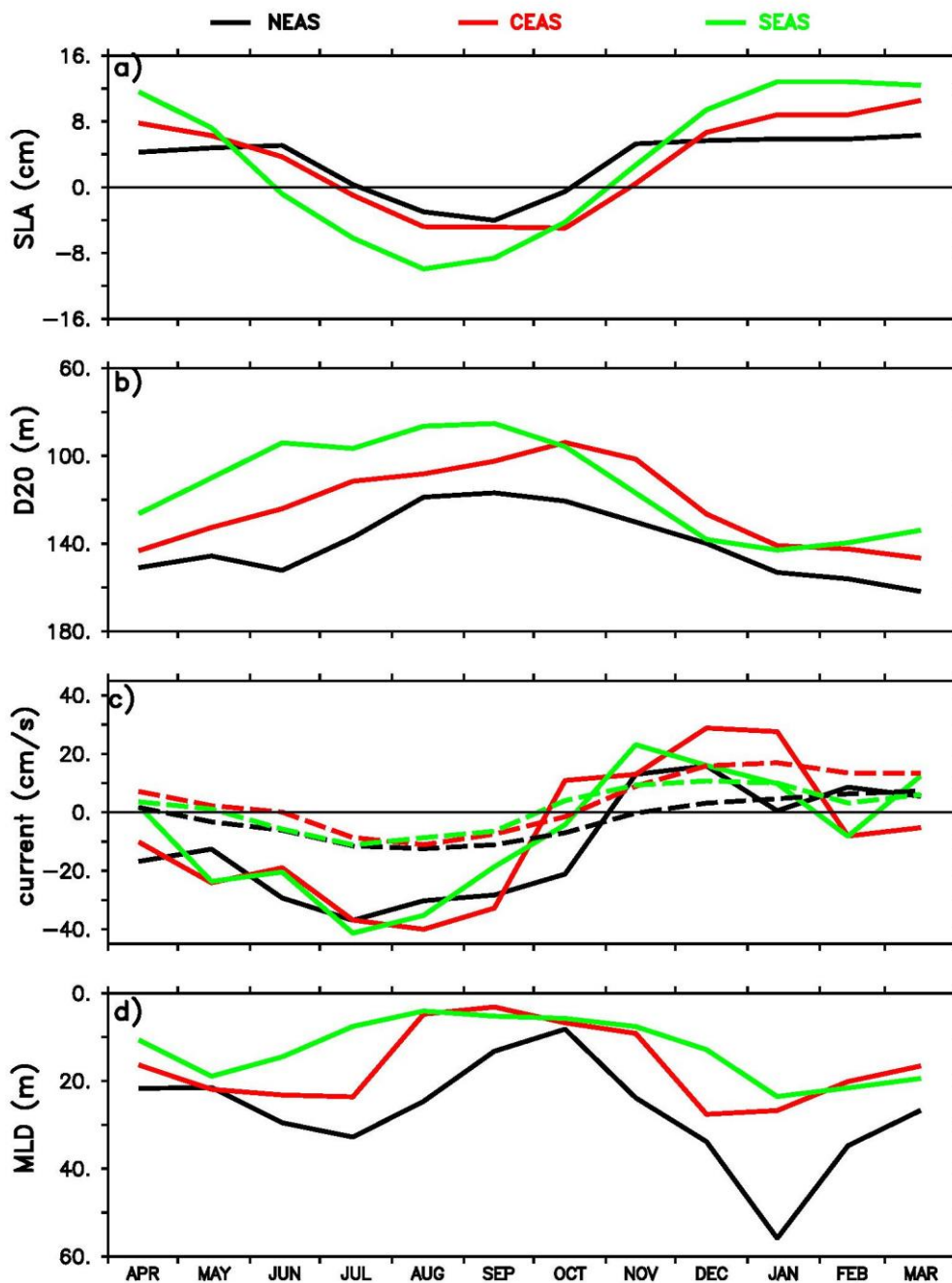


**Fig. 4.** Seasonal cycle of (a) sea-level anomaly (SLA, cm; AVISO, 1996), (b) depth of 20°C isotherm (D20, m; Chatterjee et al, 2012), (c) alongshore current (cm/s), and (d) mixed-layer depth (MLD, m; Chatterjee et al, 2012) at the three ADCP mooring locations. The black, red, and green curves are for the moorings at 20°N (NEAS), 15.5°N (CEAS), and 9°N (SEAS), respectively. In the panel for alongshore current, the solid curves are for the ship drifts (Mariano et al, 1995) and the dashed curves for the OSCAR currents (Bonjean and Lagerloef, 2002).

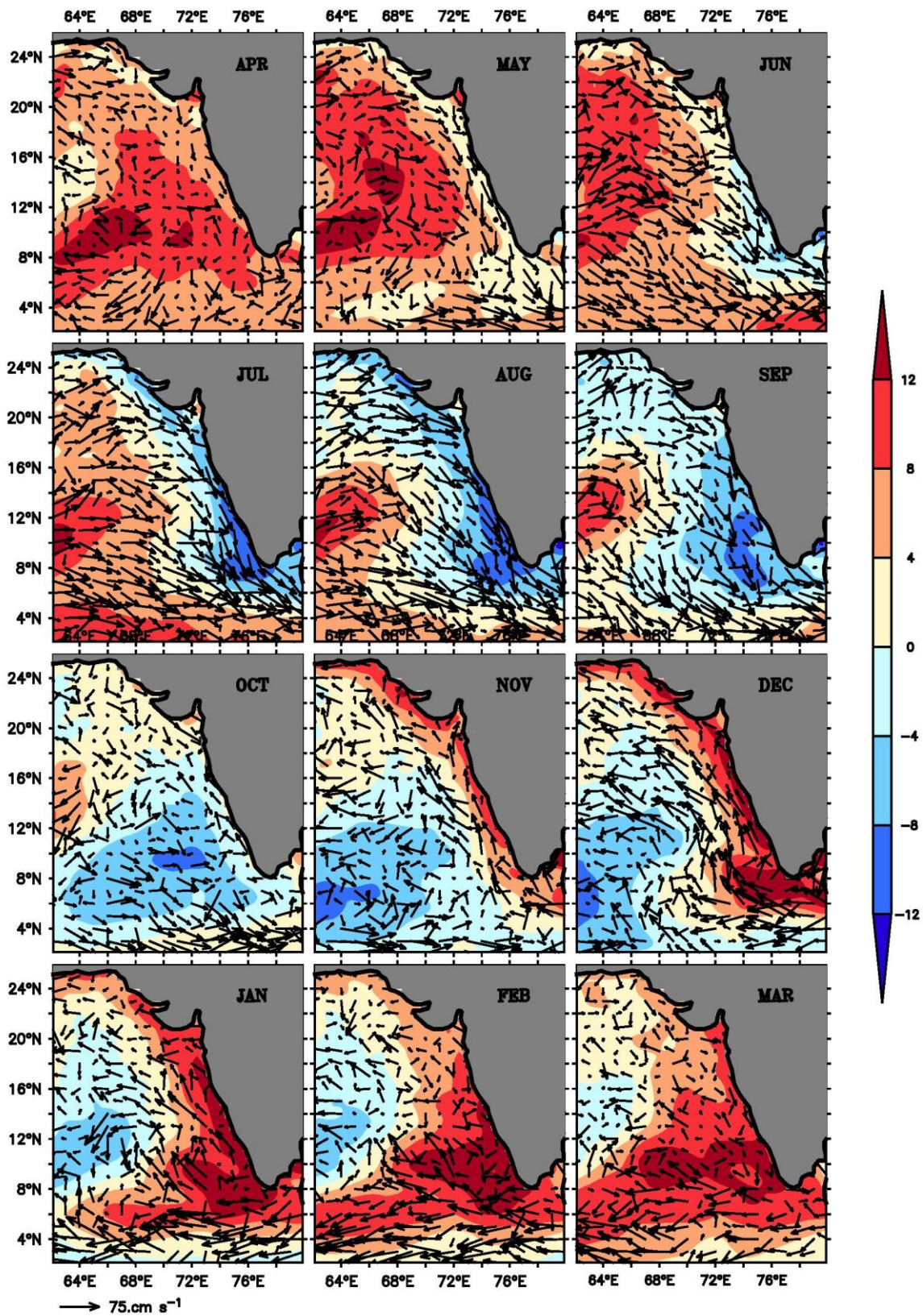


**Fig. 5.** Spatial maps of SLA (cm, colour fill) and the near-surface currents (overlaid vectors) from ship drifts (cm/s; Mariano et al, 1995). The vector scale is shown at the bottom left corner.

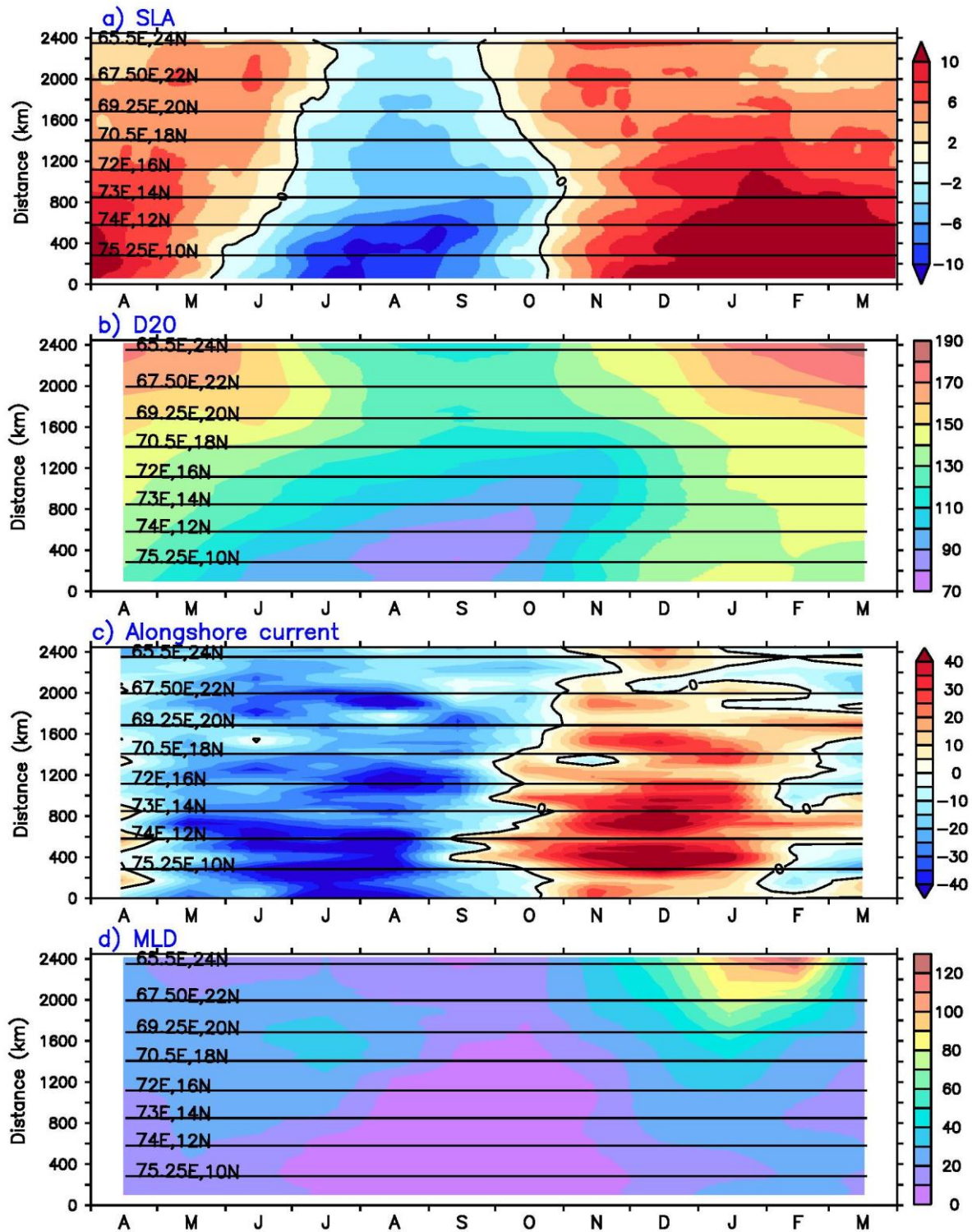


**Fig. 6.** Variation along the 1000 m isobath of (a) SLA (cm; AVISO, 1996), (b) D20 (m; Chatterjee et al, 2012), (c) alongshore current from ship drifts (cm/s; Mariano et al, 1995), and (d) MLD (m; Chatterjee et al, 2012). The abscissa is time and the ordinate is distance (km) along the 1000 m isobath from 8°N. The data are available at different resolutions and are plotted at the original resolution following interpolation to the appropriate longitude on the 1000 m isobath. The horizontal lines mark the latitudes, which are unequally spaced since the distance is measured along the isobath.

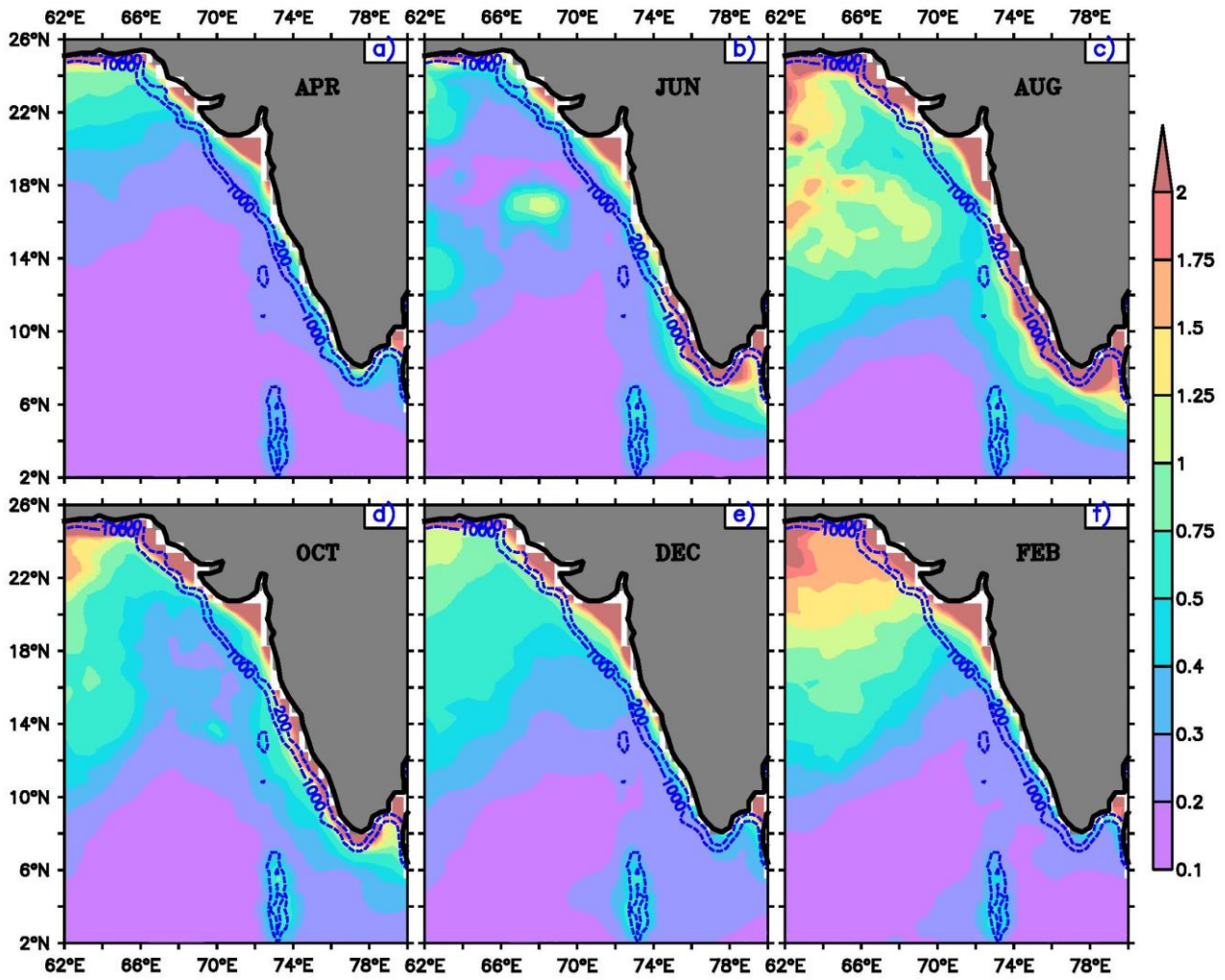


**Fig. 7.** Bimonthly maps of the observed climatology of chlorophyll-*a* ( $\text{mg}/\text{m}^3$ ; Lévy et al, 2006) in the EAS. (a) April; (b) June; (c) August; (d) October; (e) December; (f) February. The dashed blue curves represent the 200 m (shelf break) and 1000 m isobaths.

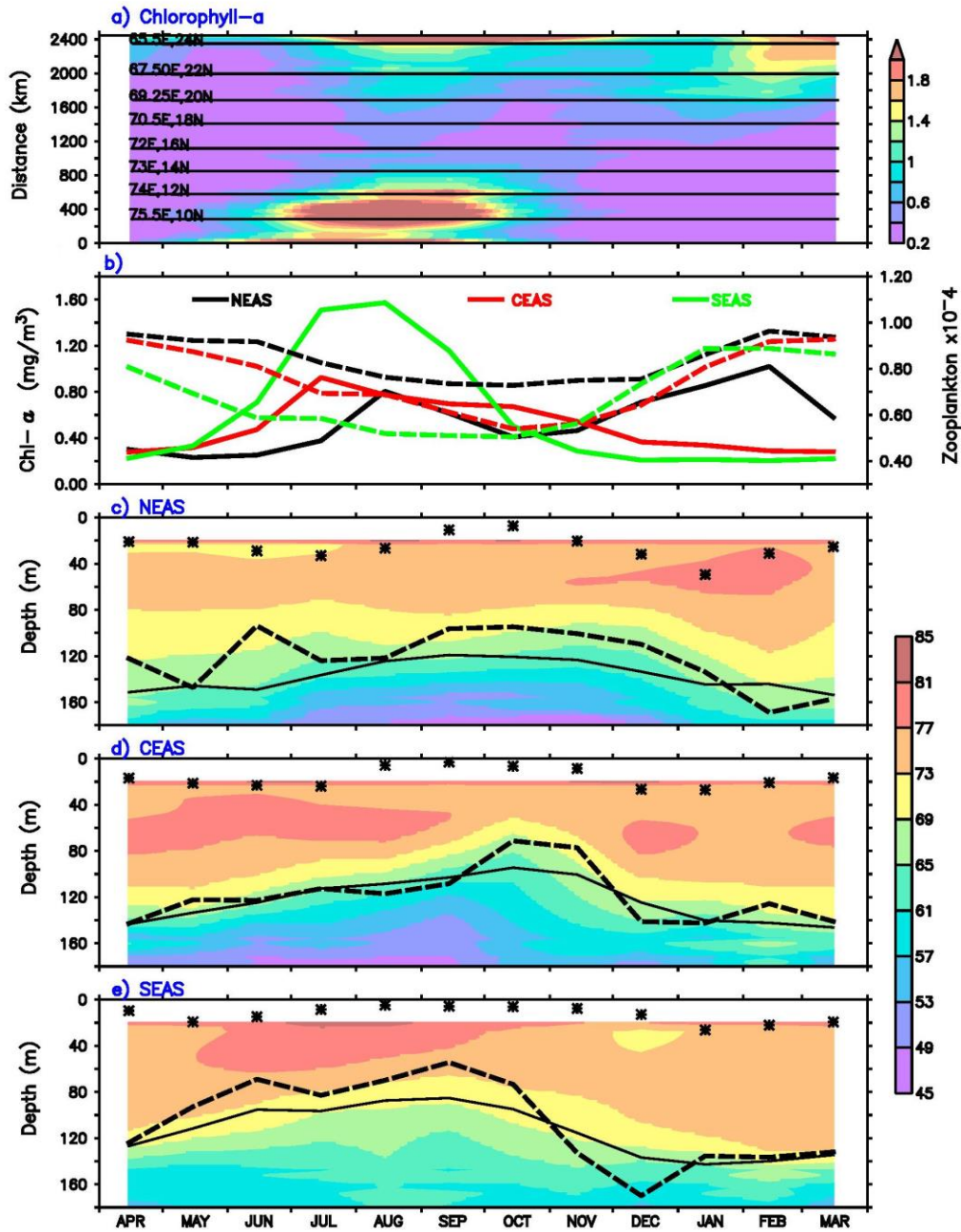


**Fig. 8.** (a) SeaWIFS chlorophyll-*a* concentration ( $\text{mg}/\text{m}^3$ ) plotted as a function of distance (km) along the 1000 m isobath from south to north (ordinate, measured from  $8^\circ\text{N}$ ) and time (abscissa). The horizontal lines mark the latitudes, which are unequally spaced since the distance is measured along the isobath. (b) SeaWIFS chlorophyll-*a* concentration ( $\text{mg}/\text{m}^3$ ; solid curves) plotted as a function of time at the three ADCP mooring locations. As in Fig. 4a–d, the black, red, and green curves are for the moorings at  $20^\circ\text{N}$  (NEAS),  $15.5^\circ\text{N}$  (CEAS), and  $9^\circ\text{N}$  (SEAS), respectively. Also shown is the integral of the ADCP backscatter (dashed curves) over the depth of the ocean above D20 (see Fig. 6b); these curves are also at the ADCP mooring locations. The ADCP backscatter (dB) is a proxy for zooplankton biomass; therefore, its integral over the depth range from the surface to D20 (arbitrary units) is a proxy for the zooplankton standing stock in the upper ocean. Since ADCP data are not available in the top  $\sim 20$  m, the value in the top bin is extrapolated to the surface for computing the integral. (c) ADCP backscatter (dB), a proxy for zooplankton biomass, is plotted as a function of time (abscissa) and depth (m, ordinate) at the mooring location at  $20^\circ\text{N}$  (NEAS). The solid curve denotes D20 and the dashed curve denotes the 0.6 ml/l oxygen curve based on the oxygen data from the World Ocean Atlas (Garcia et al, 2014); the asterisks denote the MLD (m). D20 and MLD are based on the temperature and salinity data from Chatterjee et al (2012); the MLD was estimated using the density criterion of Shenoi et al (2004). (d) As in (c), but for the mooring at  $15.5^\circ\text{N}$  (CEAS). (e) As in (c), but for the mooring at  $9^\circ\text{N}$  (SEAS). The oxygen curve in this panel is plotted for 1.2 ml/l instead of 0.6 ml/l at  $20^\circ\text{N}$  and  $15.5^\circ\text{N}$ .



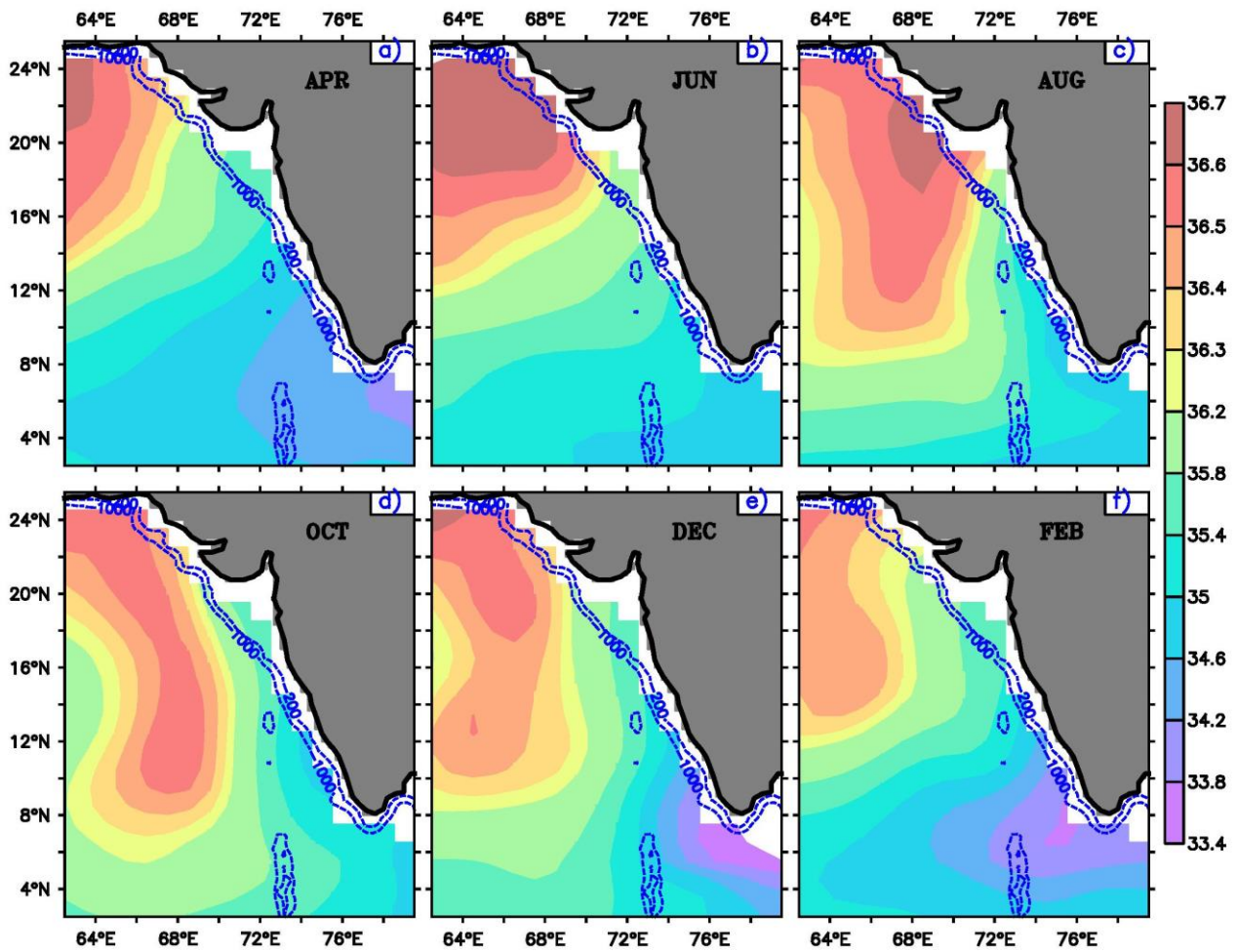


**Fig. 9.** Bimonthly maps of the observed climatology of surface salinity (psu; Chatterjee et al, 2012) in the EAS. (a) April; (b) June; (c) August; (d) October; (e) December; (f) February. The dashed blue curves represent the 200 m (shelf break) and 1000 m isobaths.

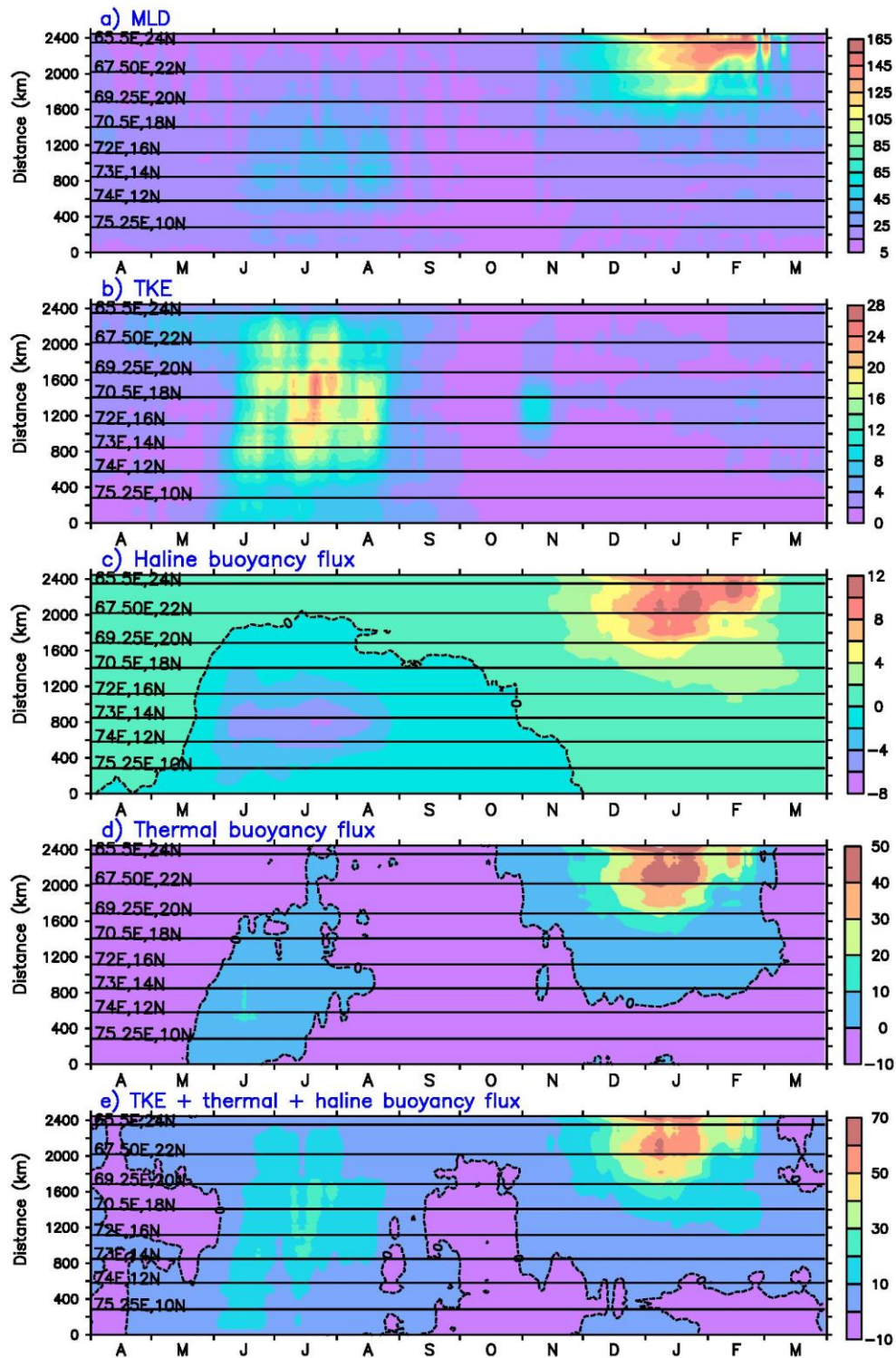


**Fig. 10.** Variation along the 1000 m isobath of (a) MLD (m; repeats Fig. 4d for convenience), (b) the turbulent kinetic energy (TKE) input by the wind, (c) haline buoyancy flux, (d) thermal buoyancy flux, and (e) the sum of the wind-forced TKE and thermal and haline buoyancy fluxes along the 1000 m isobath during April–March. The unit for panels b–e is  $10^{-7} \text{ m}^3/\text{s}^3$  (the values have been multiplied by  $10^7$  before plotting). The thermal and haline buoyancy fluxes were smoothed with a 15-day running mean to damp the noise in the daily fields. The abscissa is time and the ordinate gives the distance (in hundreds of kilometres) poleward from  $8^\circ\text{N}$ ; the latitude and longitude are marked by horizontal lines. This figure extends the results of Shankar et al (2016; see their Figure 14) to the entire year and the entire EAS.

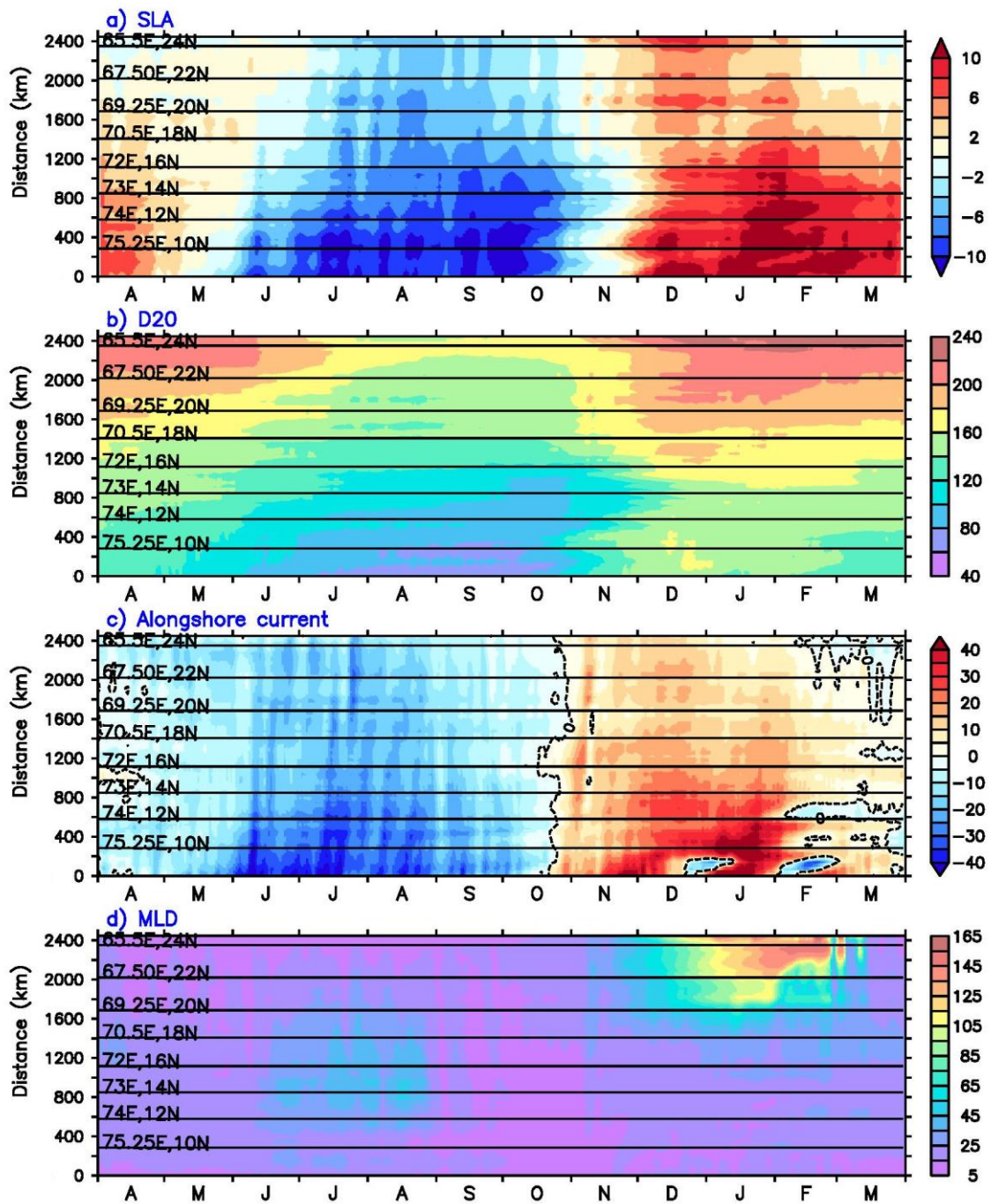


**Fig. 11.** Variation along the 1000 m isobath of the model (MOM; Shankar et al, 2016) (a) SLA (cm), (b) D20 (m), (c) alongshore current (cm/s), and (d) MLD (m). The abscissa is time and the ordinate is distance (km) along the 1000 m isobath from 8°N. The data are available at different resolutions and are plotted at the original resolution following interpolation to the appropriate longitude on the 1000 m isobath. The horizontal lines mark the latitudes, which are unequally spaced since the distance is measured along the isobath.

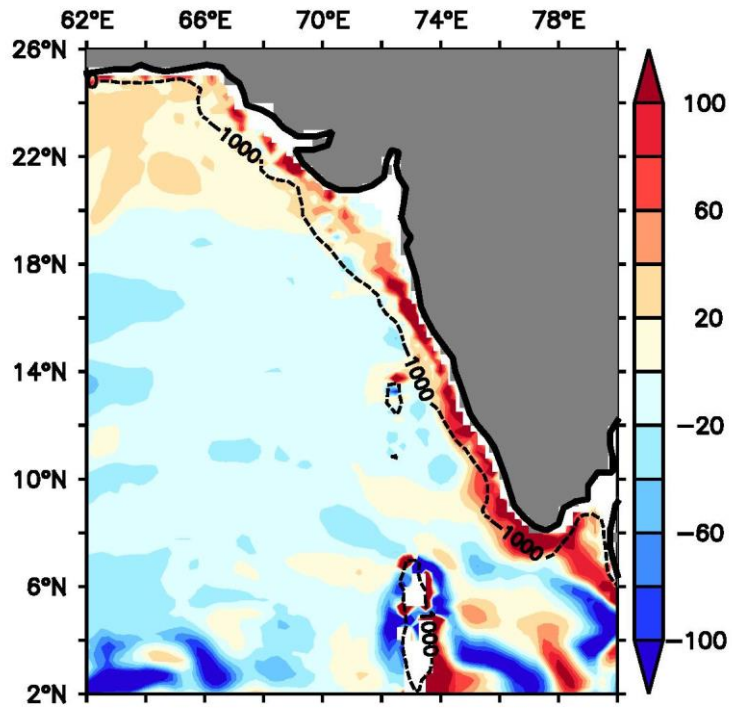


**Fig. 12.** Cumulation of vertical velocity (m) at 30 m depth during 1-July to 30-September in the EAS. The cumulation is based on the model simulation of Shankar et al (2016). Red (blue) colour denotes upwelling (downwelling) or an upward (downward) vertical velocity.

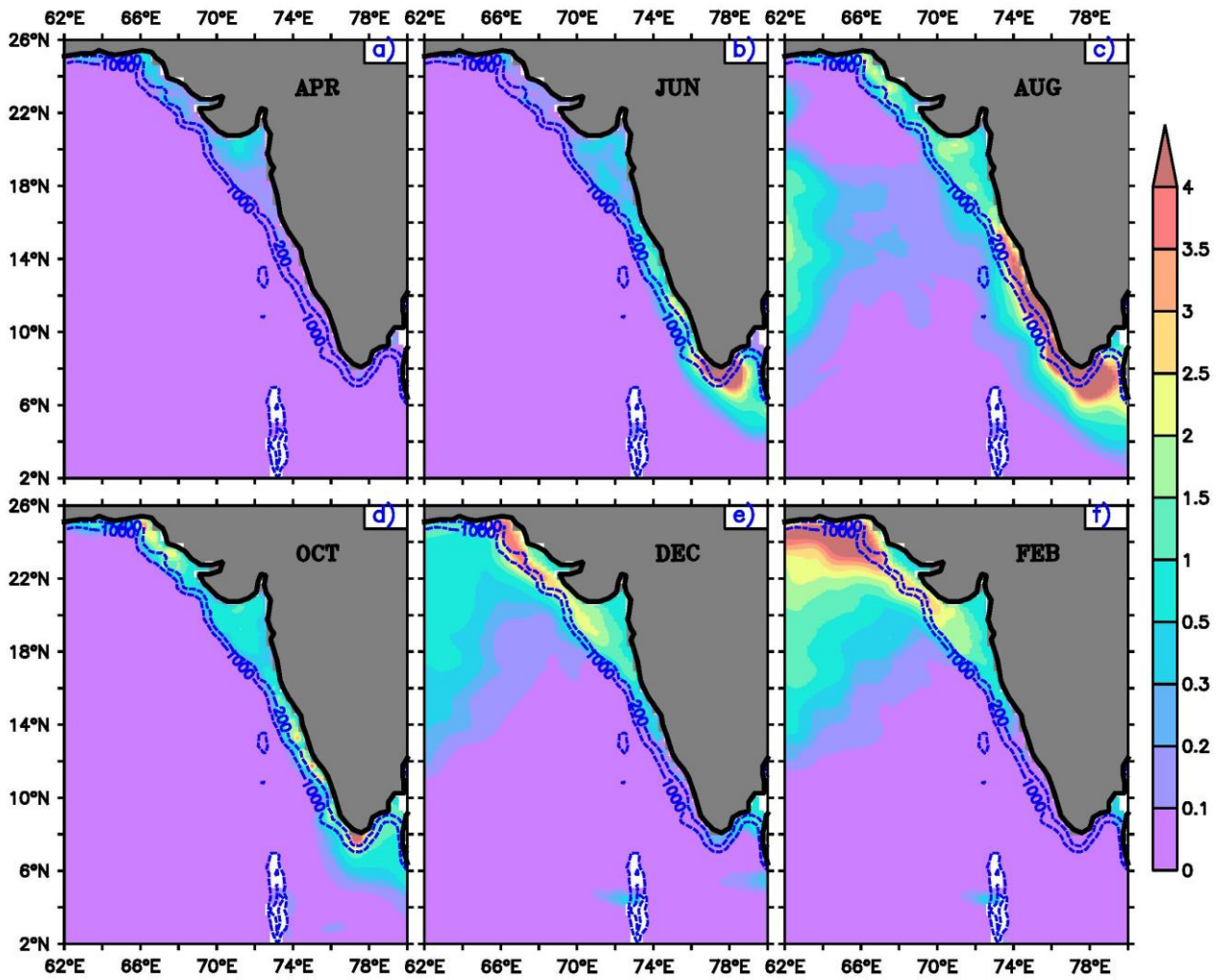


**Fig. 13.** Bimonthly maps of the model climatology of surface nitrate ( $\mu\text{mol/kg}$ ) in the EAS. (a) April; (b) June; (c) August; (d) October; (e) December; (f) February. The dashed blue curves represent the 200 m (shelf break) and 1000 m isobaths. These results are based on the TOPAZ simulation reported by Vijith et al (2016), but they showed the results only for the NEAS during October–March.

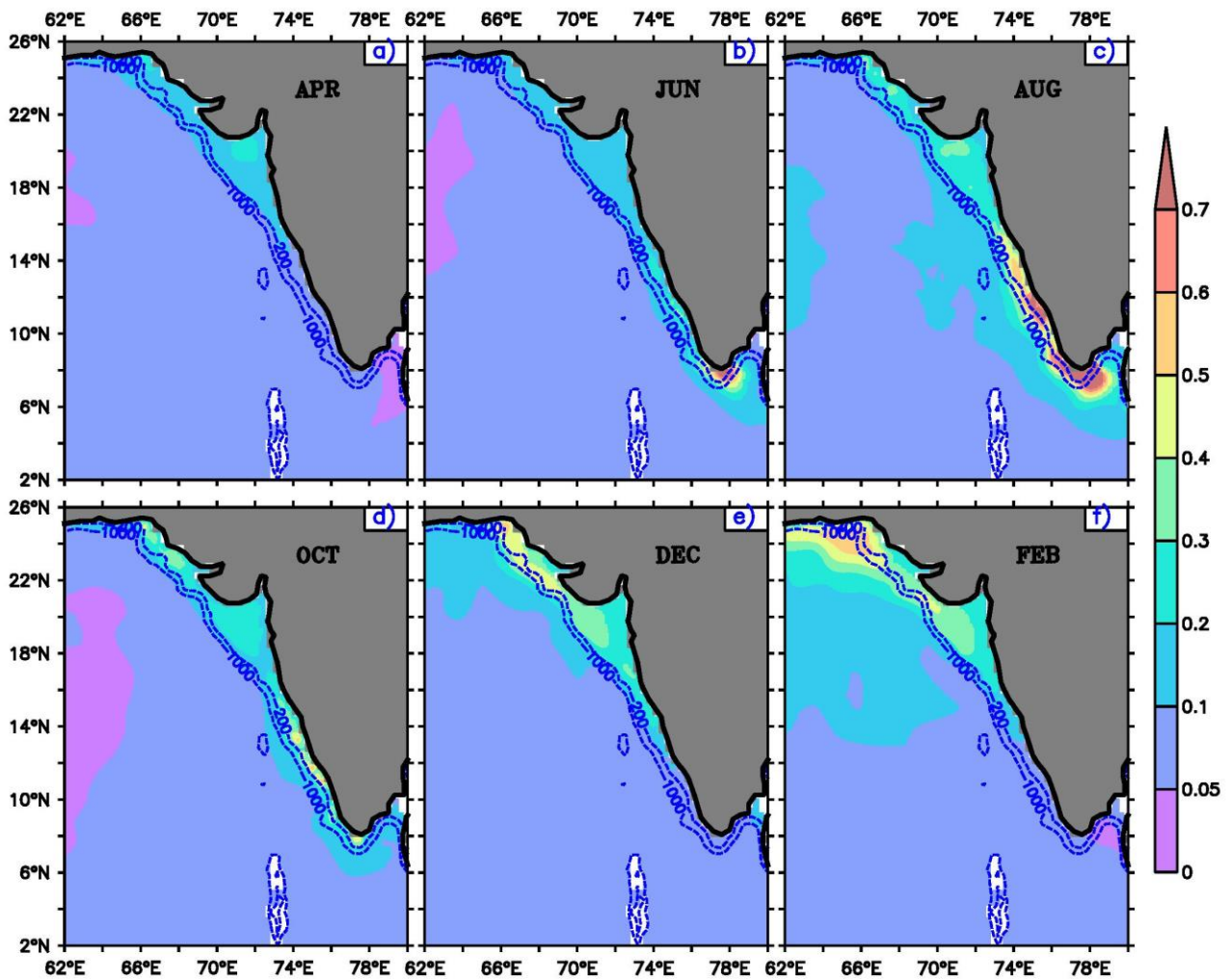


**Fig. 14.** Bimonthly maps of the model climatology of surface phosphate ( $\mu\text{mol/kg}$ ) in the EAS. (a) April; (b) June; (c) August; (d) October; (e) December; (f) February. The dashed blue curves represent the 200 m (shelf break) and 1000 m isobaths. These results are based on the TOPAZ simulation reported by Vijith et al (2016), but they showed the results only for the NEAS during October–March.

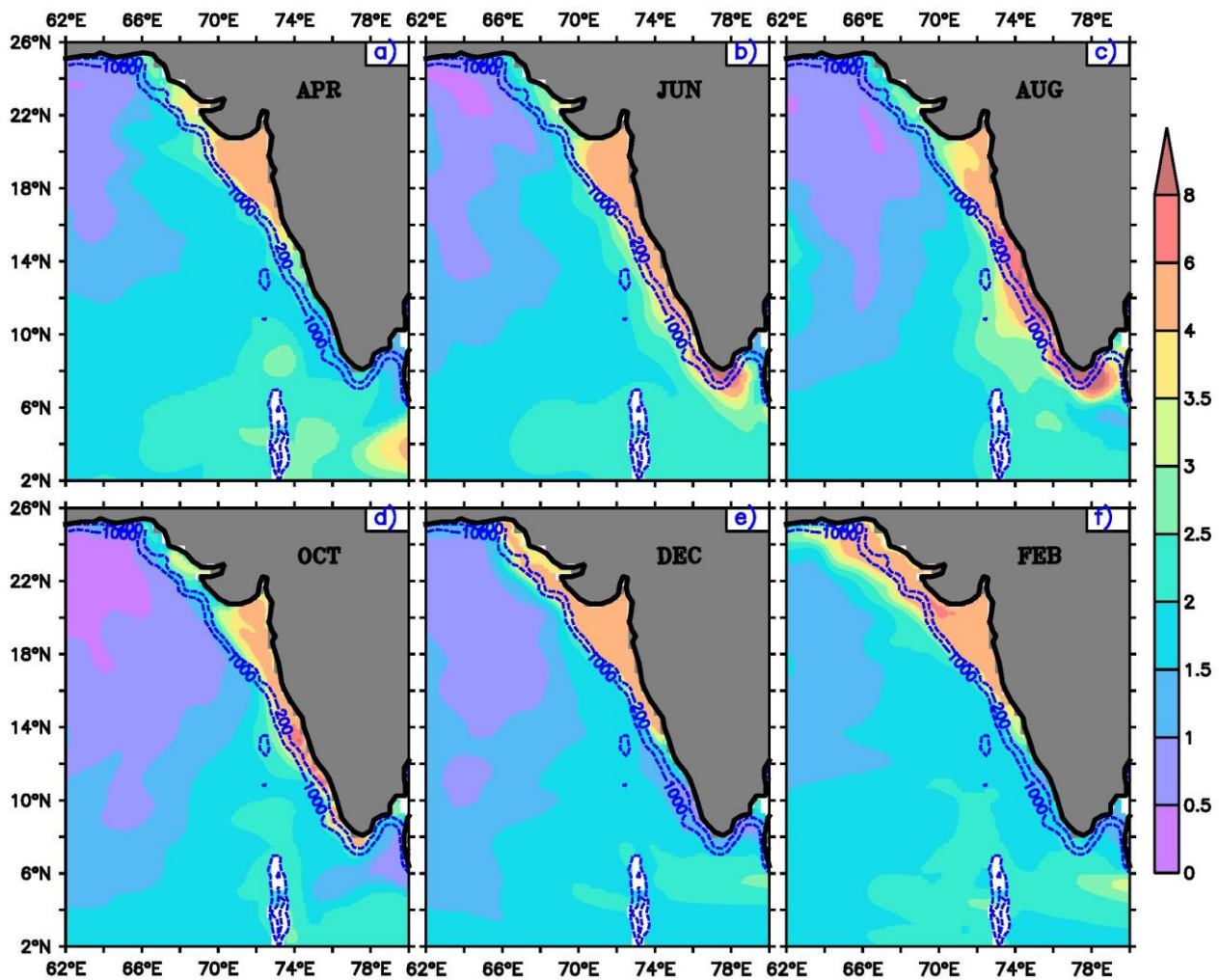


**Fig. 15.** Bimonthly maps of the model climatology of surface silicate ( $\mu\text{mol/kg}$ ) in the EAS. (a) April; (b) June; (c) August; (d) October; (e) December; (f) February. The dashed blue curves represent the 200 m (shelf break) and 1000 m isobaths. These results are based on the TOPAZ simulation reported by Vijith et al (2016), but they showed the results only for the NEAS during October–March.

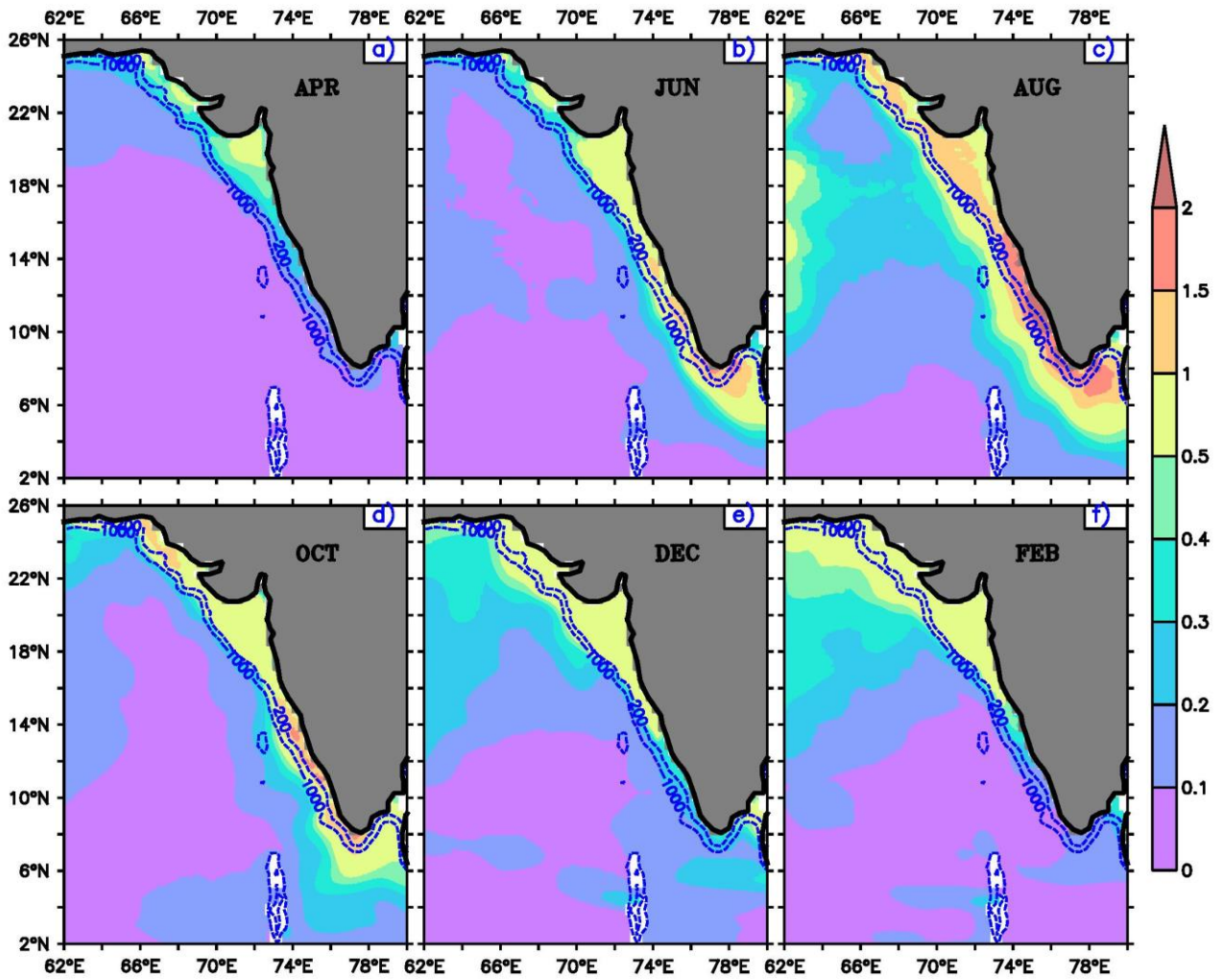


**Fig. 16.** Bimonthly maps of the model climatology of surface chlorophyll ( $\mu\text{g}/\text{kg}$ ) in the EAS. (a) April; (b) June; (c) August; (d) October; (e) December; (f) February. The dashed blue curves represent the 200 m (shelf break) and 1000 m isobaths. These results are based on the TOPAZ simulation reported by Vijith et al (2016), but they showed the results only for the NEAS during October–March.



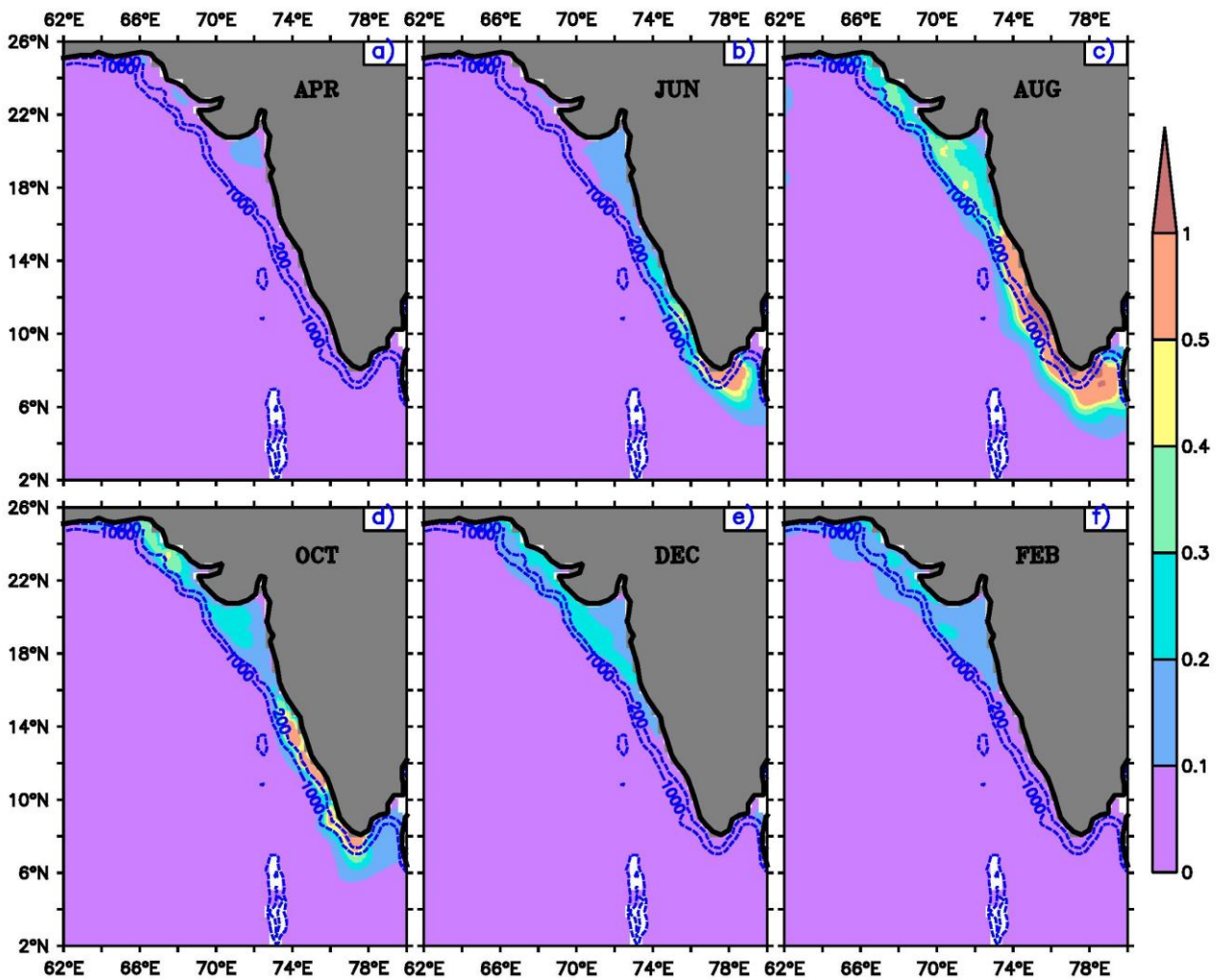


**Fig. 17.** Bimonthly maps of the model climatology of surface chlorophyll ( $\mu\text{g}/\text{kg}$ ) due to large phytoplankton in the EAS. (a) April; (b) June; (c) August; (d) October; (e) December; (f) February. The dashed blue curves represent the 200 m (shelf break) and 1000 m isobaths. These results are based on the TOPAZ simulation reported by Vijith et al (2016), but they showed the results only for the NEAS during October–March.

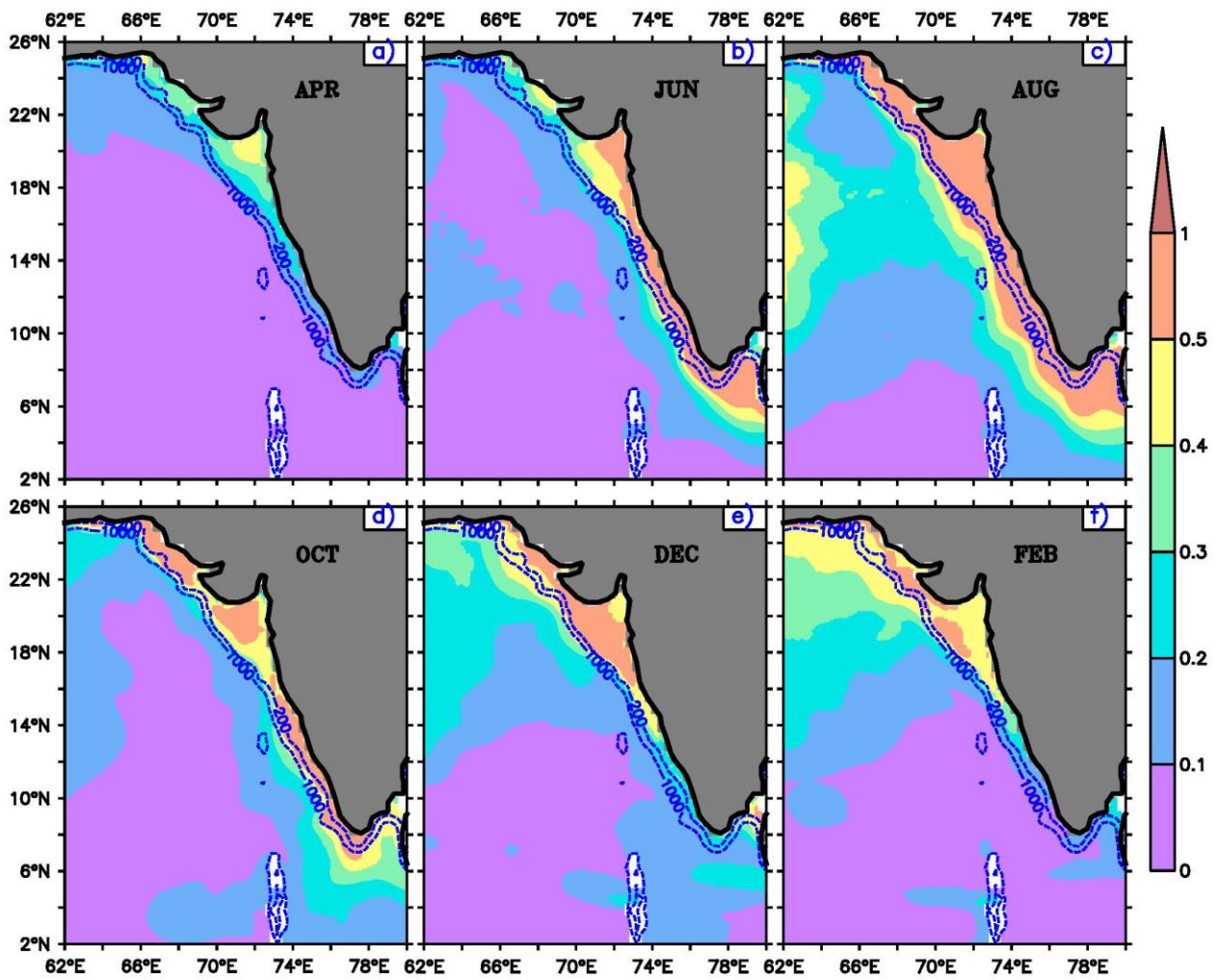


**Fig. 18.** Bimonthly maps of the model climatology of surface chlorophyll ( $\mu\text{g/kg}$ ) due to small phytoplankton in the EAS. (a) April; (b) June; (c) August; (d) October; (e) December; (f) February. The dashed blue curves represent the 200 m (shelf break) and 1000 m isobaths. These results are based on the TOPAZ simulation reported by Vijith et al (2016), but they showed the results only for the NEAS during October–March.

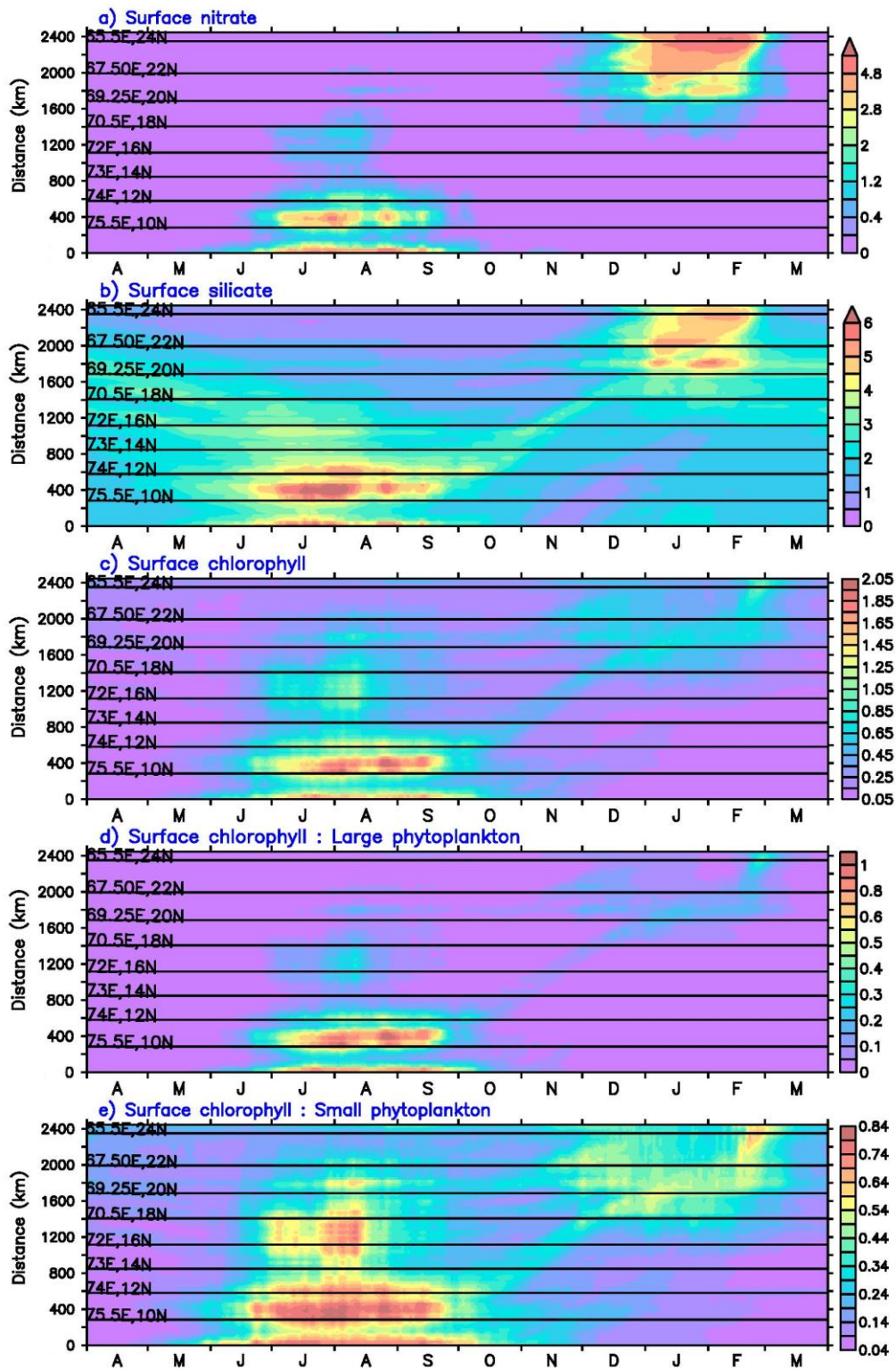
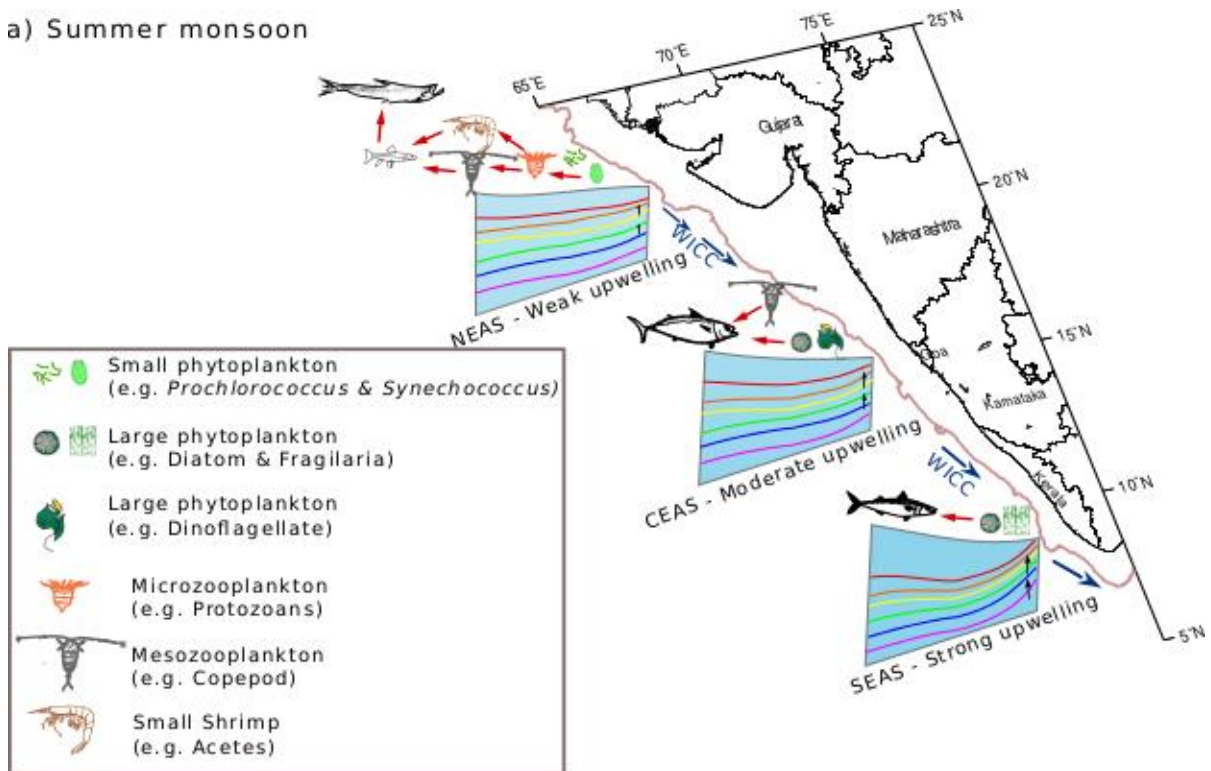


**Fig. 19.** Variation along the 1000 m isobath of the model (TOPAZ; Vijith et al, 2016) (a) surface nitrate ( $\mu\text{mol}/\text{kg}$ ), (b) surface silicate ( $\mu\text{mol}/\text{kg}$ ), (c) surface chlorophyll ( $\mu\text{g}/\text{kg}$ ), (d) chlorophyll due to large phytoplankton at surface ( $\mu\text{g}/\text{kg}$ ), and (e) chlorophyll due to small phytoplankton at surface ( $\mu\text{g}/\text{kg}$ ). The abscissa is time and the ordinate is distance (km) along the 1000 m isobath from  $8^\circ\text{N}$ . The data are available at different resolutions and are plotted at the original resolution following interpolation to the appropriate longitude on the 1000 m isobath. The horizontal lines mark the latitudes, which are unequally spaced since the distance is measured along the isobath. These results are based on the TOPAZ simulation reported by Vijith et al (2016), but they showed the results only for the NEAs during October–March.

a) Summer monsoon



b) Winter monsoon

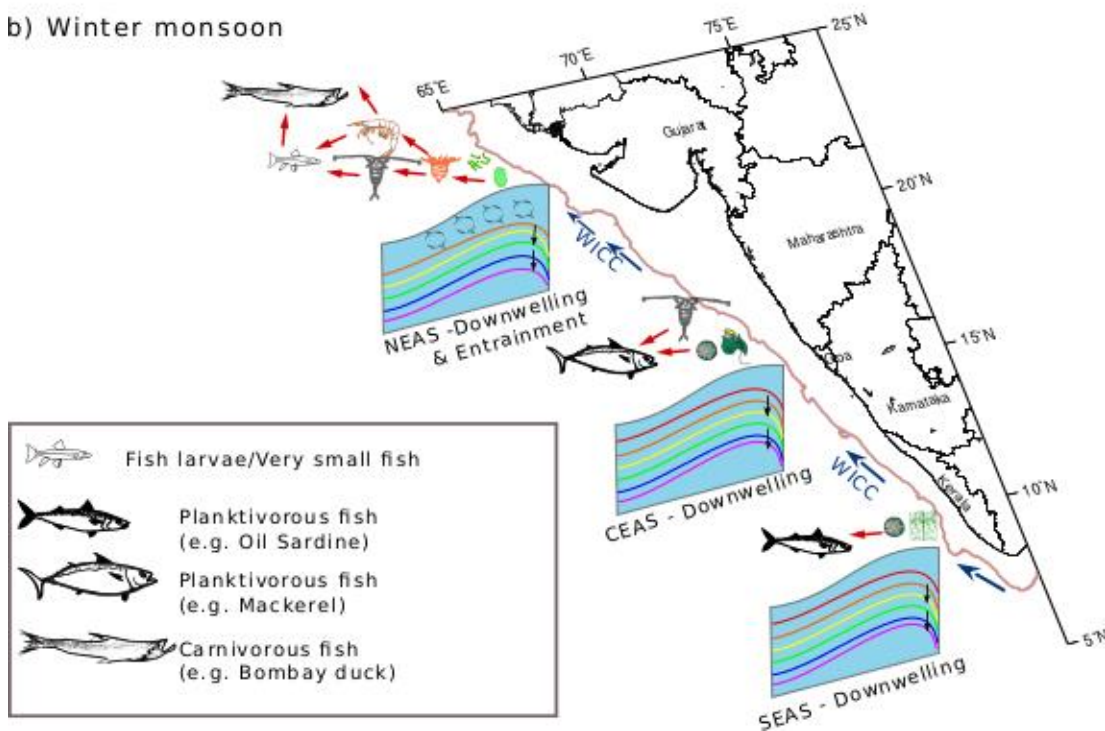


**Fig. 20.** Schematic diagram summarizing the spatial variation of major physical processes and the response of the ecosystem in the EAS during the (a) summer monsoon and (b) winter monsoon. The schematic shows dominant food chain in the SEAS, CEAS, and NEAS as discussed in this paper. Note that the quantity of fish catch reduces in the SEAS and CEAS after the withdrawal of the summer monsoon. Nevertheless, the nature of the dominant fishery during winter monsoon seems to remain the same as that during the summer monsoon.

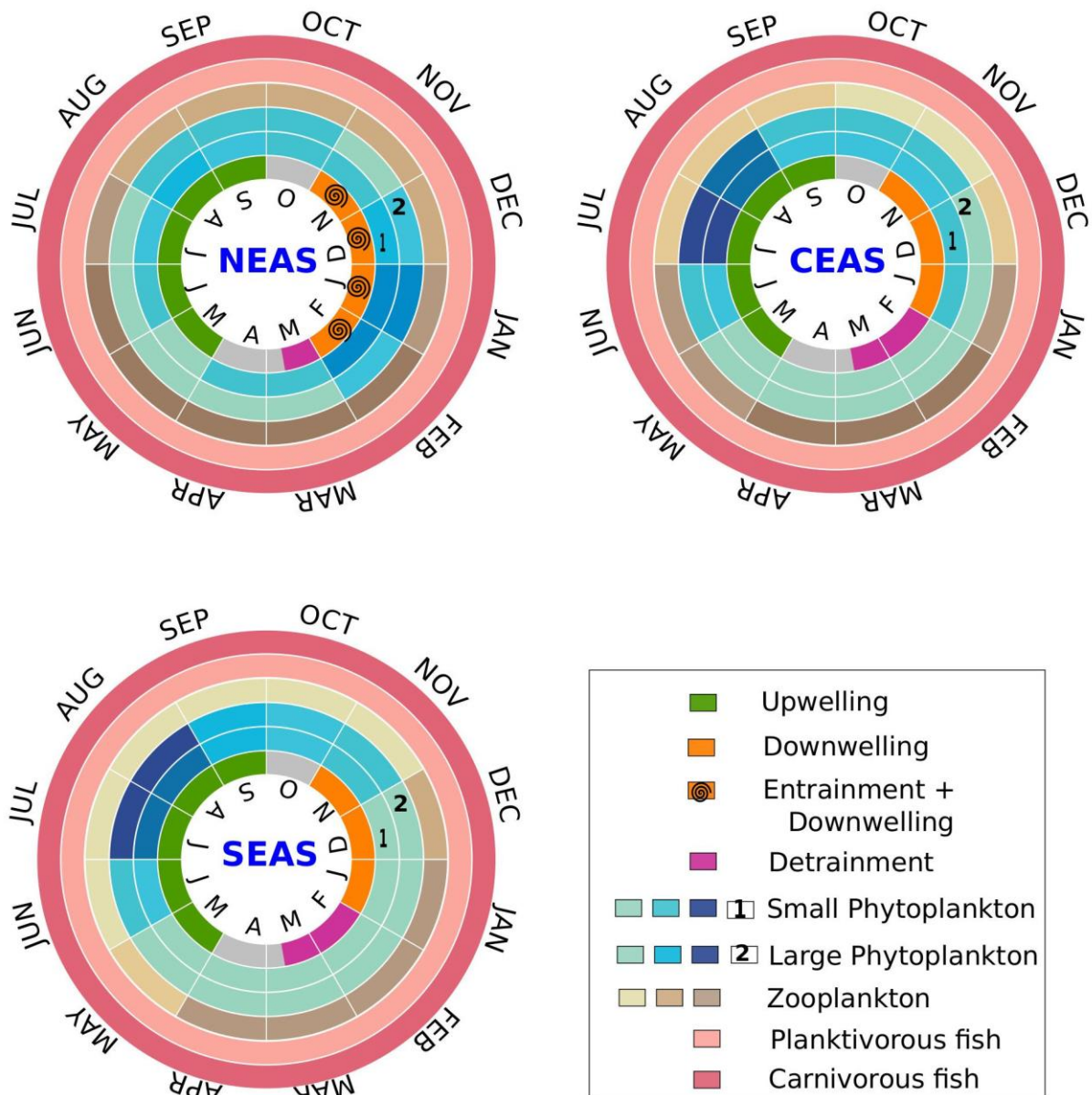


**Fig. 21.** Schematic diagram summarizing the temporal variation of major physical processes and the response of the ecosystem in the NEAS, CEAS, and SEAS. The concentric rings represent the physical forcing (innermost ring), small and large phytoplankton (the second and third rings), zooplankton standing stock (fourth ring), and planktivorous (fifth ring) and carnivorous (outermost ring) fish. The strength of the forcing and the phytoplankton biomass and zooplankton standing stock vary with season and the lighter (darker) shade represents a weaker (stronger) forcing and lower (higher) biomass in the rings for the physical forcing and plankton. Note that downwelling is accompanied by entrainment mixing during winter in the NEAS, but not in the CEAS and SEAS. For the fishery, seasonality is not shown. This neglect does not imply a lack of seasonal variation in the fisheries in the EAS; it merely reflects the discussion in this paper, in which the seasonal changes in the physical forcing are related to the annual catch.